Spatial patterns of humidity, fuel moisture, and fire danger across a forested landscape

by

Derek W. van der Kamp

BSc., Physics and Ocean Sciences, University of Victoria, 2005

MSc., Geography, The University of British Columbia, 2008

A THESIS SUBMITTED IN PARTIAL FULFILLMENT
OF THE REQUIREMENTS FOR THE DEGREE OF

Doctor of Philosophy

in

THE FACULTY OF GRADUATE AND POSTDOCTORAL
STUDIES

(Geography)

The University of British Columbia

(Vancouver)

August 2017

Abstract

Spatial variability in fuel moisture driven by changes in microclimate is an important bottom-up factor determining spatial wildfire behaviour, as fuel moisture impacts fire intensity, severity, and spread probability. However, few studies have examined how landscape scale patterns in near-surface microclimates impact fuel moisture patterns. This study quantified patterns of near-surface atmospheric conditions within a heterogeneous forested landscape, and determined how those patterns impact the spatial variability of fuel moisture and fire danger across the landscape. Observations across a forested landscape demonstrated that, in general, spatial variability in near-surface relative humidity and temperature was highest during dry, clear-sky conditions. However, daytime relative humidity was an exception, being relatively homogenous across the landscape and only weakly related to weather conditions. Canopy cover and above-canopy radiation load predicted a significant portion of the spatial patterns in relative humidity and temperature. Changes in canopy cover had the largest impact on near-surface conditions. Open sites saw higher relative humidity, on average, due to nocturnal longwave cooling. A novel fuel moisture model was presented that predicted between 76% and 93% of the variance in observations from independent sites or time periods, which is an improvement on a more complex model currently used operationally. This model was combined with meteorological observations to quantify spatial patterns in fuel moisture and potential fire danger across the landscape. Daytime fuel moisture and potential fire danger exhibited low spatial variability, regardless of weather conditions, and only 1-hour fuel moisture was related to canopy cover or radiation load. Fuel moisture and potential fire danger were more variable at night and that variability increased during cool, moist periods with low wind speeds. Patterns in

fuel moisture and potential fire danger were dominated by differences in nocturnal longwave cooling due to changes in canopy cover. Open sites had lower daily mean potential fire danger. When fire danger was extrapolated over a larger study region, daytime conditions remained homogenous. Moreover, radiation load and canopy cover did not have a large enough direct influence on daytime fuel moisture to generate patches within the landscape that remain significantly wetter than the surrounding landscape.

Lay Summary

Fires play an important role in forests, and it is important to understand how fires spread and how the severity and intensity of a fire changes across a forest. The goal of this thesis was to determine how fuel moisture, which has a significant influence on fire behaviour, changes across a forested landscape due to changes in aspect and the density of the canopy. It was found that the density of the canopy had an impact on fuel moisture. Open sites had wetter fuels and lower fire danger due to increased cooling at night. Terrain aspect had a secondary impact on the moisture of smaller fuel elements, but not on fire danger. In general, however, fuel moisture did not vary substantially across the landscape during the afternoon, suggesting that aspect and canopy density alone cannot create significant changes in fuel moisture across the landscape.

Preface

The following thesis was completed under the supervision of Dr. R. Dan Moore and Dr. I.G. McKendry. Dr. Moore and Dr. McKendry provided guidance and suggestions on the study design and analyses, as well as editorial revisions. Derek van der Kamp was the lead author and led the conceptualization, design, data collection, data analyses and writing of this thesis.

A version of Chapter 4 has been published as:

van der Kamp, D. W., Moore, R.D., and McKendry, I.G. 2017 A model for simulating the moisture content of standardized fuel sticks of various sizes. *Agricultural and Forest Meteorology* 236: 123-134.

Table of Contents

List of Tables

List of Figures

xiv

xvi

xviii

List of symbols for Chapter 4

Variables

α Albedo

β Cloud type constant

ε Emissivity

κ Thermal diffusivity of air (1.9×10^{-5} m^2 s^{-1})

λ Energy required to transition a unit mass of water to vapour (J Kg^{-1})

ν Kinematic viscosity of air (1.51×10^{-5} m^2 s^{-1})

Ω Aerodynamic resistance (sm^{-1})

ϕ Solar elevation angle (rad)

ρ Density (kg m^{-3})

σ Stephan-Boltzmann constant (5.67×10^{-8} W m^{-2} K^{-4})

τ Atmospheric transmissivity

θ Angle relative to the horizontal (rad)

a Surface area (m^2)

A, B Empirical constants related to the equilibrium moisture content

C Conduction into the core (W)

c Specific heat (J K^{-1} kg^{-1})

D Diffusion into the core (kg s^{-1})

d Bulk moisture diffusion coefficient (m^2 s^{-1})

E Moisture flux between the outer layer and the atmosphere (kg s^{-1})

f Fraction of the stick volume taken up by the outer layer

g Specific gravity of the stick

I Isotropic diffuse radiation (W m^{-2})

K Shortwave radiation (W m^{-2})

k Bulk conductivity (J m^{-1} s^{-1} K^{-1})

L Longwave radiation (W m^{-2})

l Length of the stick (m)

M Molecular mass of water (0.0180 kg mol^{-1})

m Cloudiness factor

m Moisture content (% of oven-dry weight)

n Clearness index

Nu Nusselt number

P Precipitation (kg s^{-1})

Q Turbulent heat flux (W m^{-2})

q Vapour density(kg m^{-3})

r Radius of stick (m)

R Gas constant (8.314 $\times 10^{-3}$ kPa m^3 mol^{-1} K^{-1})

Re Reynolds number

RH	Relative humidity (%)
s	Canopy view-factor
T	Temperature (K)
u	Wind speed (m s^{-1})
V	Volume (m^3)
w	Precipitable water content (cm)

Subscripts

a	Ambient air
abs	Absorbed by stick
c	Inner core of stick
d	Downwelling radiation
diff	Diffuse radiation component
dir	Direct radiation component
e	latent heat flux
emitt	Emitted by stick
fsp	Fibre saturation point
g	Ground
h	Sensible heat flux
inc	Incident
max	Maximum allowable value
mid	Mid-point radius (m)
o	Outer layer of stick

s	Entire stick
sat	Saturation
surf	At the stick surface
u	Upwelling radiation

Acknowledgments

I want to begin by thanking my co-supervisors, Dan Moore and Ian McKendry, for their support and encouragement throughout my thesis. They provided me with both the freedom to develop and pursue my own research direction, as well as useful guidance when I needed it. I couldn't have asked for better supervisors. As well, my committee members, Meg Krawchuk and Steve Mitchell, provided me with very useful advice at the outset of the project. This thesis also benefited immensely from their careful reading and thoughtful comments. I would also like to thank Meg for letting me tag along to her field sites so that I could "smell the numbers." It was great to be able to work on this thesis alongside my good friends and officemates, Joel Trubilowicz and Jason Leach who provided me with a lot of great advice and timely distractions. Thanks to my parents and family for all the support over the years.

I am grateful to J.D. Carlson for providing us with the Oklahoma fuel moisture dataset. Thanks to Dr. Christopher A. Fiebrich of the Oklahoma Climatological Survey for providing the Oklahoma Mesonet data. Thanks also to Lawrence Bird for his assistance in the field. Funding for this research was provided by the Natural Science and Engineering Research Council. NSERC provided me with a Canada Graduate Scholarship and Discovery Grants to both Dan Moore and Ian McKendry. Dan K. Thompson and Ralph M. Nelson provided useful comments on an earlier manuscript of Chapter 4.

Finally, I want to thank Alison for all her support. I am so lucky that I had my best friend and partner just down the hall over the last few years.

Chapter 1

Introduction

1.1 Motivation

Wildfire is a significant source of disturbance in many ecosystems and the spatial patterns that fires leave on a landscape affect both ecosystem structure and ecosystem function (McKenzie et al., 2011). For instance, the successional pathway of a forested ecosystem following fire is strongly dependent on burn severity patterns. Species richness and community composition are impacted by the size and severity of burned patches (Turner et al., 1997). Patterns in post-fire seedling establishment can be influenced by the location of stands of surviving mature trees that act as seed sources (Pierce and Taylor, 2011), or by burn severity patterns in organic soils (Johnstone and Chapin, 2006). The heterogeneity and connectivity of vegetation patterns resulting from fires are also important in creating suitable habitat for fauna; a more heterogeneous landscape provides species with a larger range of habitat conditions (Smith et al., 2000). Wildfire patterns also influence subsequent fire activity (Parks et al., 2014).

Understanding the spatial behaviour of fires is important from a management perspective, as accurate predictions of fire behaviour are crucial for protecting lives and values at risk. As well, current management practices emphasize that reducing suppression efforts and allowing more fires to burn will help achieve management goals and create more resilient forests (Stephens and Ruth, 2005; Canadian Council of Forest Ministers, 2005). Increasing our understanding of fire behaviour across

1

the landscape will increase the confidence of fire managers to allow more fires to burn (Collins et al., 2007). The planning and execution of prescribed fires and fuel treatments would also benefit from an increased ability to predict the patterns and ecological consequences of wildfires.

The spatial behaviour of wildfire across a landscape is dependent on the three elements of the "fire triangle": fuels, topography, and weather, all of which vary at multiple scales (McKenzie et al., 2011). At the finer scales, fire patterns are influenced by patterns in fuel type, fuel amount, and connectivity across different slope aspects (Lertzman et al., 1998); the impact of slope steepness on fireline intensity (Cohen and Deeming, 1985); and the influence of terrain on local wind fields (Sharples, 2009).

A number of researchers have identified patterns in fuel moisture driven by changes in microclimate across different slope aspects as an important bottom-up factor determining spatial wildfire behaviour (e.g., Heyerdahl et al. 2001). It has also been postulated that reduced wind speeds and radiation below dense forest canopies lead to cool moist microclimates and wetter fuels (Collins et al., 2007). A number of studies have pointed to variability in fuel moisture across the landscape as a driver of burn severity patterns derived from satellite imagery (e.g., Holden et al. 2009; Birch et al. 2015; Kane et al. 2015; Dillon et al. 2011). Spatial patterns in fuel moisture may also alter fire spread probability. In the extreme case where the landscape is homogeneously dry, a fire can spread unimpeded through a region. However, in moderate fire weather conditions, particular areas of the landscape may be dry enough to support fire spread while other areas are too wet, and in this case the pattern of fuel moisture becomes important. If fuel moisture changes gradually across the landscape, a fire will be more likely to spread across the drier portion of the region, given ideal weather conditions and fuel types. Alternatively, if the fuel moisture pattern is patchier, a fire will be less likely to move across the entire landscape as patches of wet fuels will impede its progress (Miller and Urban, 2000; Littell and Gwozdz, 2011).

Patterns in microclimates impact fuel moisture directly though changes in radiation, wind speed, cold air pooling, or soil moisture. They can also have an indirect effect through their influence on vegetation density and composition. Cool, north-facing slopes may have increased biomass in both the overstory and understory that

2

decreases the amount of solar radiation and wind speed available to dry out surface fuels (Zou et al., 2007; Birch et al., 2015). Increased vegetation may, in turn, increase near-surface humidity through enhanced transpiration (Renaud et al., 2011; Estes et al., 2012). Nyman et al. (2015b) demonstrated that the influence of aspect on fuel moisture is significantly enhanced by the indirect influence of increased vegetation, and deeper, wetter soils on cooler slopes. In this way the indirect effects and direct effects compound one another. However, this relationship between the direct and indirect impact may be decoupled due to disturbance history, or in wetter, energy-limited forests that often have homogeneous vegetation across different aspects (Ohmann and Spies, 1998). It would therefore be useful to decouple these direct and indirect impacts of microclimate patterns on fuel moisture and examine each factor in isolation.

That fuel moisture is a primary driver of wildfire patterns is a reasonable conclusion, considering that moisture has a strong influence on the energy released by the propagating fire front (Rothermel, 1972) and the amount of forest floor duff and larger fuel elements that are consumed (Sandberg, 1980, Knapp et al., 2005). However, limited work has been done directly measuring patterns in fuel moisture across forested landscapes, and many of the studies that are available have found low variability, especially during dry periods (Whitehead et al., 2006; Estes et al., 2012; Banwell et al., 2013; Gibos, 2010). As well, even though the literature often cites microclimate as a primary driver of fuel moisture patterns, there are few studies that examine landscape scale patterns in microclimate with the explicit purpose of determining how these patterns in near-surface conditions, in turn, influence fuel moisture patterns. For instance, previous analyses have primarily focused on temperature, rather than relative humidity, which is a primary driver of fuel moisture (Viney, 1991).

Given that 1) patterns in fuel moisture are often considered to be a primary driver of fire behaviour, 2) direct observations of fuel moisture variability are limited, and 3) few studies in microclimate variability are designed with fuel moisture in mind, it would be worthwhile to examine, in detail, how microclimatic conditions vary across forested landscapes, and how that variability translates into fuel moisture patterns. In the following section, a brief literature review will summarize the processes impacting fuel moisture, provide an overview of different approaches

to fuel moisture modelling, and discuss how microclimates and fuel moisture may vary across a forested landscape.

1.2 Literature review

1.2.1 Processes impacting fuel moisture

Dead fuel moisture content plays a significant role in determining the rate and intensity of fire spread as the latent heat of vaporisation represents a significant portion of the energy required to bring a fuel to ignition (Rothermel, 1972). Dead surface fuels gain and lose moisture through a number of processes. Fuel elements can gain moisture through the adsorption of water vapour from the surrounding air by cell walls via molecular bonding, or through absorption, in which liquid water is drawn into cavities within the fuels though capillary flow. Adsorption can only raise moisture up to a "fibre saturation point" (around 30% of the dry weight of the fuel), beyond which moisture must be gained through the absorption of liquid water (Viney, 1991). When liquid water is introduced to a fuel element, rapid absorption occurs within the first few hours, after which the absorption rate decreases as the fuel reaches saturation, which can range anywhere from 150 to 400% of the dry weight of the fuel (Simard, 1968). Previous research suggests that waxy resins on the surface of the elements can reduce moisture absorption. As fuels decompose, this wax coating is lost, and the rate at which fuel elements absorb moisture increases (Van Wagner, 1969). These processes will continually move fuel moisture towards an equilibrium moisture content (EMC). The EMC for a particular meteorological condition is the moisture content reached by a fuel element if it is given enough time to come to an equilibrium with that condition.

Precipitation has an obvious impact on fuel moisture. However, the amount of incident precipitation that is actually absorbed by fuel elements is dependent on intensity and antecedent moisture (Nelson, 2000); precipitation will more readily be absorbed by fuels if the rate of precipitation is low, and if the fuels are dry. Condensation can also signficantly increase fuel moisture in the absence of precipitation (Viney, 1991). There is also evidence that surface fuels gain moisture from underlying wet soils due to capillary draw (Hatton et al., 1988; Samran et al.,

1995). Fuel elements lose moisture through gravitational drainage of liquid water from larger pores and the evaporation of liquid water from the fuel surface and free liquid water drawn to the surface via capillary forces. Evaporation of liquid water is followed by the desorption of bound water from the cell walls (Viney, 1991).

Free liquid water within the cells and surfaces of the fuel elements is likely present only during brief windows following precipitation, snowmelt or condensation (Van Wagner, 1979; Viney, 1991). As liquid water is quickly removed from the fuel elements, the fibre saturation point is reached and adsorption and desorption then become dominant and represent the primary method of moisture exchange throughout the fire season. This transfer of water vapour to and from molecularly bound water in the cell walls of fuel elements is thermodynamically different than evaporation and condensation, as bound water within cellulose has a lower energy state than liquid water (Skaar, 1988), i.e., it takes more energy to remove the water from the fuel element.

1.2.2   Modelling fuel moisture

Numerous researchers have developed models for simulating fuel moisture (see Viney (1991) and Matthews (2013) for reviews). These models can be divided into two broad categories: empirical models and process-based models. Empirical models are often generated by regressing measured fuel moisture content against a suite of meteorological and site variables (e.g., McArthur 1962; Pook and Gill 1993; Marsden-Smedley and Catchpole 2001; Ferguson et al. 2002; Lin 2004; Alves et al. 2009). Matthews (2013) reviewed the literature to determine predictors of fuel moisture commonly used by these regression models. Relative humidity was the most common predictor, followed by temperature.

A number of empirical models of EMC have been developed. Van Wagner (1972) let different fuel types come to equilibrium with conditions precisely controlled in a drying chamber. The author found that the EMC was a sigmoidal function of atmospheric relative humidity, and that the shape of the function changed with temperature and fuel type. Importantly, fuel moisture exhibited a hysteresis behaviour: the shape of the function also depended on whether the fuel was drying towards the EMC or getting wetter. Van Wagner (1972) fit a semi-empirical

function to the data. This sigmoidal behaviour, along with the presence of hysteresis has been repeated in other studies (e.g., Anderson 1990b), and is a part of the fuel moisture indices within the Canadian Fire Weather index system (Van Wagner, 1987). Nelson (1984) developed a semi-physical model for EMC based on thermodynamic arguments. At the core of the model is the assumption that the change in the Gibbs free energy that occurs when liquid water becomes molecularly bound within the cellulose of the fuel is an exponential function of the fuel moisture. Using this assumption, Nelson (1984) derived a sigmoidal EMC function similar to what was found in previous empirical studies.

The EMC can be used to model actual fuel moisture using the differential equation:

$$\frac{dm}{dt} = \frac{m_e - m}{\tau} \tag{1.1}$$

where m is the fuel moisture content given as a percentage of the dry weight, m_e is the EMC, and τ is the response time of the fuel, which determines how quickly the fuel approaches the EMC. This formulation has been used by a number of researchers (e.g., Fosberg et al. 1981; Catchpole et al. 2001), is utilized by the Canadian Fire Weather Index system (Van Wagner, 1987), and has recently been integrated into a coupled fire-weather model (Vejmelka et al., 2016). Numerous studies have measured the response time, τ, of various fuels and attempted to relate these drying rates to weather conditions (e.g. Anderson 1990a; Hille and den Ouden 2005). Van Wagner (1979) demonstrated that the drying rate increases with temperature and decreases with relative humidity, although that relationship is less clear below 60% relative humidity. Van Wagner (1979) also found that the drying rate increases with wind for low wind speeds (<2 km/h), but is relatively insensitive to speeds above that threshold.

The Canadian Fire Weather Index system (Van Wagner, 1987) is used operationally in Canada and globally to estimate fire weather severity. At the core of this system are three moisture indices: the Fine Fuel Moisture Code (FFMC), the Duff Moisture (DMC) Code, and the Drought Code (DC). The FFMC represents small diameter surface litter, such as needles, cured grasses, and small twigs, the DMC represents the layer of decomposing, loosely packed organic material,

and the DC represents the moisture of the deep layer of compact organic material. These indices are calculated using an accounting approach whereby yesterday's fuel moisture is increased though precipitation, or reduced via drying. The FWI system uses the approach outlined in Equation 1.1, and the response time of the fuel is smallest for the FFMC, and largest for the DC. In the case of the FFMC, the drying rate calculation uses the relationships found by Van Wagner (1979) and the EMC is a sigmoidal function of relative humidity. In contrast, the DMC has a constant EMC of 20%, and the logarithm of the drying rate has a positive linear relationship with temperature and the length of day, and is negatively related to relative humidity. Daily moisture loss for the DC is estimated from temperature only, using a empirical linear relationship.

A crucial component of the American National Fire Danger Rating System (NFDRS) is the four fuel moisture variables: 1-hour, 10-hour, 100-hour, and 1000-hour fuel moisture (Cohen and Deeming, 1985). These metrics were developed to simulate the moisture of standardized fuel sticks of various sizes. They were assumed to, in constant conditions, behave according to equation 1.1 and approach the equilibrium moisture content, m_e, along an exponential curve defined by the response time of the fuel, τ, which was independent of conditions, and increases from 1 hour to 1000 hours.

Fuel moisture for the 1-hour and 10-hour fuel sizes are calculated using the approach of Fosberg and Deeming (1971). The authors developed a differential equation that related the change in moisture content with the trend in m_e over the late morning and early afternoon. Using climatological data from a single study, Fosberg and Deeming (1971) developed equations in which the mid-afternoon 1-hour and 10-hour fuel moisture was a simple linear function of the mid-afternoon m_e. It is important to note that these two metrics are not related to precipitation. For the 100-hour and 1000-hour fuels the NFDRS follows the procedure outlined by Fosberg et al. (1981) whereby the change in moisture from some initial value is directly related to the difference between that initial moisture content and the m_e, and τ. For the 100-hour fuel, the day's moisture content is calculated using the previous day's value and the average m_e for the last 24 hours, while for the 1000-hour fuel the moisture content from seven days ago is used along with the m_e averaged over the last week. The influence of precipitation is included by increasing m_e by

an amount dependent on precipitation amount.

Nelson (2000) developed a sophisticated model for simulating the moisture of standardized fuel sticks as an alternative to the relatively simple approach used previously in the NFDRS. This model is used operationally by a number of fire management agencies. It simulates the energy and moisture exchange at the surface as well as the transport of moisture and heat within the interior of the stick. The model uses a linearised energy budget in which net longwave radiation is estimated as a function of the difference between the stick temperature and the apparent sky temperature.

1.2.3 Spatial variability of microclimate and fuel moisture at the landscape scale

All of the processes influencing fuel moisture will vary spatially at a host of different scales. For instance, fuel moisture is heavily influenced by near-surface temperature and humidity, which can vary significantly in complex terrain. Temperatures generally decrease with altitude due to adiabatic cooling (Barry, 2008) and increase with increasing radiation load (Geiger, 1965; Barry, 2008). A number of studies have examined the influence of terrain on surface conditions and fuel moisture. Hayes (1941) found that, in the absence of a canopy, fuel moisture was always higher on north slopes. However, Gibos (2010) found no significant difference between a north and south aspect under dense canopy. Nyman et al. (2015a) found that, in both dry or wet forests where canopy is either homogeneously dense or open, aspect had little effect on fuel moisture, as radiation was either consistently low, or high across sites. Aspect had the largest impact in a forest with moderate canopy cover. Sullivan and Matthews (2012) used a model validated on field data to simulate differences in fuel moisture across different aspects. They found that differences in modelled fuel moisture mainly occurred during the morning on steep slopes due to lower morning sun angles. Holden and Jolly (2011) used empirical relationships between terrain indices and weather observations to model fire danger across complex terrain. Their analysis indicated that south facing slopes had drier fuels, due, in part, to increased radiation.

Stand structure can have a significant influence on near-surface microclimates during the fire season. Near-surface temperatures are often lower than above canopy

conditions during the day and warmer at night (Fridley, 2009). Wind speeds diminish with increased canopy cover (Oke, 1990). However, significant evaporation can occur when large eddies penetrate the canopy and ventilate the surface with relatively warm or dry air (Denmead and Bradley, 1985). The presence of a significant understory will enhance both the decreased ventilation and decreased moisture deficit directly above the forest floor. Within the understory, moisture levels are often near saturation and wind speeds can be close to zero (Oke, 1990). As well, net radiation levels are obviously controlled by canopy and understory structure. Studies examining the influence of canopy cover on temperature have found that, overall, a forest canopy acts to reduce diurnal variability in temperature by reducing incoming solar radiation and nocturnal radiative cooling (Chen et al., 1999). The influence of canopy cover on relative humidity is partly driven by temperature variability. Compared to open sites, cooler daytime conditions below dense canopies lead to higher relative humidity while relative humidity is lower at night when nocturnal cooling is reduced (Chen et al., 1993; Renaud et al., 2011). However, this effect is more modest and less consistent than for temperature. A handful of studies have examined the influence of canopy cover on fuel moisture (e.g., Whitehead et al. 2006; Estes et al. 2012; Banwell et al. 2013). Generally, it was found that canopy cover has the strongest impact on fuel moisture during periods of low to moderate fire weather; extreme fire weather leads to more homogeneous moisture levels.

Variability in canopy cover and precipitation interception will impact spatial patterns in fuel moisture. The amount of interception by vegetation is strongly dependent on antecedent precipitation (dry canopies have a higher capacity to retain moisture than wet canopies), wind speeds, and air temperature, which influence evaporation and precipitation rates. Mean annual interception rates are dependent on canopy densities and weather and range from 3 to 30% of total precipitation, depending on forest stand characteristics and climate conditions (Winkler et al., 2010). The amount of infiltrating precipitation that will be stored within the litter layer is dependent on antecedent moisture conditions and precipitation rates. Sato et al. (2004) found that the rate of moisture accumulation fell quickly upon initiation of precipitation, plateauing at a maximum storage amount that was itself dependent on the precipitation rate. Within the Canadian Fire Weather Index sys-

tem, precipitation adds moisture content to the fine fuels at a rate that decreases with increasing precipitation rate and initial moisture content (Van Wagner, 1987).

Mesoscale air flows driven by buoyancy differentials can also change surface climates. For instance, the negative buoyancy experienced by cool surface air forms down-slope katabatic drainage flows during clear nights. This will lead to cooler air with higher relative humidity levels pooling in valley bottoms and hollows (Lundquist et al., 2008). Simulated maps of fire danger generated for a mountainous terrain by Holden and Jolly (2011) found that nocturnal drainage led to diminished fire danger in valley bottoms. A similar pattern of relatively low fire danger in valley bottoms was found by Schunk et al. (2013).

High fuel moisture may also be found in topographically convergent and/or poorly drained areas within a landscape. Late-successional stands with lower fire frequencies are more likely to occur within riparian zones (Camp et al., 1997; Dwire and Kauffman, 2003). Lateral flows of water through the duff and litter layers themselves are more ephemeral and occur at a smaller spatial scale than lateral flow within mineral soils (Kim et al., 2005; Keith et al., 2010b). It is likely, therefore, that any hydrological impact on fuel moisture patterns is due to lateral flow within the underlying mineral soil, which then influences fuel moisture.

Such an influence could happen in a number of ways. Fuels could be inundated if the water table reaches the surface. High water tables mainly occur in regions of hydrological accumulation such as regions of confluence, on perched water tables, or within valley bottoms (Winkler et al., 2010). This effect may be reduced during dry periods; Dyer (2009) found that cool climates found in valley bottoms are less pronounced during the growing season. Secondly, as mentioned in the previous section, it may be possible for the moisture of surface fuels to be influenced by the underlying soil moisture through upwards capillary draw, although the literature is unclear on this topic. While a few observational studies have indicated that surface fuels gain moisture from the underlying soils (Hatton et al., 1988; Samran et al., 1995; Nyman et al., 2015b), exclusion experiments by Keith et al. (2010a) indicated that during dry conditions diurnal cycles in duff moisture were driven by evaporation from the surface; capillary draw had no impact. A number of models of litter moisture (Ogée and Brunet, 2002; Matthews, 2006) assume no upwards capillary draw.

10

Hydrology may also have an indirect control of fuel moisture by first influencing near-surface atmospheric conditions. Temperatures have been found to be lower near streams (Bolstad et al., 1998; Lookingbill and Urban, 2003; Fridley, 2009) due to increased evaporative cooling. Moreover, Dobrowski (2011) pointed out that relatively moist soils can temper the diurnal range of near-surface temperature due to increased thermal inertia. The cooler, more slowly varying microclimates found above moist soils could, in turn, lead to slowly varying fuel moisture.

1.3   Thesis objectives and outline

From the overview of the literature presented above, it is clear that there are a number of research gaps that have yet to be filled. Specifically, it is unclear whether changes in near-surface atmospheric conditions can lead to substantial variability in fuel moisture and fire danger over a forested landscape within complex terrain. There is also little information about the relative influence of different factors controlling fuel moisture patterns. Finally, there has been a lack of research on separating the direct and indirect impacts of microclimates on fuel moisture. Therefore, the overall objective of this thesis is to quantify the spatial variability in near-surface atmospheric conditions, examine how this variability translates into patterns in fuel moisture and fire danger, and determine the relative influence of canopy cover, radiation load, and elevation on these patterns.

Radiation load is defined here as the intensity of solar radiation on the forest floor if the canopy were to be removed, and will vary with slope and aspect. Canopy cover is defined here in terms of a canopy gap fraction estimated from hemispherical photos. In the interest of producing a focused study, and given resource limitations, the potential influences of cold-air pooling and groundwater patterns on fuel moisture patterns are not examined here.

As mentioned above, wind, slope and fuel amount influence fire danger in addition to fuel moisture. However, this thesis will focus on the contribution of fuel moisture to fire danger rating. Consequently, the Energy Release Component (ERC) of the US National Fire Danger Rating System will be used as a metric for potential fire danger. The ERC is strongly dependent on fuel moisture, and is not related to wind or slope. The ERC is used operationally in the United States as a

metric for potential fire behaviour.

The thesis objectives will be addressed through four analysis chapters. Following a description of the field site and methodology in Chapter 2, the analysis in Chapter 3 focuses on the spatial patterns of observed near-surface temperature and relative humidity. Specifically, a network of humidity and temperature sensors was established at sites representing a range of both radiation load and canopy cover. The locations were chosen so that the two dimensional parameter space described by canopy cover and radiation load was sampled as evenly as possible. This sampling approach allows for the influence of both factors to be assessed independently and for their relative influence to be compared. The objective of this chapter is to quantify the amount of spatial variability in near-surface atmospheric conditions that is seen across a small (<4 km^2) forested landscape, how weather conditions control that variability, and the relative influence of radiation load and canopy cover on spatial patterns in near-surface conditions. Sites were chosen with consistent understory vegetation in order to focus on the direct impacts of changing radiation loads on fuel moisture.

In order to determine how micrometeorological conditions impact fuel moisture, a novel fuel moisture model was developed that explicitly simulates heat and moisture exchange between the atmosphere and standardized fuel sticks. This model is described and evaluated in Chapter 4. The new model builds on the model used operationally by fire management agencies by increasing the sophistication of the treatment of radiative and turbulent heat transfers. This increased sophistication will allow for a more detailed examination of how changing micrometeorological conditions alter fuel moisture. A focus on elevated fuel moisture sticks avoids the requirement to simulate the potential influence of underlying soil moisture on fuel moisture.

In Chapter 5 the network of near-surface weather observations presented in Chapter 3, and the fuel moisture model presented in Chapter 4, are combined to simulate fuel moisture variability across the field site. These data are then used to examine the influence of micrometeorology and site characteristics on spatial patterns in fuel moisture and fire danger. As in Chapter 3, the spatial variability in fuel moisture and fire danger is quantified, and the relative influence of canopy cover and radiation load is assessed. This chapter examines if either radiation load

12

or canopy cover have the ability to create significant patterns in fuel moisture and fire danger that persist over multiple days. In order to examine how changing microclimates on different slope aspects directly impact fuel moisture, a sampling approach will be used which separates the influence of radiation load and canopy cover and uses sites with consistent understory. Chapter 5 also attempts to quantify the relative influence of precipitation and radiation on fuel moisture and fire danger.

Finally, in Chapter 6 rasters of fuel moisture are developed to examine patterns in fire danger across a larger study region of 140 km^2. In this way the analysis of spatial patterns in fire danger and fuel moisture is extended beyond point measurements made within a small ($<$4 km^2) area. Additionally, this final analysis introduces the impact of elevation. The required rasters of relative humidity and temperature are estimated using a non-linear machine learning approach that is trained on the near-surface observations used in Chapter 3.

Final conclusions are provided in Chapter 7, beginning with a summary of major findings. This is followed by a discussion of the implications of the findings and potential future research directions.

Chapter 2

Field site and methodology

2.1 Overview

A network of near-surface humidity and temperature sensors was established across a forested landscape with a wide range of both radiation load and canopy cover. In order to isolate the influence of these two factors, and given the focus on the landscape scale, the network sampled a relatively small area (<4 km^2) with little change in elevation. This sampling design ensured that there were no larger scale climatic gradients, and that all sites were forced by the same above-canopy conditions. Sites were selected so as to sample as much of the two dimensional space described by canopy cover and radiation load as possible, which helped to avoid collinearity and its effects on the stability of estimated regression coefficients. As mentioned in the introduction, this thesis will attempt to isolate the direct impact of patterns in microclimate on fuel moisture due to increased radiation from the indirect impacts, which are attributable to the fact that vegetation is often denser in cooler and wetter microclimates. Therefore, sites were chosen which had relatively consistent vegetation with little understory vegetation. As a complement to this network, fuel moisture, solar radiation, precipitation, and wind speed were measured at a subset of sites.

2.2 Field site

The field location was selected based on several criteria. At a broad scale, the Interior Douglas-fir (IDF) Biogeoclimatic Ecological Classification (BEC) zone (Pojar et al., 1987) was chosen as a suitable ecosystem type for this field work for several reasons. Firstly, this region is characterized by relatively long seasons of intense fire weather and was likely to provide a wide range of conditions including protracted dry periods. Secondly, this BEC zone is characterized by a relatively sparse understory which allowed me to focus on the influence of the overstory independently of the influence of shrubs and understory trees. At a finer scale, I focused on locating regions of Crown land that were accessible by major logging roads but were not being actively logged. Finally, I looked for regions characterized by high spatial variability in canopy cover and radiation load so that a wide range of these factors could be sampled within a relatively small area.

Based on these criteria, a broader region of interest was selected located 20 km north-west of Kamloops, just west of the Lac du Bois Grasslands Protected area with an average elevation of 1170 m. The plateau region exhibits a rolling terrain, and logging activity has left a mosaic of stand structures. Within the drier regions of BC, such as the IDF and Ponderosa Pine BEC zones, canopy cover increases with decreasing radiation load due to decreased water deficit. However, the logging at the field location has, to a certain extent, decoupled this relationship; logging on cool north facing slopes has provided sites with low radiation load and low canopy cover. This decoupling provided an opportunity to sample the entire canopy cover/radiation load parameter space.

A smaller field site was then selected within this broader region. Its location is shown in Figure 2.1. Using Landsat imagery, the Vegetation Resource Inventory database (http://www. for.gov.bc.ca/hts/vri/), and Google Earth, canopy cover was mapped across the broader region. Combining these layers with maps of radiation load calculated using ArcGIS 10 (ESRI), the region was divided into 16 strata, each with a unique combination of low, low-moderate, high-moderate, and high levels of both canopy cover and radiation load. A smaller region was then identified within which as many of the 16 strata as possible were represented. Having selected the specific study area, these strata were then used to to select individual measurement

sites so that as much of the two-dimensional parameter space was sampled as possible. In Chapter 6 I produce 30-m resolution rasters of fire danger across a 34 km^2 study region centred around the field site. The location of this study region is also shown in Figure 2.1

2.3 Field methodology

The network of stations comprised 24 sites, each of which had a LogTag Haxo-8 relative humidity/temperature sensor, which took measurements every 30 minutes. A detailed map of the field area along with the site locations is shown in Figure 2.2, and site characteristics are provided in Table 2.1. Site locations were chosen to minimize among-site variation in understory structure, with a preference for sites dominated by a needle bed interspersed with grasses and/or mosses. Shrubs and thick understory vegetation were avoided as much as possible. Observations were made from May 6 to September 22, 2014. The field site was established soon after the area was accessible, and ended when the likelihood of a period of high fire danger occurring had diminished. Each LogTag was placed within a custom radiation screen constructed from corrugated plastic sheets and reflective foil tape, based on the design by Holden et al. (2013). As these data will be used to drive the fuel moisture stick model developed in Chapter 3, the sensors were placed 30.5 cm above the ground, which is the standard measurement height for fuel moisture sticks.

At each site, hemispherical photos of the canopy were taken to estimate canopy cover. A Nikon FC-E8 fisheye lens and a Nikon Coolpix 4500 4.0 mega pixel camera were used to take the images at the highest image quality. These images were processed with the Gap Light Analyser software (Frazer et al., 1999), which generated canopy gap fractions as a function of zenith angle and azimuth. A total canopy gap fraction, which was taken to represent canopy cover, was then generated by integrating over the half sphere. The hemispherical photos were also used to model below-canopy shortwave radiation load. The details of this modelling are provided in Chapter 5. Aspect was estimated at each site using a compass, and slope gradients were estimated at each site by averaging both the downslope and upslope gradient over a distance of 10 m using an inclinometer. Aspect and slope were then
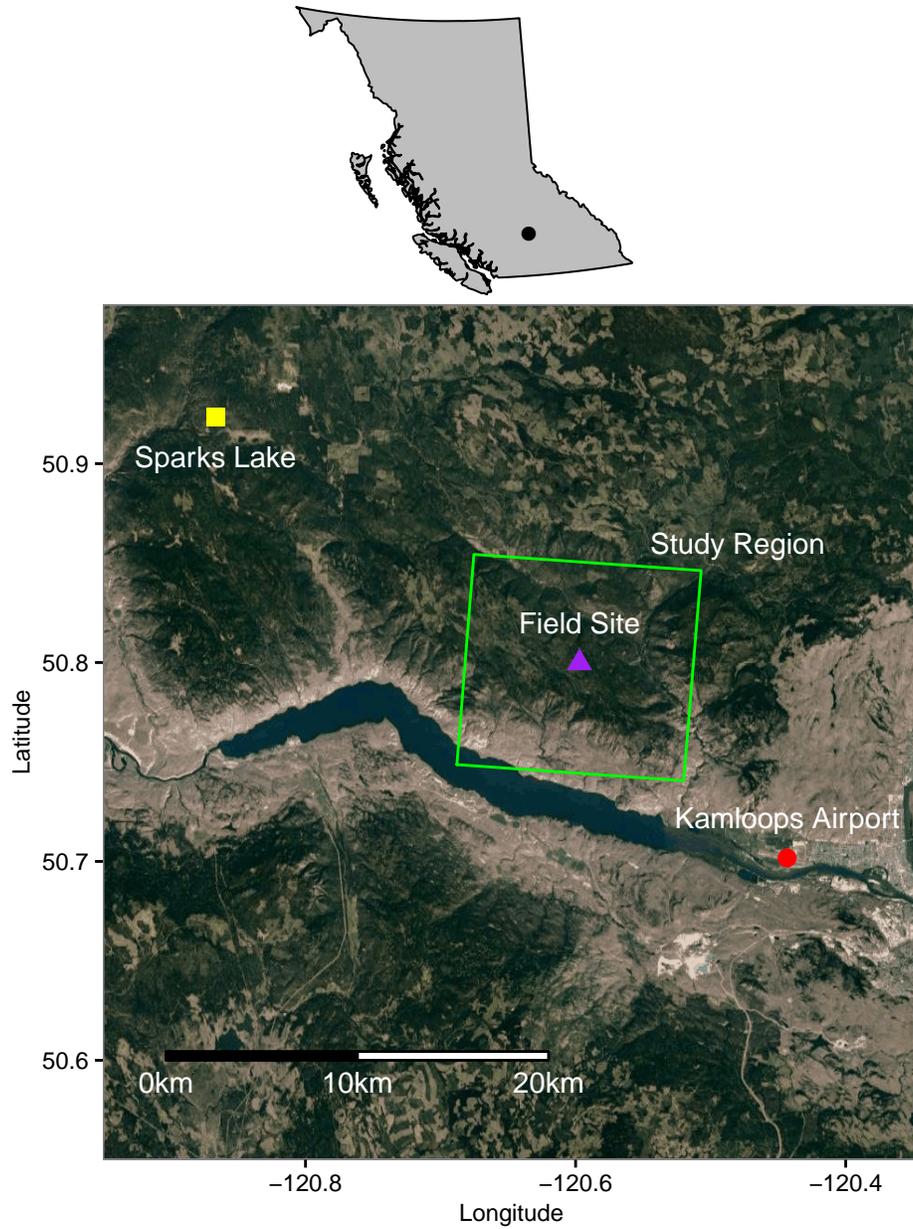
Figure 2.1: Map of study area, including the Field site location (*purple triangle*), the Sparks Lake fire weather station used in Chapter 5 (*yellow square*) , and the study region (*green square*) and Kamloops Airport weather station (*red circle*) used in Chapter 6. The location of the study area within BC is indicated by the black point in the map at top.

17
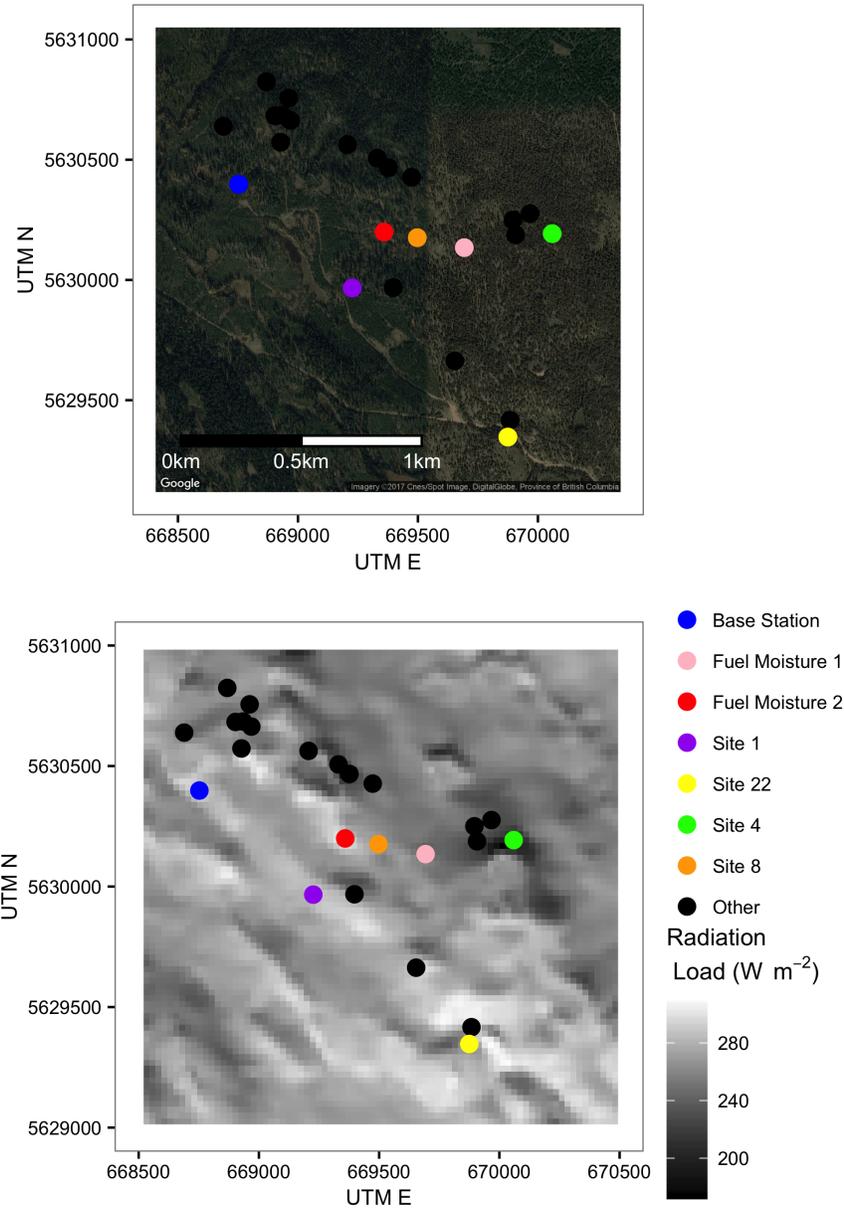
Figure 2.2: Detail of the field site. *Top:* aerial photography of site. *Bottom:* radiation load averaged over the entire field season (calculated using a 30-m resolution digital elevation model developed by Rosin (2010)). Sites referred to in text are indicated by colour.

18

used to calculate radiation load at each site using the equations of Iqbal (1983). At each site, flux densities of solar radiation parallel to the forest floor were calculated assuming clear sky conditions and no canopy cover. These hourly data were then averaged over the entire field season to generate average radiation loads for each site.

At three of the sites, Fuel Moisture 1, Fuel Moisture 2, and the Base Station, Campbell Scientific CS506 Fuel Moisture Sensors made 10-hour fuel moisture observations at a standard height of 30.5 cm. This sensor is composed of a time domain reflectometer probe embedded within a standard moisture stick with a radius of 0.65 cm and a length 50.8 cm. Co-located with each fuel moisture sensor was a Rotronic HC-S3 humidity and air temperature sensor (also at a height of 30.5 cm), a Rainwise tipping bucket raingauge, and a Kipp And Zonen CM3 pyranometer. In addition, at the Base Station wind speed was measured by a Met One anemometer, which has a stall speed of 0.4 m s^1, and temperature and humidity measurements were also taken at a height of 1.62 m. Wind speed was interpolated to 30.5 cm from 1.62 m using a neutral logarithmic wind profile. The aerodynamic roughness length was set to 0.01 m, which is appropriate for short grass (Oke, 1990). Fuel moisture, temperature, humidity, wind speed, and solar radiation measurements were made at 10 minute intervals. Finally, precipitation was also measured at Site 8 and at Site 1. Example photos of the instrumentation are shown in Figure 2.3.

A number of steps were taken to assess the accuracy of the Logtag sensors. Firstly, to assess any intrinsic biases of individual sensors, the LogTags were set to measure ambient temperature and humidity in the lab for three days before and after the field season. Secondly, the LogTag observations were compared to higher quality co-located Rotronic HC-S3 observations made at three of the sites. Results from this analysis can be found in Appendix A.

Even though the pine dowels used in the automatic fuel moisture sensors are carefully selected and standardized, it is likely that the sensors used here would provide slightly different results. With respect to sensor accuracy, the manufacturer reports that the root mean square error is $\pm$ 0.74% for moisture content below 10%, $\pm$ 0.90% for moisture between 10% to 20%, $\pm$ 1.94% for moisture between 20% and 30% and $\pm$ 2.27% for values above 30% (Campbell Scientific, 2015). To check the consistency between the sensors, two comparison periods were undertaken on

19

Figure 2.3: Field instrumentation. *Left:* Base Station; *Top Right:* LogTag Haxo-8 humidity and temperature sensor; *Bottom Right:* Radiation screen installed at Site 6. Instrumentation was surrounded by chicken wire to protect against grazing cattle.

either end of the field season in which the sensors were co-located for a total of 35 days. Using these co-located data, biases between the sensors were calculated and then removed to bring the three sensors into agreement. Details of this fuel moisture sensor calibration is detailed in Appendix A.

2.4 Supplementary weather observations

In order to provide context for the single season of fire danger estimated at the field site in Chapter 5, 26 years of fire weather data from a nearby British Columbia

Wildfire Management Branch fire weather station, Sparks Lake, were used to generate a regional climatology of fire danger. The station's location, shown in Figure 2.1, is at a similar elevation and forest type as the field site. The data, which were taken from Pacific Climate Impact Consortium's Data Portal (https://www.pacificclimate.org/data), include hourly observations of wind speed, precipitation, and relative humidity and temperature at a screen height of 2 m. Shortwave radiation was not measured at these stations and was therefore extracted from the Daymet dataset, which is a 1-km resolution daily interpolated weather dataset (Thornton et al., 1997). Daily mean shortwave radiation was converted to the required hourly resolution using the technique outlined by Liu and Jordan (1960). Any fire season (May 15th to October 1st) that had a data gap wider than four days was not used in the analysis and any data gap less than four days was in-filled using linear interpolation. Although this is not a particularly accurate method, it does not likely have a large impact on the resulting fire danger climatology derived from 26 fire seasons.

The analysis in Chapter 6 requires the calculation of temperature and humidity lapse rates. These lapse rates were calculated using the field observations combined with observations at the Kamloops Airport, which is at an elevation of 345 m above sea-level, compared to the field site's elevation of 1170m (See Figure 2.1 for location). The Kamloops Airport data were produced by Environment and Climate Change Canada and also acquired via the Pacific Climate Impact Consortium's Data Portal.

Table 2.1: Site characteristics.

Site Name	Longitude (Degrees)	Latitude (Degrees)	Radiation Load (Wm^{-2})	Canopy Gap Fraction (%)	Aspect (Degrees)	Slope (Degrees)
Site 1	-120.5991	50.7969	293	32	239	17
Site 2	-120.5967	50.7969	282	28	294	5
Site 3	-120.5930	50.7942	291	18	241	25
Site 4	-120.5873	50.7989	208	16	21	29
Site 5	-120.5886	50.7997	223	18	22	25
Site 6	-120.5896	50.7995	291	31	227	4
Site 8	-120.5953	50.7988	268	60	44	11
Site 9	-120.5956	50.8011	268	30	22	9
Site 10	-120.5970	50.8014	241	28	8	18
Site 11	-120.5976	50.8018	245	47	28	18
Site 12	-120.5994	50.8023	266	46	332	10
Site 13	-120.6033	50.8024	294	21	232	29
Site 14	-120.6067	50.8030	262	32	307	15
Site 15	-120.6042	50.8046	274	46	299	10
Site 16	-120.6029	50.8040	268	17	27	9
Site 17	-120.6032	50.8034	238	14	12	19
Site 18	-120.6037	50.8033	265	32	27	10
Site 19	-120.6028	50.8032	246	14	34	18
Site 21	-120.5898	50.7920	294	33	237	19
Site 22	-120.5899	50.7913	232	10	10	21
Site 23	-120.5895	50.7989	232	19	41	24
Base Station	-120.6058	50.8008	298	68	216	11
Fuel Moisture 1	-120.5925	50.7984	237	18	47	24
Fuel Moisture 2	-120.5972	50.7990	303	52	207	15

Chapter 3

Spatial variability of near-surface temperature and humidity across a heterogeneous forested landscape

3.1 Introduction

Near-surface atmospheric conditions drive fuel drying rates (Cohen and Deeming, 1985; Van Wagner, 1987) and can vary significantly at a range of scales within a heterogeneous forested landscape. Spatial patterns in near-surface conditions can be due to a number of factors including aspect and elevation (Barry, 2008), cold-air pooling (Holden et al., 2011b), patterns in canopy cover due to natural and anthropogenic disturbances (Chen et al., 1999), precipitation, and soil moisture dynamics (Lookingbill and Urban, 2003). Any large fire (>1 km^2) will likely encounter a mosaic of conditions as all of these factors vary at a range of scales, leading to complex patterns in fire behaviour and effects. It is therefore important to understand what are the most important drivers of patterns in near-surface conditions at the scale of large fires (1 km^2 to 100 km^2), how weather conditions enhance or diminish their effects, and how the impact of elevation, aspect, cold-air-pooling,

canopy cover, precipitation, and soil moisture interact.

Relative humidity is often taken to be the master variable that determines fuel moisture (Viney, 1991; Matthews, 2013). Fuel moisture is primarily driven by adsorption and desorption, especially at lower moisture levels. These sorption processes are constantly moving fuel towards some equilibrium moisture content, which is the moisture level the fuel would obtain if left to come into equilibrium with some constant atmospheric condition. By analysing the thermodynamics of sorption, Nelson (1984) demonstrated that this equilibrium moisture content is directly related to relative humidity. This dependence on relative humidity is an important distinction that sets sorption apart from evaporation and condensation, which are more strongly related to humidity deficits: vapour pressure deficit or vapour density deficit (Oke, 1990). Consequently, relative humidity will be the primary focus of this study. However, variability in relative humidity is, to a large extent, driven by variability in temperature, particularly at the daily time scale where vapour pressure is less variable. Temperature also has a direct but secondary impact on fuel moisture (Viney, 1991). Temperature will therefore be included in this analysis primarily because it provides insight into the observed trends in relative humidity. Due to its direct impact on relative humidity, absolute humidity will be examined here as well using vapour pressure.

The relative influence of canopy cover and radiation load on near-surface conditions will be examined in this study. Canopy cover and radiation load also merit study due to possible interactions (Nyman et al., 2015b). The influence of aspect is likely diminished below dense canopies, and canopy cover may not be as important on very cool terrain facets where radiation levels are already low.

In general, temperatures increase with increasing radiation load (Geiger, 1965; Barry, 2008). Within open sites there is a positive linear relationship between radiation load and surface temperatures (Chung and Yun, 2004; Vercauteren et al., 2013) (unless otherwise stated, the literature reviewed here examines mid-latitude temperate forests). This influence of solar radiation is seen primarily during the day (Bolstad et al., 1998; Lookingbill and Urban, 2003; Dingman et al., 2013). This influence of aspect is strongest during winter months when lower sun angles lead to larger spatial variability in radiation load (Smith, 2002; Dobrowski et al., 2009), and is reduced during cloudy conditions (Dobrowski, 2011; Suggitt et al.,

2011). Dingman et al. (2013) found that the impact of radiation load on temperature increased closer to the ground.

There is little evidence in the literature of any significant impact of aspect on absolute humidity. In many cases the dewpoint temperature is assumed to equal the daily minimum temperature (e.g., Thornton et al. 1997). Given the lack of variability in nocturnal temperatures across different terrain facets, this approach implicitly assumes that there is no influence of aspect on absolute humidity. Changes in relative humidity with aspect are therefore driven largely via its impact on temperature. For instance, given constant absolute humidity, one would expect that daytime minimum relative humidity would be lower on warmer slopes. Indeed, Holden and Jolly (2011) found that, averaged over the fire season, daytime relative humidity levels were lowest on south-west facing slopes.

Canopy cover also has a significant impact on forest floor conditions. Overall, a forest canopy acts to reduce diurnal variability in temperature by reducing incoming solar radiation and nocturnal radiative cooling (Chen et al., 1999). Stathers (1989) found that the probability of seedling frost damage was reduced below dense canopies. Because of counteracting effects of longwave cooling and solar heating, canopy cover has less impact on daily mean temperatures. Canopy influence is most strongly felt near the ground (Whitehead et al., 2006; Suggitt et al., 2011), during summer months due to increased sun angles (Suggitt et al., 2011; Smith, 2002), and during fair weather conditions (Chen et al., 1993). Working in New South Wales, Australia, Ashcroft and Gollan (2011) demonstrated that canopy cover is more important than both elevation and distance to the coast in determining a site's extreme temperatures. However, this influence is only seen at very high canopy densities. An opposite result was obtained by Vanwalleghem and Meentemeyer (2009) where stand density played only a minor role in determining the spatial variability of temperature at monthly, daily, and sub-daily time scales.

As with aspect, the influence of canopy cover on relative humidity is partly driven by temperature variability. Compared to open sites, cooler daytime conditions below dense canopies lead to higher relative humidity while relative humidity is lower at night when nocturnal cooling is reduced (Chen et al., 1993; Renaud et al., 2011). However, this effect is more modest and less consistent than for temperature. Meyer et al. (2001), Whitehead et al. (2006), and Brooks and Kyker-

Snowman (2008) all found little to no impact of canopy cover on relative humidity differences, while Latif and Blackburn (2010) found lower nocturnal relative humidity within natural treefall gaps. Chen et al. (1993) found that absolute humidity within a forested site was higher during the day and lower during the night as compared to an open site, suggesting that some of the variability in relative humidity was due to changes in absolute humidity. Again, this is not a robust result as Valigura and Messina (1994) found no real impact of canopy cover on absolute humidity.

Fridley (2009) and Dobrowski (2011) demonstrated that relatively moist soils can temper the diurnal range of near-surface temperature due to increased thermal inertia. These results are echoed by Ashcroft and Gollan (2013a), who found that canopy cover only gains importance as a factor for near-surface conditions during drier situations.

The above literature leaves room for further research aimed at a specific goal of this thesis: the quantification of spatial variability in near-surface conditions at the landscape scale, with an emphasis on humidity and fuel moisture. For instance, many of the above mentioned studies have focused on screen-level measurements. However, conditions can change significantly within the first few metres of the atmosphere (Oke, 1990). Both Dingman et al. (2013) and Suggitt et al. (2011) demonstrated that the landscape-scale variability in temperature seen near the surface was largely absent at heights above 1.5 m. Consequently, since surface fuel moisture is driven by conditions at the forest floor, results based on screen-level measurements may be misleading. Another gap in the literature is that most topoclimatology studies focus on large ($>$100 km^2) areas and elevation gradients, while a spreading fire interacts with the mosaic of terrain, fuels, and moisture at a smaller scale of around 1 km^2. As well, while the literature focuses on temperature, fuel moisture is primarily driven by relative humidity, which can have different spatial patterns and driving factors than temperature. In addition, there has been little focus on the impact of weather events on spatial patterns. In most cases the focus has been on long-term or monthly averages, which removes the impact of shorter-term weather variability that drives extreme fire weather conditions.

Finally, few studies have attempted a focused and systematic analysis of the relative impact of aspect and canopy cover or their interaction. Vanwalleghem and

Meentemeyer (2009) found that the spatial pattern of temperature across a 274 km^2 study area was more closely related to stand structure than radiation load at monthly time scales, while the opposite was true at daily time scales. However, these were just two of a number of different explanatory variables examined. Suggitt et al. (2011) found that the monthly mean temperature differences between south and north-facing slopes were similar to the differences between open and forested sites, although these results were from two different study regions. Zou et al. (2007) measured shortwave radiation at sites with different combinations of aspect, slope, and canopy cover. The results suggest an interaction between radiation load and canopy cover during the summer. The impact of aspect on below-canopy solar radiation was muted under dense canopies, and canopy cover had a larger impact on south aspects compared to north aspects.

Given the gaps in the literature and the goals of this thesis, this chapter will address the following research questions:

1. How much variability is seen in near-surface temperature and humidity at the landscape scale across a heterogeneous forested environment with complex terrain?

2. How do weather conditions act to either enhance or diminish this spatial variability in near-surface temperature and humidity?

3. What is the relative influence of radiation load and canopy cover on spatial patterns in near-surface temperature and humidity, and do these two factors interact?

The analysis will be guided by the following specific hypotheses that are based on results from the literature and preliminary analysis of the field data:

1. Spatial variability in near-surface conditions is enhanced during fair-weather, dry conditions.

2. canopy cover and radiation load have an interacting influence on spatial patterns of near-surface temperature and relative humidity.

3. canopy cover and radiation load are better predictors of spatial patterns in near-surface temperature than relative humidity.

27

This chapter begins with a description of the analysis methods in Section 3.2. Results presented in Section 3.3 include quantification of the variability of near-surface humidity and temperature (Section 3.3.1) and analysis of the relative influences of radiation load and canopy cover on these near-surface conditions (Section 3.3.2). This is followed by a discussion of results in Section 3.4 and conclusions in Section 3.5

3.2 Methods

Acquisition and processing of field data are described in Chapter 2. The first step in the analysis for the current chapter involved calculating the daily mean, maximum, and minimum values for relative humidity, vapour pressure, and temperature at each of the 24 sites described in Chapter 2.2. These data were originally measured at 30 minute intervals. Spatial variability was quantified by calculating daily site-specific anomalies from the daily intersite mean for each of the variables. The daily anomaly time-series of these nine variables formed the core of this chapter's analysis. For the purpose of calculating the maximum and minimum values, the day was taken to start at sunrise rather than midnight. That is, the hours before sunrise are assumed to belong to the previous day. During a particularly cold night, the temperature and humidity at midnight could be more extreme than the previous morning's conditions. In this case, ending days at midnight would lead to a double counting of these extreme conditions for both days. Ending the day at sunrise avoids this truncation issue.

Due to the strong diurnal cycles in temperature and relative humidity, maximum and minimum values were chosen as indicators of daytime and nocturnal extremes. Daytime extremes are important as they provide an indication of how severe the afternoon fire weather will become. It is often during the afternoon that the most intense fire behaviour occurs. The nocturnal extremes are important because they indicate the extent to which fuel moisture can increase, or recharge, during the night. The daily mean values were highlighted as they indicate the average seasonal trends in relative humidity and temperature, which play a large role in determining the seasonal trends in fuel moisture, especially for the larger fuel elements.

To address the first two research questions, anomalies were compared across sites to identify the variables and periods of the day that exhibited the widest spread across stations. This spread was quantified by calculating, for each day and for each of the nine variables, both the standard deviation and the maximum range (that is, the difference between the warmest and coolest site, or the wettest and driest site) of the variables. These daily standard deviations and ranges were averaged for each month and for all days with and without rain. To specifically address the second research objective, daily time series of these ranges were compared to time series of weather variables measured at the Base Station that could potentially be influencing temporal changes in the the spread of conditions across sites.

To address the third research question, longer term averages of the anomalies were calculated over the entire field season for days with and without rain, and for each month, resulting in seven averaging periods (five months + all rain days + all dry days). For each combination of the nine variables and the seven averaging periods, optimal linear regression models were developed using canopy gap fraction, radiation load, and their interaction as possible predictors of these average anomalies. Collinearity between predictors was assessed by calculating variance inflation factors (VIF). As well, exploratory analysis using Cook's distance suggested that Site 22 was a significant outlier during the night time and was therefore excluded from the following analysis. Consequently, these 23 data points were used to fit the models. An examination of bi-plots between predictors and predictands did not uncover any obvious non-linear relationships. Therefore, no transformations were deemed necessary.

The optimal models were selected using the following stepwise approach. First, single predictor models were developed for both explanatory variables. Second, starting with the strongest single predictor model, analysis of variance was used to determine if the addition of the second predictor, and then an interaction term, significantly improved the model. That is, for each additional term, the null hypothesis that the term's regression coefficient was equal to zero was tested. The term was added to the optimal model only if the null hypothesis was rejected at the 95% confidence level.

In order to compare the relative influence of canopy gap fraction and radiation load, the predictors and predictands were first normalized by subtracting the mean

29

and dividing by the standard deviations. In this way the relative sizes of the estimated regression coefficients indicated the relative influence of each predictor on the spatial patterns in near-surface conditions.

Throughout this analysis two sites were chosen to represent end-members of the sample. Site 4 was located on a steep north-facing slope with a closed-canopy. The Fuel Moisture 2 site was in an open location on a south-facing slope. These sites are highlighted in the results section. In addition, Site 22 was identified as a significant outlier due to its unusual nocturnal conditions relative to other similarly placed sites. This site was also singled out in the following results.

3.3   Results

3.3.1   Quantifying variability in near-surface humidity and temperature and the impact of weather conditions

The seasonal trends in near-surface conditions are presented in Figure 3.1. There was a warming trend through May, June, and into July with cooling through August and September. There was also an unseasonally cool period in the second half of July centred around a significant precipitation event. Absolute humidity remained relatively steady during the first three months of the season. In August there was a substantial increase in vapour pressure, which was followed by a drying trend into September. Relative humidity generally decreased through May, June, and July. Two low-humidity periods occurred in mid-July and late July / early August. The last dry period ended with the increase in vapour pressure. In general, precipitation was associated with high relative humidity values across all sites.

Figure 3.2 shows 29 days of humidity and temperature data for all 24 sites at a resolution of 30 minutes. Both relative humidity and temperature had large diurnal cycles while for vapour pressure the diurnal signal was weaker. The largest amount of spatial variability occurred during the afternoon and early morning. Nocturnal variability in relative humidity across sites was particularly large. At times the differences between sites were over 40%. For all three variables the spatial variability among sites tended to increase during warm, dry periods with no rain, while precipitation acted to collapse the spread among stations. Fuel Moisture 2, which
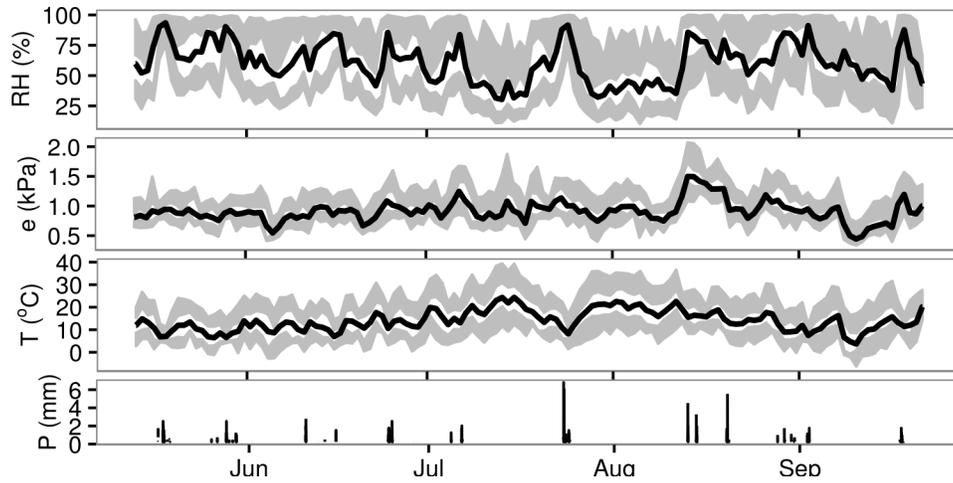
Figure 3.1: Daily relative humidity, vapour pressure, and temperature observations. The *thick black lines* are the daily intersite means. The *grey ribbons* show the intersite range of the daily minimum and maximum values. Hourly precipitation observations at the Base Station are presented in *bottom plot*.

had little canopy cover, was consistently warmer during the day and cooler at night compared to the closed canopy Site 4. There was no consistent difference between sites. The Fuel Moisture 2 site also saw larger diurnal cycles in relative humidity with wetter nights and drier afternoons. Compared to the similarly placed Site 4, the diurnal cycle was much larger at Site 22 due to its cool and wet nocturnal conditions. Indeed, the nocturnal conditions at Site 4 were similar to those at the open Fuel Moisture 2 site.
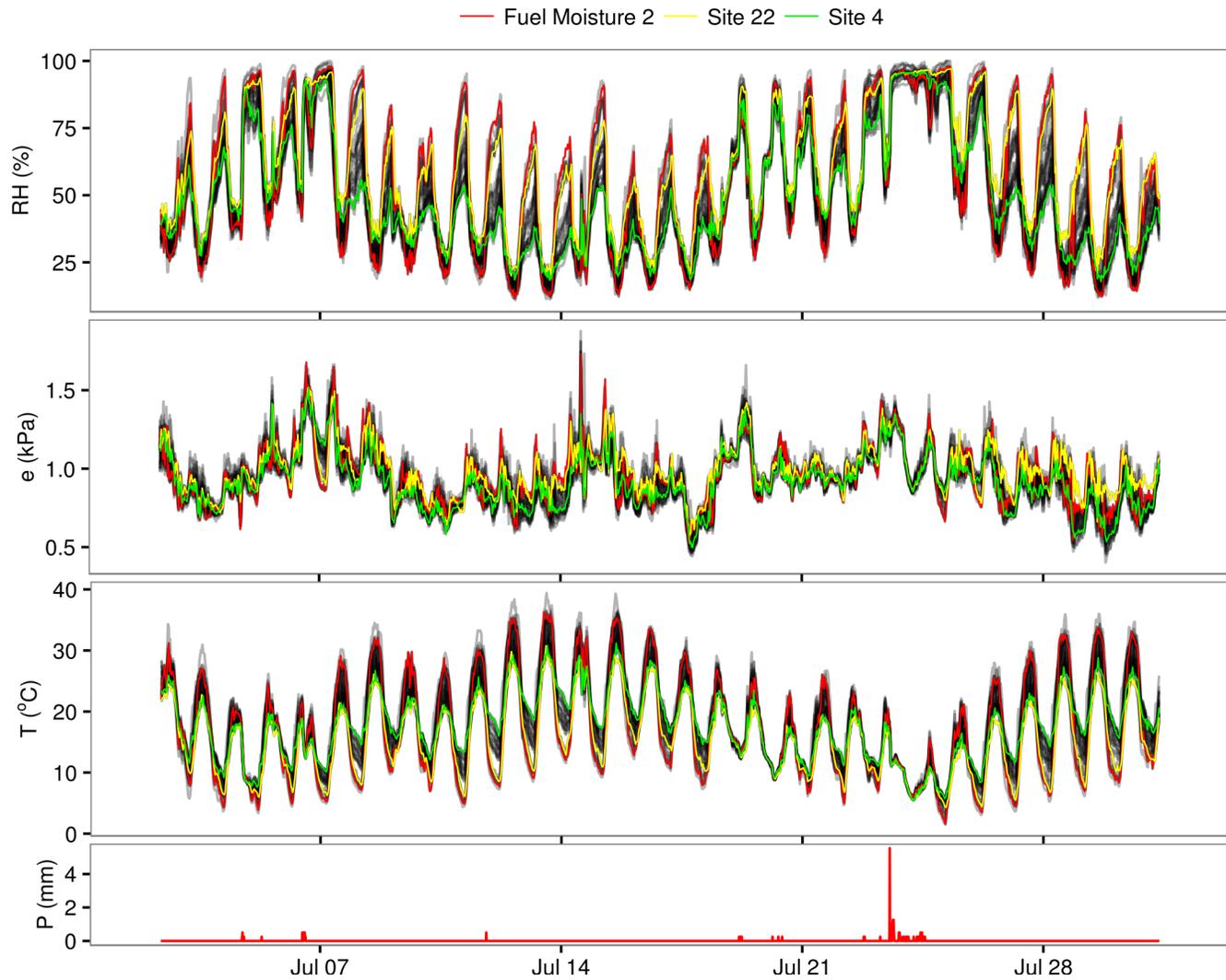
Figure 3.2: A sample of hourly relative humidity, vapour pressure, temperature, and precipitation (*bottom*) observations for all sites (*grey lines*). Fuel Moisture 2, Site 22, and Site 4 are highlighted.

The spatial variability in temperature and humidity is highlighted in Figure 3.3. A summary of these anomalies is presented in Table 3.1. In general, variability increased over the first three months of the season. The daily mean values saw less spread across sites while nocturnal conditions were generally the most variable, especially for relative humidity. Other than minimum relative humidity, precipitation acted to reduce the spread across stations.

Figure 3.3 also demonstrates the consistent warm/dry daytime conditions and cool/wet nocturnal conditions at the Fuel Moisture 2 site seen in Figure 3.2. It further demonstrates that the anomalies in daytime conditions (Figures 3.3B and D) were relatively steady throughout the field season, regardless of weather conditions. This consistent variability is in contrast to the nocturnal conditions (Figures 3.3A and E), which exhibited obvious shifts between periods of low and high variability. Figure 3.3 demonstrates that the role of precipitation in reducing spatial variability was strongest at night.

Anomalies in mean vapour pressure (Figure 3.3C) were less consistent than for relative humidity and temperature. However, daily mean vapour pressure was generally lower at Site 4 while the last half of the season saw a large moist anomaly at Site 22. July exhibited two periods of more significant spread in vapour pressure which coincided with similar large ranges in the nocturnal relative humidity and temperature.

Even though the outlying Site 22 was similar to Site 4 in its placement (north-facing closed-canopy), it was generally much cooler with higher relative humidity at night. Site 22 also consistently had the lowest temperature and highest relative humidity of all sites during the day. Absolute humidity at Site 22 did not show such strong anomalies, although it exhibited relatively high vapour pressure during August, July, and September.

The spread in near-surface conditions and the influence of rain events are highlighted in Figure 3.4. The impact of precipitation is easily identified here. For most variables, rain events acted to reduce the spatial variability, reflecting the results in Table 3.1. The impact of precipitation is most evident during the night (Figures 3.4A and E) when rain created substantial reductions in the spatial range of maximum relative humidity and minimum temperature. A similar but less severe pattern is seen in the maximum temperatures (Figure 3.4D). Precipitation had the opposite
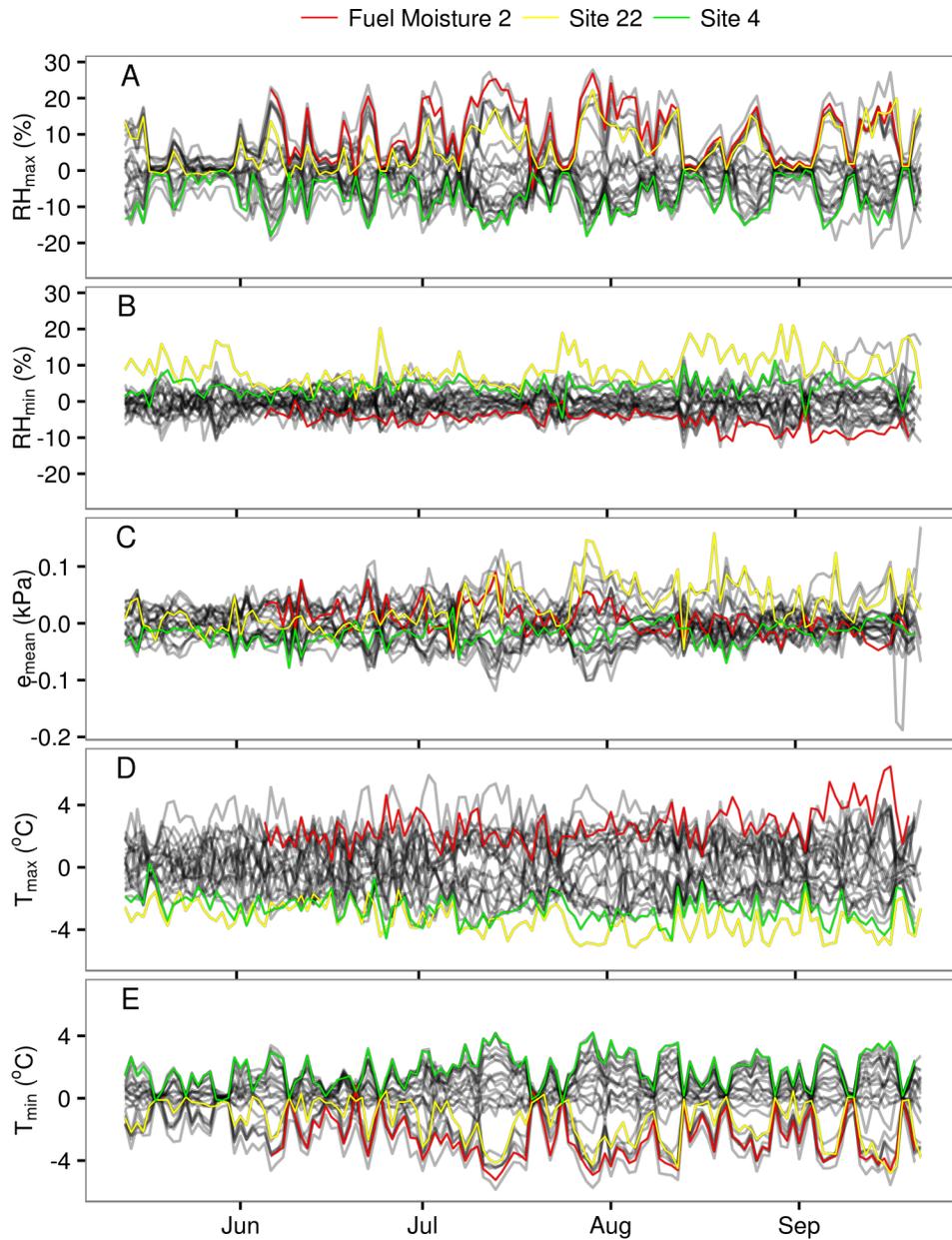
Figure 3.3: Daily anomalies from the intersite mean for maximum and minimum relative humidity and temperature, and daily mean vapour pressure at all sites (*grey lines*). As in Figure 3.2, Fuel Moisture 2, Site 22, and Site 4 are highlighted.

Table 3.1: Daily standard deviation (SD) and maximum range (Range) of temperature and humidity variables averaged across each month and across all days with and without rain.

Period	RH$_{min}$ (%) SD	Range	T$_{max}$ (°C) SD	Range	RH$_{max}$ (%) SD	Range	T$_{min}$ (°C) SD	Range	RH$_{mean}$ (%) SD	Range	T$_{mean}$ (°C) SD	Range
May	3.9	16.1	1.5	5.6	4.2	15.5	0.9	3.2	2.8	11.3	0.5	2.2
June	3.3	13.0	1.7	6.0	6.4	22.5	1.3	4.5	3.5	12.2	0.5	2.3
July	3.4	14.0	2.1	7.6	8.5	28.6	1.9	6.3	3.9	14.4	0.7	3.4
Aug.	4.5	19.3	2.0	6.9	6.2	21.4	1.6	5.2	3.6	14.5	0.6	2.9
Sept.	5.7	23.0	2.0	7.5	7.8	28.6	1.8	5.8	5.0	19.8	0.9	3.8
Dry Days	4.0	16.4	2.0	7.4	8.1	27.4	1.8	5.8	4.1	15.5	0.7	3.4
Rain Days	4.3	17.6	1.5	5.4	3.9	15.1	1.1	3.7	3.0	11.8	0.4	2.0

impact on minimum relative humidity, which generally became more variable after significant rain (Figure 3.4B). Examination of Figure 3.3B demonstrates that these significant increases in the total range were primarily due to the outlying Site 22. However, post-rain increases are seen to a certain degree in the standard deviation as well, suggesting that this effect was felt broadly across all sites. The impact of precipitation on vapour pressure (Figure 3.4C) is less clear; rain acted to both increase and decrease variability while in other cases there did not seem to be any impact.

The influence of weather conditions on the spread across stations is further demonstrated in Figure 3.5 where the daily standard deviation of maximum and minimum relative humidity and temperature (the grey lines in Figures 3.4A, B, D, and E) are plotted against days since rain, solar radiation (K_d), daily precipitation amounts, and daily mean wind speed. Again, the impact of precipitation is clear. In addition, the left column of Figure 3.5 demonstrates that the homogenising impact of precipitation on nocturnal conditions and daytime temperatures was felt across the landscape for a number of days after precipitation ended. However, as seen in Figure 3.4B and Table 3.1, precipitation had the opposite impact on minimum relative humidity where the spread across stations was highest during and immediately after precipitation.

Increased solar radiation was associated with increased variability for all but minimum relative humidity, for which there was a small negative relationship (middle column). The relationship was strongest for daytime temperatures (bottom
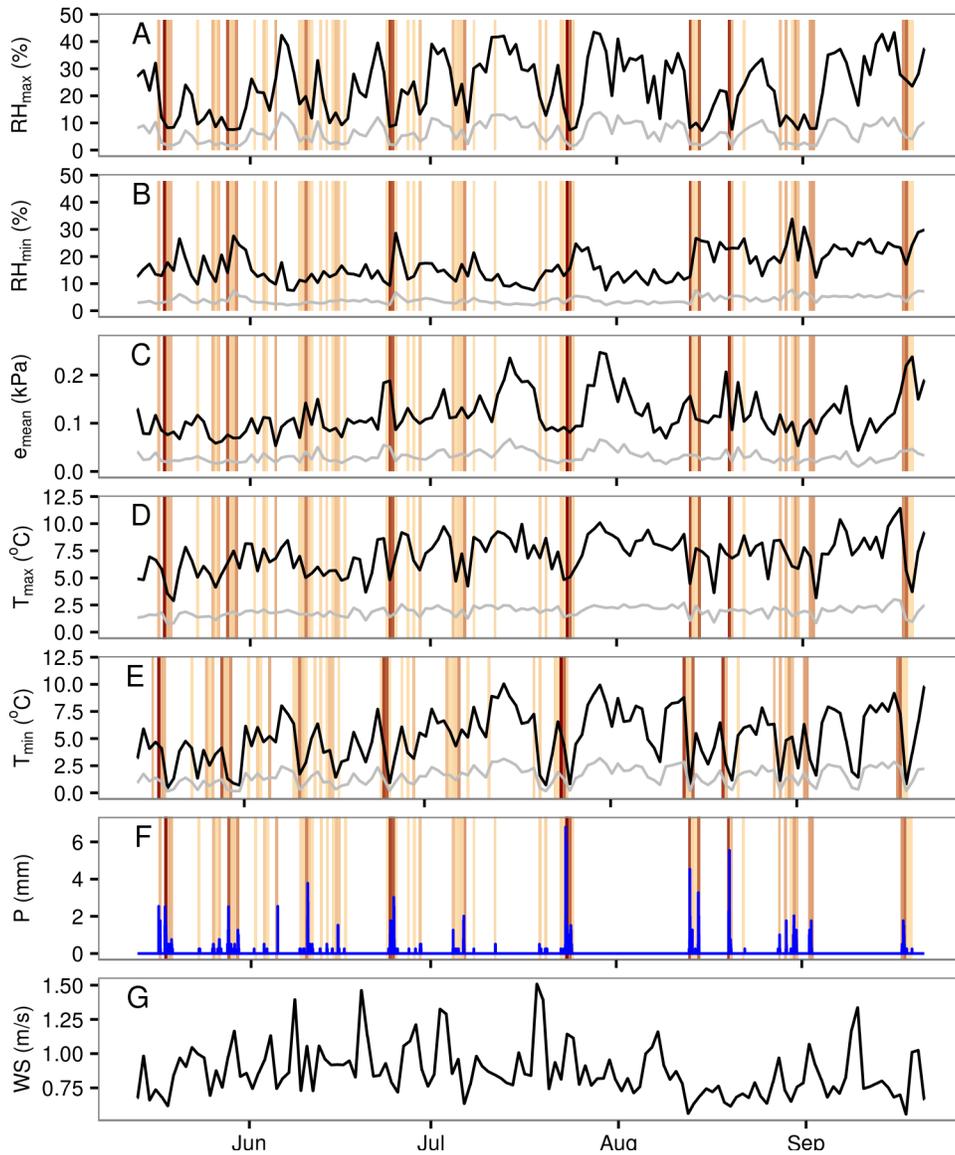
Figure 3.4: Range (*black line*) and standard deviation (*grey line*) of daily maximum and minimum relative humidity (*A, B*), mean vapour pressure (*C*), and maximum and minimum temperature (*D, E*). Hourly precipitation (*F*), and daily average wind speed (*G*) are also provided. Precipitation amounts are also shown with *maroon shading*.

36
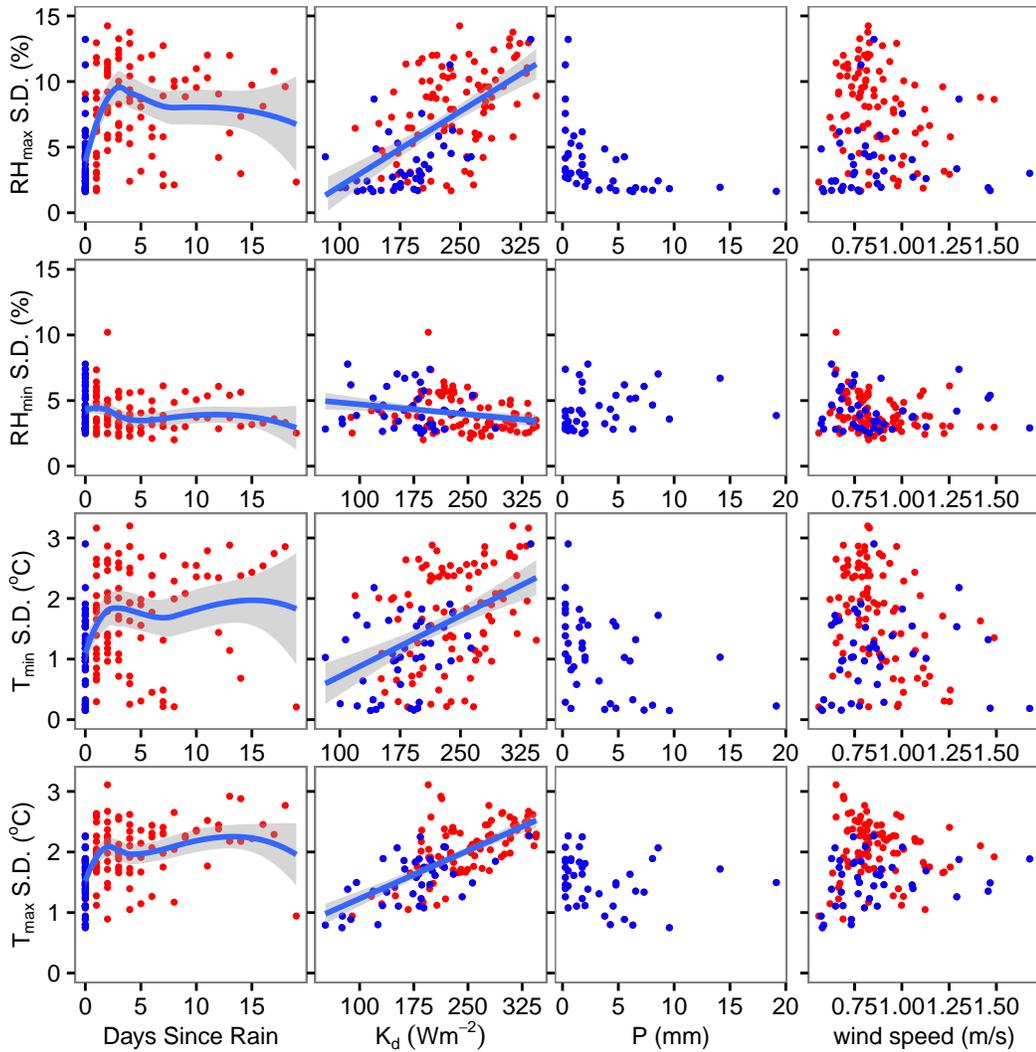
Figure 3.5: Daily standard deviation of maximum and minimum humidity (*top two rows*) and minimum and maximum temperature (*bottom two rows*) plotted against days since rain (*first column*), solar radiation (*second column*), daily precipitation (*third column*), and mean wind speed (*fourth column*). Days are divided into days with rain (*blue points*) and without (*red points*). For maximum humidity and minimum temperature solar radiation is calculated as a running average of the current and following days. Loess curves with a two-degree polynomial are fit to the relations with days since rain while linear regressions are fit to the solar radiation plots (*solid blue lines*) The 95% confidence intervals for these fits are included (*grey ribbons*).

row). For the nocturnal variables (top row and third row) solar radiation is calculated as an average of the current day and the following day and can be thought of as a metric of "sky clearness" and radiative cooling at night. Consequently, the physical link to near-surface variability is less direct than for maximum temperature, for which solar radiation is for the current day only, leading to decreased correlations in the nocturnal case. The spread in nocturnal conditions is reduced during periods with heavy precipitation or high wind speeds, especially for nocturnal conditions.

3.3.2 Quantifying the impact of radiation load and canopy cover

The correlation between radiation load and canopy cover ranged from 0.44 to 0.56, depending on the averaging period chosen. VIFs (Montgomery and Peck, 1992) for all averaging periods remained below 2 in all cases, suggesting that collinearity is not a major concern (Zuur et al., 2007).

The results of the model selection procedure are shown in Table 3.2. In all cases, an interaction term did not improve the model at the 95% confidence level and is therefore not included in the following analysis. For the sake of brevity, results are presented only for June, September, and the full season. The relationship between predictands and predictors is generally what would be expected. Cooler conditions with higher relative humidity are found at north-facing, closed-canopy sites during the day and at open canopy sites during the night. Notably, there is a relatively strong positive relationship between maximum vapour pressure and canopy gap fraction; higher vapour pressure is generally found at open sites.

Overall, canopy gap fraction was the strongest predictor. That is, for almost all cases, canopy gap fraction explained more of the spatial pattern in near-surface conditions and had larger or comparable standardized regression coefficients than radiation load. However, it is important to note that radiation load was a strong predictor of minimum relative humidity. On average, the temperature models were the most skillfull (assessed using the coefficient of determination), while the vapour pressure models performed the poorest. Models of daily mean values were generally poorer than for maximum and minimum values. Indeed, the two variables had no significant explanatory power (at the 5% confidence level) for average temperatures during periods of rain.

The models for "All Dry Days" summarized in Table 3.2 are shown graphically in Figure 3.6. In general, there was a wider range in nocturnal conditions than during the day, which is consistent with Figure 3.3. canopy cover had a significant effect on both daytime and nocturnal conditions. Moreover, compared to radiation load the influence of canopy cover was stronger for daytime temperatures and approximately equal for daytime relative humidity. The abnormal nocturnal conditions seen at Site 22 (which was not included in the regression analysis) are clear from this figure. Compared to similar sites surrounding it within the parameter space, it was cooler and had higher relative humidity levels.

3.4 Discussion

There were a number of significant findings from this study. Firstly, near-surface conditions were generally more heterogeneous during dry, clear-sky conditions, and spatial variability was reduced during, and for a few days following, precipitation. In particular, spatial variability in daytime relative humidity was low and relatively unaffected by weather conditions. Secondly, while canopy cover had weak drying effect on daytime humidity due to solar heating, canopy cover also had a stronger impact on nocturnal relative humidity, which was higher at open sites due to longwave cooling. Consequently, open sites experienced higher daily mean relative humidity.

3.4.1 Quantifying variability in near-surface humidity and temperature and the impact of weather conditions

Significant variability was seen across the relatively small study area, especially at night. For instance, the daily ranges in both minimum and maximum temperatures were often comparable to over a kilometre of elevation change, assuming a typical lapse rate of ca. $6°C$ per kilometre. In some cases, nocturnal relative humidity was close to 100% at open sites but around 50% at closed-canopy sites. Spatial contrasts in daytime relative humidity were less pronounced. Some of the above results reflect similar findings in the literature. For instance, the presence of a canopy significantly reduced the diurnal variability of relative humidity and temperature (Chen et al., 1993), and higher temperatures were found on south-facing
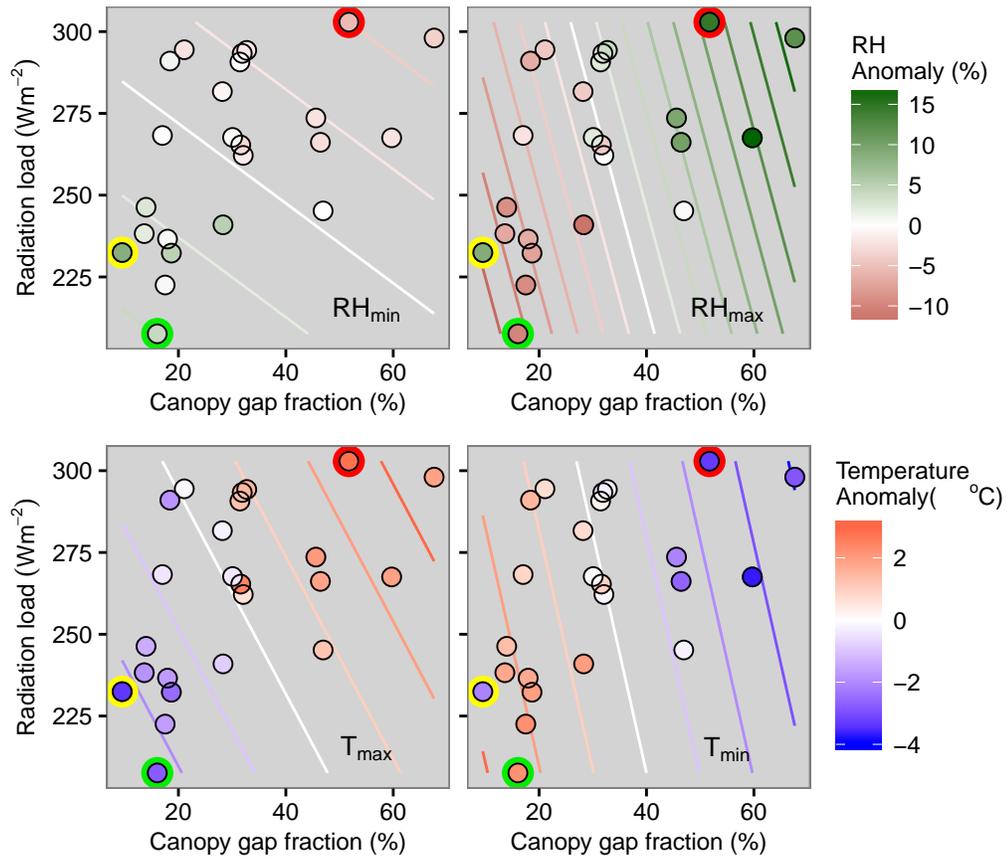
Figure 3.6: Average anomalies of daily maximum and minimum relative humidity (*top row*) and temperature (*bottom row*) for all non-rain days plotted on the radiation load - canopy gap fraction parameter space. The *right column* shows daytime conditions (maximum temperature and minimum relative humidity), while the *left column* shows night time conditions (minimum temperature and maximum relative humidity). The anomaly values predicted by the linear regression models summarized in rows 1-4 of Table 3.2 are indicated by the *contour lines*. Specific sites are highlighted as in Figures 3.3 and 3.2: Site 22 (*yellow*), Fuel Moisture 2 (*red*), and Site 4 (*green*).

slopes (Barry, 2008).

As was hypothesized, variability was generally enhanced during dry, clear-sky conditions, although this study revealed further details and caveats that expand on this relatively simple prediction. For instance, the impact of precipitation is strongest for nocturnal relative humidity and temperature. As well, this homogenizing influence of precipitation persisted for a number of days following rain. It is likely that increased moisture following precipitation led to increased thermal inertia of near-surface conditions (Fridley, 2009; Dobrowski, 2011), which, in turn, reduced heterogeneity across the landscape. As well, variability in daytime minimum relative humidity increased during and immediately after rainfall and was negatively related to solar radiation, supporting what was seen in Figure 3.4.

It is likely that some of the fluctuation between high and low variability of maximum relative humidity is due to the 100% saturation ceiling. That is, precipitation followed by nocturnal cooling will bring many of the sites to saturation, decreasing variability substantially. This saturation effect explains the strong relationship between precipitation amount and the spread in maximum humidity seen in Figure 3.5.

Site 22 is an interesting outlier in this dataset. Even though it had the densest canopy of any site, its nocturnal conditions were similar to that of an open site: cool with high relative humidity. It also saw a substantial cold/wet daytime anomaly compared to all other sites. The sensor in this case was located within 15 m of a draw that remained wet throughout the season. It is likely that an elevated water table at the site led to enhanced near-surface moisture, leading, in turn, to elevated relative humidity compared to other closed-canopy locations. Indeed, during the last half of the season when the rest of the sites dried out, this extra source of moisture kept vapour pressure anomalously high at Site 22 (see Figure 3.3C), explaining the elevated relative humidity throughout the day. The cold anomaly could be attributed to evaporative cooling that would occur as drier surrounding air was advected through the site. The cold anomaly could also be partially explained by the fact that groundwater is typically cooler than summer air temperatures. Another potential explanation is that cool air was draining downslope from an open area located upslope of the site. However, because this cold advection would have only occurred during clear nights, it cannot explain the consistent cold anomaly

41

present during all times of day and weather conditions.

3.4.2 Quantifying the impact of radiation load and canopy cover

In most cases, canopy gap fraction and radiation load were able to account for a large amount of the spatial variability of near-surface conditions. The fitted relations were stronger during the night than during the day. The best results were achieved for nocturnal temperature during dry conditions, for which the model explained up to 85% of the spatial variability. Canopy gap fraction emerged as the most important predictor, even for daytime temperature and daytime relative humidity during days with rain. Even for variables with radiation load as the strongest single predictor, the standardized regression coefficient values where comparable between the two predictors. This suggests that the amount of solar radiation being absorbed at a particular site is more dependent on canopy interception than the solar angle relative to the slope of the forest floor. Considering that the impact of radiation load increases closer to the forest floor (Dingman et al., 2013), it is also possible that skin temperatures of the forest floor would be more strongly influenced by radiation load, and that this impact is diminished at the 30.5 cm measuring height used here.

It was hypothesized that canopy cover and radiation load would be stronger predictors of temperature than humidity. This prediction is borne out in the results where the temperature models were the most skillfull, followed by relative humidity and then vapour pressure. It is possible that variability in humidity is more dependent on site characteristics such as the amount and type of understory vegetation and the resulting rates of transpiration. Although an effort was made to maintain consistent understory vegetation across sites, the variability that did occur may have been enough to increase unexplained variability in relative humidity.

The analysis also revealed higher vapour pressure at more open sites, especially for mean and maximum vapour pressure. This result is slightly counter-intuitive, as one might expect that more open canopies would allow for greater mixing with drier air aloft, leading to a negative relationship. However, it is also possible that as canopy cover decreases, the amount of moisture removed from the forest floor via transpiration within the overstory would also decrease. It is unlikely that increased

precipitation at open sites led to increased vapour pressure as these results demonstrated that precipitation had little impact on vapour pressure. It may also be the case that heating of the Logtag sensors by solar radiation led to a positive bias in temperature and vapour pressure at open sites. However, if this radiation influence were present, one would expect a bias at higher temperatures. Yet, following the removal of temperature biases in the Logtag sensors (see Appendix A), no such bias was apparent.

An important result here is the homogeneity of daytime humidity, which was relatively constant regardless of weather conditions. For instance, in contrast to the other variables, precipitation did not act to decrease the variability in minimum relative humidity across sites while solar radiation had a small negative impact (see Figure 3.5). The positive relationship between canopy gap fraction and vapour pressure may explain this reduced spatial variability in daytime relative humidity and its weak relationship with canopy gap fraction. That is, higher levels of vapour pressure at open sites were balanced by higher daytime temperatures, resulting in less variability in minimum relative humidity across sites.

It is significant that daily mean relative humidity and temperature are generally less variable across sites and were more poorly predicted than minimum and maximum values. Indeed, during periods of rain the spatial pattern in daily mean temperatures was not related to either explanatory variable. Chen et al. (1999) suggested that due to the counteracting impact of canopy cover on daytime versus nocturnal conditions, average conditions will likely be less related to canopy cover and will therefore be less spatially variable.

The lack of interaction between the two predictors is also notable. It was originally hypothesized that increased canopy cover would diminish the impact of radiation load on near-surface conditions, while canopy cover would be less important on cool north-facing aspects where the radiation load is already low. However, no evidence for this was found in this study, although it is possible that a larger dataset would produce significant interaction terms.

3.4.3 Implications for fuel moisture

These findings have a number of implications for fuel moisture. With respect to relative humidity, which is the primary driver of fuel moisture, the spread across sites is smaller during the day than at night. Therefore, in the afternoon, when fires are often the most active, spatial variability in fuel moisture may be small. As well, relative humidity patterns across the landscape are not strongly dependent on weather conditions, suggesting that the daytime spatial variability in drying potential may not increase during particularly dry periods.

Air temperature does have a secondary impact on fuel moisture. However, these results suggest that the nocturnal and daytime variability of near-surface temperature (both of which are driven primarily by canopy cover) are of equal magnitude but opposite sign. This balance between daytime and nocturnal conditions means that there would be no persistent temperature anomaly that could drive a significant divergence in fuel moisture across sites.

This behaviour is in contrast to that of relative humidity, which varied more at night than during the day, leading to the positive relationship between canopy gap fraction and daily mean relative humidity seen in Table 3.2. Therefore, as will be hypothesized in Chapter 5, nocturnal moisture recharge may overwhelm the daytime drying at the open sites, leading to higher fuel moisture at open sites.

Being quicker to respond, the smaller fuel elements will likely follow this diel cycle of relative humidity: increased moisture and spatial variability at night followed by drier, less variable fuel moisture during the day. For the larger fuel elements with their longer response times, the impact of increased daily mean relative humidity at open sites, integrated over time, may actually lead to higher fuel moisture at open sites. In any case, canopy cover, being a stronger predictor of relative humidity anomalies than radiation load, will, in turn, be the primary driver of spatial patterns in fuel moisture.

3.5 Conclusions

The largest variability in near-surface conditions was seen at night, while daily mean values were less variable than both daily minimum and maximum values. At night, sites with dense canopies remained warmer than open sites due to down-

welling longwave radiation. Consequently, there were some instances in which open sites were near or at saturation while relative humidity was around 50% at closed-canopy sites. During the day, cool, north-facing slopes were often significantly cooler than nearby warm south-facing slopes. For temperature and nocturnal relative humidity, precipitation acted to reduce variability across the landscape while variability increased during clear sky conditions. However, radiation and precipitation had the opposite impact on daytime relative humidity variability. The homogenizing influence of precipitation persisted for a number of days after rain ceased, and the impact of weather conditions on spatial variability was largest at night. One site, located next to a draw that remained wet throughout the season, recorded anomalously wet, cool conditions relative to other similarly placed sites. As other sites dried out over the course of the season, the site's high water table provided a source of moisture, which also led to evaporative cooling.

Together, canopy gap fraction and radiation load predicted up to 85% of the spatial variability in near-surface climate. Patterns in temperature were better predicted than relative humidity, while vapour pressure was poorly predicted. Overall, canopy gap fraction was a better predictor of average near-surface conditions than radiation load. Notably, mean relative humidity was positively correlated with canopy gap fraction during both dry and wet conditions, suggesting that open sites are on average wetter than closed sites, even after periods with no rain.

The results of this study have a number of implications for fuel moisture. Firstly, spatial variability in daytime relative humidity is relatively limited and not strongly impacted by weather conditions, suggesting that afternoon fuel moisture will remain homogenous across the landscape and throughout the fire season. Secondly, because open sites are wetter compared to closed-canopy sites, it is possible that open sites will see higher fuel moisture. Finally, areas where a high water table persists throughout the season will likely have wetter fuels relative to the surroundings.

The implications for fuel moisture will be studied in more detail in Chapters 5 and 6 where the fuel moisture model developed in Chapter 4 will be combined with the above dataset and canopy interception models of precipitation and radiation to generate modelled patterns of fuel moisture across the landscape.

Table 3.2: Results of model selection. Standardized regression coefficients are shown in the Canopy Gap and Rad Load columns. Bold values indicate the predictor with the strongest single variable model as determined by the coefficient of determination. Missing values indicate that the addition of the predictor did not substantially improve the model performance. Standard error of the estimate is provided in the units of the predictor (Temperature: °C, Relative Humidity: %, Vapour Pressure: kPa).

Predictand	Period	Canopy Gap	Rad Load	Adj. R^2	Std. Error
RH_{min}	All Dry Days	-0.39	**-0.56**	0.64	1.66
T_{max}	All Dry Days	**0.64**	0.36	0.74	0.89
RH_{max}	All Dry Days	**0.78**	0.23	0.82	3.50
T_{min}	All Dry Days	**-0.82**	-0.2	0.85	0.72
RH_{mean}	All Dry Days	**0.83**		0.68	1.84
T_{mean}	All Dry Days	**-0.61**		0.34	0.34
e_{min}	All Dry Days				
e_{max}	All Dry Days	**0.74**		0.53	0.03
e_{mean}	All Dry Days	**0.56**		0.28	0.02
RH_{min}	All Rain Days	**-0.59**	-0.43	0.76	1.33
T_{max}	All Rain Days	**0.74**	0.25	0.76	0.64
RH_{max}	All Rain Days	**0.75**		0.54	2.40
T_{min}	All Rain Days	**-0.92**		0.84	0.44
RH_{mean}	All Rain Days	**0.59**		0.32	1.82
T_{mean}	All Rain Days				
e_{min}	All Rain Days	**-0.43**		0.15	0.02
e_{max}	All Rain Days	**0.76**		0.56	0.03
e_{mean}	All Rain Days	**0.52**		0.23	0.02
RH_{min}	June	-0.46	**-0.49**	0.65	1.36
T_{max}	June	**0.81**		0.64	0.88
RH_{max}	June	**0.85**		0.71	3.04
T_{min}	June	**-0.92**		0.85	0.48
RH_{mean}	June	**0.77**		0.57	1.77
T_{mean}	June				
e_{min}	June				
e_{max}	June	**0.83**		0.68	0.03
e_{mean}	June	**0.73**		0.51	0.02
RH_{min}	September		**-0.77**	0.57	2.83
T_{max}	September	**0.56**	0.54	0.85	0.68
RH_{max}	September	**0.84**		0.69	3.83
T_{min}	September	**-0.92**		0.84	0.68
RH_{mean}	September	**0.73**		0.51	2.52
T_{mean}	September	**-0.71**		0.48	0.40
e_{min}	September	**-0.53**		0.25	0.02
e_{max}	September				
e_{mean}	September				

Chapter 4

A model for simulating the moisture content of standardized fuel sticks of various sizes

4.1 Introduction

Dead fuel moisture is an important determinant of wildfire behaviour as it influences a fire's intensity and rate of spread (Rothermel, 1972). Metrics of fuel moisture are at the core of both the Canadian and U.S. fire danger rating systems (Cohen and Deeming, 1985; Van Wagner, 1987). Moisture content of the 1-hour, 10-hour, 100-hour and 1000-hour fuel sizes is a major component of the American National Fire Danger Rating System and is used to estimate, among other things, ignition potential, fireline intensity, flame length, and rate of spread. Given constant environmental conditions, fuel elements are assumed to dry following an exponential decay to some equilibrium moisture constant. The names of the fuel sizes are in reference to the decay constant of these exponential drying curves.

Traditionally, the moisture of the smaller two fuel sizes was estimated by weighing standardized *Pinus ponderosa* (ponderosa pine) dowelling. Recently, automated measurements have become more common in which moisture sensors are integrated directly into the fuel sticks, allowing for remote real-time observations

47

(Nelson, 2000). However, fuel moisture observations are not always available, especially for larger fuel sizes. Simple models were therefore developed within the National Fire Danger Rating System that related fuel moisture to the equilibrium moisture constant by assuming exponential drying curves (Cohen and Deeming, 1985). These models used climatological data from a single study to estimate moisture. Consequently, the diurnal cycle forcing the model is assumed to be constant even though the model is applied across a range of sites and weather conditions.

A more sophisticated process-based model was developed by Nelson (2000), which simulates the moisture content of the fuel sticks at sub-daily resolution (referred to here as the Nelson model). An updated version of the Nelson model is a component of the FlamMap (Finney, 2006) and FARSITE (Finney, 2004) fire modelling tools that are used by a number of fire management agencies to simulate spatial patterns in fuel moisture and fire behaviour. The Nelson Model is also integrated into the USDA Weather Information Management System. Andrews (2014) suggested that the Nelson model be used within the BehavePlus fire modelling system.

The Nelson model simulates the energy and moisture exchange at the surface as well as the transport of moisture and heat within the interior of the stick. Internal moisture transport can occur within the model through the diffusion of water vapour, the diffusion of bound water, or capillary flow. It also includes semi-empirical modelling of rainwater absorption.

The radial and temporal variation of moisture and heat within fuel sticks can be described by a two-dimensional partial differential equation expressed in radial coordinates. In order to simplify the problem, the Nelson model uses a linearised energy budget in which net longwave radiation is estimated as a function of the difference between the stick temperature and the apparent sky temperature. The model assumes two constant apparent sky temperatures, one for the daytime and one for the nighttime. However, the accuracy of the linearised energy budget diminishes when the difference between the fuel temperature and apparent atmospheric temperature increases. Indeed, during periods of high radiation this temperature difference exceeds 30 °C.

Moreover, a linearized energy budget does not allow for variations in downwelling longwave radiation due to canopy coverage or changes in sky conditions

such as cloud cover. Including the impact of the canopy on longwave radiation may be particularly important for simulating the impact of changing canopy cover on the spatial patterns of fuel moisture across forested landscapes. However, because FARSITE and FlamMap use the Nelson model, they are not able to include variations in longwave radiation due to canopy coverage because the Nelson model, as mentioned above, does not have this functionality.

In addition, the transport of moisture between the stick surface and the atmosphere is modelled by assuming that the fuel stick acts as a wet bulb. That is, it is assumed that sensible and latent heat flux are the only components of the energy budget, and all sensible heat is converted to latent heat, driving evaporation. However, if the stick is exposed to direct sunlight, shortwave radiation would dominate the energy budget, and the wet-bulb assumption becomes invalid.

This chapter presents a model for simulating the fuel moisture of standard fuel sticks. The model uses a linear approximation of the internal transport of heat and moisture but solves the energy and moisture budgets numerically, whereas the Nelson model uses a linear form of the energy budget and solves the internal transport equations numerically. By solving the energy and moisture budgets numerically, incoming and outgoing longwave radiation can be modelled directly. This approach allows for the incoming radiation to vary due to both canopy coverage or changing sky conditions. As well, the transport of moisture to and from the surface of the stick, and its corresponding latent heat flux, is calculated using an aerodynamic resistance approach. This approach avoids the assumption made in the Nelson model that the stick acts like a wet-bulb. However, it does require the inclusion of wind speed as an input variable, which is avoided in the Nelson model. With respect to internal transport, the new model divides the stick into two layers and calculates an energy and moisture budget for each layer at every time step.

Moisture observations of fuel sticks are used to calibrate and evaluate the model. Two independent datasets were used: a previous dataset of moisture content of 1-hour, 10-hour, 100-hour, and 1000-hour fuel sticks used to evaluate the Nelson model, and the observations of 10-hour fuel stick moisture content collected at the Base Station and Fuel Moisture 2 site (see Chapter 2). An additional analysis will examine the sensitivity of the model to its forcing variables.

This chapter begins with a full description of the model in Section 4.2 (a list

of symbols is provided at beginning of the thesis), followed by a description of the model calibration and evaluation and sensitivity analysis in Section 4.3. Model evaluation results are then presented and discussed (Sections 4.4 and 4.5), followed by conclusions in Section 4.6.

4.2   Model description

4.2.1   Overview

The model requires hourly values of air temperature, relative humidity, precipitation, shortwave radiation, and wind speed. The stick is assumed to be suspended at a standard 30.5 cm above the forest floor. The stick is divided into two zones: a thin outer layer that reacts to atmospheric forcing, and a larger central core. The thickness of the outer layer changes with the different stick sizes, but remains below 8 mm. This division will allow the model to respond to changes in atmospheric conditions at the hourly scale as well as over multiple days. Temperature and moisture are assumed to be spatially constant within the outer layer and core. The average stick temperature, T_s (K), and moisture, m_s (kg of H_2O), are calculated as:

$$T_s = fT_o + (1-f)T_c \qquad (4.1)$$

$$m_s = fm_o + (1-f)m_c \qquad (4.2)$$

where T_o, T_c, m_o, and m_c are the temperature and moisture of the outer layer and inner core, respectively, and f is the fraction of the stick volume taken up by the outer layer. The variable f will be estimated via calibration.

The model is based on the assumption that diffusion and conduction only occur radially, and that transfers of heat and moisture to and from the stick only occur between the outer layer and the environment; the core will only gain or lose energy and moisture through conduction and diffusion from the outer layer. This assumption simplifies the problem and was also made by the Nelson model. Figure 4.1 provides a model schematic.

The model is composed of four differential equations which represent the en-
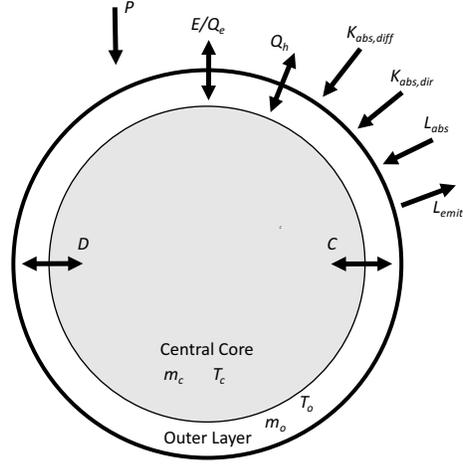
Figure 4.1: Schematic of model showing all components of the moisture and energy budgets. Please refer to the list of symbols for an explanation of the labels.

ergy and moisture budgets for each of the two zones. The energy budget for the outer layer, solved for the rate of temperature change, is:

$$\frac{dT_o}{dt} = \frac{1}{c_s \rho_s V_o} \left(L_{abs} + K_{abs,diff} + K_{abs,dir} - \right.$$

$$\left. a_s L_{emit} - a_s Q_h - (a_s - 2\pi r^2) Q_e - C \right) \quad (4.3)$$

where L_{abs} is the absorbed longwave radiation (W) , $K_{abs,diff}$ and $K_{abs,dir}$ are the absorbed diffuse and direct shortwave radiation, respectively (W), L_{emit} is the emitted longwave radiation (W m^{-2}), Q_h is the sensible heat flux (W m^{-2}), Q_e is the latent heat flux (W m^{-2}), C is the conduction into the stick's core (W), c_s is the stick specific heat (J K^{-1} kg^{-1}), which is a function of the stick moisture and temperature (see Appendix A for details), ρ_s is the stick density (400 kg m^{-3}, Nelson, 2000), V_o is the volume of the outer layer, and a_s is the surface area of the entire stick.

The energy budget of the core is composed solely of conduction from the outer layer:

$$\frac{dT_c}{dt} = \frac{C}{c_s \rho_s V_c} \tag{4.4}$$

where V_c is the volume of the core.

The moisture budget for the outer layer is composed of three components: absorbed precipitation (P_{abs}), evaporation/desorption (E), and diffusion (D) into the core:

$$\frac{dm_o}{dt} = P_{abs} - (a_s - 2\pi r^2)E - D \tag{4.5}$$

All three terms on the right-hand side are in units of kg s^{-1}. Evaporation is proportional to the latent heat flux (details below), which connects the moisture and the energy budgets.

The moisture budget for the core is composed of diffusion only:

$$\frac{dm_c}{dt} = D \tag{4.6}$$

Of note here is the use of the total stick surface area minus the area of the stick ends ($a_s - 2\pi r^2$) when calculating latent heat flux and evaporation. For the two smallest fuel sizes, the 1-hour and 10-hour fuel sticks, the area of the stick ends is small relative to their total surface area and can therefore be ignored (see Section 4.3). Moreover, the two larger 100-hour and 1000-hour fuel moisture sticks used for calibration and evaluation had wax coating their ends. This would have blocked desorption or adsorption at the stick ends. For these reasons, the latent heat flux and evaporation terms were calculated using only the lateral stick surface.

In contrast, the full surface area, a_s, is used when calculating emitted longwave and sensible heat flux as it is assumed that the wax did not impact the conductivity or emissivity of the stick ends. However, it is also assumed that there is only radial transport of heat and moisture within the stick. Therefore, while the energy exchanged between the surroundings and the stick ends is ignored, it is assumed that this energy will be exchanged via the outer layer. In effect, the outer layer has an "effective" outer surface area equal to the area of the entire stick.

The model was written in Fortran and makes use of the ODEPACK library of differential equation solvers (Hindmarsh, 1983). The deSolve package in R

52

(Soetaert et al., 2010) was used to initialize the model and input the forcing data.

4.2.2 Shortwave radiation

Because the stick is suspended above the ground, radiation inputs must be calculated from both directions. When discussing radiation components, the subscript "d" indicates downwelling inputs, "u" indicates upwelling inputs from the ground, and "emitt" indicates emitted radiation from the stick.

The downwelling shortwave radiation K_d (W m^{-2}) is divided into its diffuse, $K_{d,diff}$, and direct, $K_{d,dir}$, components following Erbs et al. (1982). Details of these calculations are presented in Appendix A. The upwelling shortwave input is calculated as $K_u = \alpha_g K_d$, where α_g is the ground albedo which is taken to be 0.185, based on values reported by Eck and Deering (1992) and Smith and Goltz (1994).

The direct solar radiation absorbed by the stick, $K_{abs,dir}$ (W), is calculated as:

$$K_{abs,dir} = a_{shadow}(1 - \alpha_s)K_{d,dir} \tag{4.7}$$

where α_s is the stick albedo. A constant albedo value of 0.65 (Nelson, 2000) is assumed. a_{shadow} is the area of the shadow cast by the stick on a horizontal plane and is a function of the sun position:

$$a_{shadow} = 2rl \csc \phi (1 - \cos^2 \phi \cos^2 \psi)^{0.5} + \pi r^2 \cot \phi \cos \psi \tag{4.8}$$

where ϕ is the solar elevation angle and ψ is the solar azimuth angle, both in radians (Monteith and Unsworth, 2008). This approach is more sophisticated than the approach by Nelson (2000), where a_{shadow} was assumed to be constant.

Appendix A provides details on the calculation of diffuse solar radiation absorbed by the stick, $K_{abs,diff}$ (W).

4.2.3 Longwave radiation

In our model, downwelling longwave radiation, L_d, varies with changing sky conditions, temperature, and canopy coverage. Changing sky conditions are accounted for with a varying atmospheric emissivity, ε_a (See Appendix A for details). Canopy coverage is accounted for using a sky-view factor, s, which is the proportion of the

sky hemisphere which is open to the atmosphere. L_d is calculated as:

$$L_d = (s\varepsilon_a + (1-s)\varepsilon_{canopy})\sigma T_a^4 \qquad (4.9)$$

where e_{canopy} is the canopy emissivity, and σ is the Stephan-Boltzmann constant $(5.67 \times 10^{-8}$ W m^{-2} K^{-4}). This approach expands upon the Nelson model, which used two constant values for downwelling longwave, one during the day and one at night, and did not allow for a changing canopy. However, because the evaluation dataset that was used to test both the present model and the Nelson model was collected only at open sites, and in the interest of providing a focused study here, the model evaluation presented below does not include an assessment of our canopy treatment. The impact of canopy on fuel moisture will be examined in Chapter 5.

The upwelling longwave input from the ground and longwave output from the stick are calculated as:

$$L_u = \varepsilon_g \sigma T_a^4, \quad L_{emitt} = \varepsilon_s \sigma T_o^4 \qquad (4.10)$$

where $\varepsilon_g = 0.95$ (Monteith and Unsworth, 2008) and $\varepsilon_s = 0.85$ (Nelson, 2000) are the emissivities of the ground and stick, respectively. Although the emissivity may change when liquid water is present on the stick surface, this only occurs during brief periods directly following precipitation. Therefore, Following Nelson (2000), the stick emissivity is assumed to remain constant. Here it is also assumed that the the ground temperature is equal to the air temperature, T_a. While this assumption is likely not valid during clear sky conditions (due to solar heating and longwave cooling), the resulting bias was not deemed large enough to warrant increasing model complexity in order to simulate the forest floor temperature.

As with diffuse shortwave radiation, Appendix A provides details on how the longwave radiation absorbed by the stick, L_{abs} (W), is calculated.

4.2.4 Sensible heat flux

Sensible heat flux is calculated using an aerodynamic resistance approach:

$$Q_h = \rho_a c_a \frac{T_o - T_a}{\Omega} \qquad (4.11)$$

where ρ_a is the density of air (1.093 kg m^{-3}) and c_a is the specific heat of air (1005 J kg^{-1} K^{-1}). T_a is the temperature of the ambient air and Ω is the aerodynamic resistance (s m^{-1}), which is calculated following Monteith and Unsworth (2008):

$$\Omega = \frac{2r}{\kappa Nu} \tag{4.12}$$

where r is the radius of the stick (m), κ is the thermal diffusivity of air (1.9×10^{-5} m^2 s^{-1}), and Nu is the Nusselt number, which, in the case of a cylinder exposed to the range of wind speeds observed in the field, can be assumed to be a function of the Reynolds Number, Re:

$$Nu = 0.17Re^{0.62} \tag{4.13}$$

where

$$Re = \frac{u2r}{v} \tag{4.14}$$

where u is the wind speed (m s^{-1}) and v is the kinematic viscosity of air (1.51×10^{-5} m^2 s^{-1}). When the wind speed fell below the stall speed of the anemometer (0.4 m s^{-1}), the wind speed was set to the stall speed. The approach may have over-estimated evaporation during low wind conditions. However, as will be shown later in this chapter, fuel moisture was relatively insensitive to wind speeds, so this approximation likely did not have a significant impact on model output.

4.2.5 Water vapour and latent heat flux

The mass flux of water vapour to and from the stick, E (kg m^{-2} s^{-1}), is computed as:

$$E = \frac{q_{surf} - q_a}{\Omega} \tag{4.15}$$

where q_a is the vapour density of the ambient air (kg m^{-3}) and q_{surf} is the vapour density at the stick surface. Here the aerodynamic resistance of water vapour is assumed to be the same as the resistance for sensible heat flux, Ω.

In order to calculate q_{surf}, desorption and adsorption within the stick needs

to be accounted for. These sorption processes were included using the following approach. When the stick's moisture content is above the fibre saturation point of 30%, the stick surface is near or at saturation, and it is assumed that liquid water is present, and evaporation occurs as from a liquid surface. Below the fibre saturation point desorption processes begin to dominate and resistance to moisture removal increases. This resistance occurs because an increasing proportion of the moisture within the stick would be composed of bound water, which requires extra energy to convert to water vapour and diffuse out towards the surface (Viney, 1991).

Adsorption and desorption constantly move the moisture of a fuel towards an equilibrium moisture content, which is a function of the temperature and relative humidity at the fuel surface. To account for these sorption processes it will be assumed that the surface of the stick is always at the equilibrium moisture content. Following Matthews (2006), this assumption allows us to invert the equation for the equilibrium moisture content given by Nelson (1984) to calculate the relative humidity of the air right at the stick surface, RH_{surf}, for a given stick surface temperature, T_{surf} (K), and moisture content, m_{surf} (%) :

$$RH_{surf} = \exp\left(\frac{-4.19M}{RT_{surf}}\exp(m_{surf}B+A)\right) \tag{4.16}$$

where M is the molecular mass of water (0.0180 kg mol^{-1}), R is the gas constant (8.314 $\times 10^{-3}$ kPa m^3 mol^{-1} K^{-1}), and B and A are unitless empirical constants, which will be treated as adjustable parameters during model optimization. The factor of 4.19 is required to convert the original equation of Nelson (1984) to S.I. units. RH_{surf} can then be combined with the saturation vapour density, q_{sat}, to calculate q_{surf}:

$$q_{surf} = q_{sat}RH_{surf} \tag{4.17}$$

which can then be used in Equation 4.15 to calculate evaporation rates.

The impact of m_s on RH_{surf} is presented in Figure 4.2 for a range of possible curves using A and B values suggested by the experimental work of Anderson (1990b). The influence of temperature on RH_{surf} is relatively weak, and it is ignored in this figure by setting temperature to a constant 15°C. Here we see the

aforementioned relationship between surface humidity and fuel moisture content. Above the fibre saturation point of 30%, the relative humidity at the surface is at or near 100% and evaporation is not limited. As moisture decreases below 30%, the relative humidity quickly decreases, and the resistance to moisture removal increases as sorption processes begin to dominate.
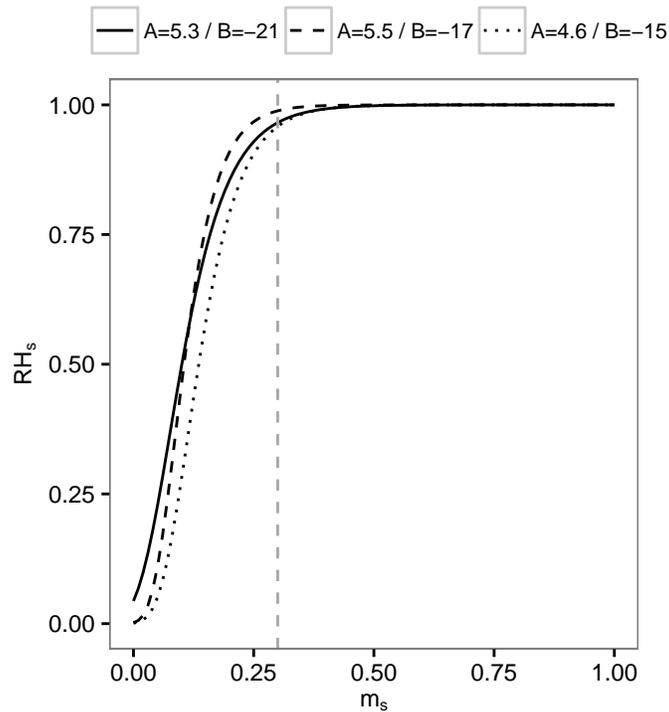
Figure 4.2: The impact of surface fuel moisture on surface relative humidity for different values of A and B. The fibre saturation point of 30% is shown by the vertical dashed grey line.

Here it will be assumed that the surface moisture and temperature are equal to the average moisture and temperature of the outer layer. In the final model, the outer layer represents a thin outer shell, whose thickness increases with fuel size but remains below 8 mm for the largest size. Therefore, this assumption is reasonable as the moisture and temperature within the thin outer layer will not likely deviate significantly from the mean value. Indeed, Matthews (2006) made

the same assumption when modelling the moisture content of eucalyptus litter elements, which also have a small but finite thickness. This approximation simplifies the model considerably by avoiding the calculation of moisture right at the surface.

In order to calculate the latent energy flux, Q_e (W m^{-2}), from the vapour mass flux, E, the lower energy state of the bound water within cellulose material compared to liquid water has to be accounted for (Skaar, 1988). Consequently, the energy required to transition a unit mass of water from its bound state to vapour (in J kg^{-1}) is the sum of the latent heat of vaporisation, λ_{vap}, and the differential heat of sorption, λ_{sorp}, so that:

$$Q_e = (\lambda_{vap} + \lambda_{sorp})E \qquad (4.18)$$

Sorption processes should become insignificant as the fuel moisture content approaches and exceeds the fibre saturation point of 30% and moisture loss is due to evaporation only. Therefore, λ_{sorp} is modelled as an exponentially decaying function of fuel moisture content (Nelson, 2000):

$$\lambda_s = \frac{21000}{M} e^{-14m_s} \qquad (4.19)$$

The dependence of λ_{vap} on temperature (Stull, 1988) is also accounted for:

$$\lambda_{vap} = 2.501 \times 10^6 - 2.37 \times 10^3 \, (T_a - 273.15) \qquad (4.20)$$

4.2.6 Conduction and diffusion

Diffusion and conduction within the stick are computed using a bulk transport approach, assuming that each layer has a constant temperature and moisture content. Using a radial coordinate system, the flux of heat between the two layers, C (W), is given as:

$$C = 2\pi l \frac{k_s \, (T_o - T_c)}{\ln(\frac{r_{o,mid}}{r_{c,mid}})} \qquad (4.21)$$

where $r_{o,mid}$ is the mid-point radius of the outer layer, $r_{c,mid}$ is the mid-point radius of the core, and k_s (J m^{-1} s^{-1} K^{-1}) is the bulk conductivity of the stick which is

58

calculated as an empirical linear function of the stick moisture:

$$k_s = g(0.1941 + 0.004064 m_s) + 0.01864 \qquad (4.22)$$

where g is the specific gravity of the stick, equal to 0.42 (Simpson and Tenwolde, 1999).

The rate of diffusion into the core from the outer layer, D (kg s^{-1}), is computed as

$$D = 2\pi l \frac{d_s \rho_s (m_o - m_c)}{\ln(\frac{r_{o,mid}}{r_{c,mid}})} \qquad (4.23)$$

where d_s, the bulk diffusion coefficient of the stick (m^2 s^{-1}), will be determined though model calibration. The stick density, ρ_s, is required to convert the moisture from a fractional weight to kg m^{-3}.

In actuality, the diffusivity will change with moisture content, and is governed by three different processes: bound water diffusion, vapour diffusion, and capillary flow (Nelson, 2000). Using a single constant parameter for controlling internal moisture transport is therefore a significant simplification. Consequently, d_s should be seen as an empirical parameter that describes the rate at which the stick responds to external forcing. Therefore, during model calibration d_s will be allowed to move beyond the range of diffusivity values reported in the literature. This reduced complexity is warranted based on the relatively simple application. Moreover, analysis not shown here demonstrated that calculating d_s as a function of the average stick moisture did not increase the skill of the model.

4.2.7   Precipitation

The amount of precipitation absorbed by the outer layer, P_{abs} (kg s^{-1}), is calculated from the incident precipitation rate, P_{inc} (kg s^{-1} m^{-2}), and the dimensions of the stick:

$$P_{abs} = 2rl P_{inc} \qquad (4.24)$$

Here it is assumed that all precipitation intercepted by the stick is absorbed, and

59

no precipitation is intercepted by the stick ends. The moisture content of the outer layer is limited to a maximum value, m_{max}. Any precipitation above this amount is assumed to run off the stick. The value of m_{max} will be determined through model calibration.

4.3 Model calibration and evaluation

Two datasets were used to calibrate and evaluate the model. The first dataset was composed of observations from the Base Station (BS) and Fuel Moisture 2 site (FM2), which were the two sites with open canopies and a full suite of meteorological and fuel moisture measurements. Each site had one fuel moisture sensor. An analysis of forest canopy impacts on fuel moisture will be left for Chapter 5. Consequently, the closed-canopy Fuel Moisture 1 site was not used in this chapter. Each site had a single fuel moisture sensor. The Rotronic HC-S3 Temperature and Relative Humidity measurements from both the 30.5 cm and 1.62 m heights were used here. Wind speed was interpolated to 30.5 cm from 1.62 m using a neutral logarithmic wind profile. The aerodynamic roughness length was set to 0.01 m, which is appropriate for short grass (Oke, 1990). Wind speed was assumed to be the same across the two sites because FM2 did not have an anemometer. Although the pine dowels used in the automatic fuel moisture sensors are carefully selected and standardized, it is likely that the two sensors used here would provide slightly different results. With respect to sensor accuracy, the manufacturer reports that the root mean square error is $\pm$ 0.74% for moisture content below 10%, $\pm$ 0.90% for moisture between 10% to 20%, $\pm$ 1.94% for moisture between 20% and 30% and $\pm$ 2.27% for values above 30%. To check the consistency between the two sensors, two comparison periods were undertaken on either end of the field season in which the two sensors were co-located for a total of 35 days.

The second dataset was collected between April 1996 and December 1997 in an agricultural field in Oklahoma and is described in detail by Carlson et al. (2007). This dataset was originally used to evaluate and train the Nelson Model. In this case, fuel moisture for the 1-hour, 10-hour, 100-hour, and 1000-hour fuel sizes was estimated by twice-daily field weighings of ponderosa pine dowels of increasing radii: 0.2, 0.64, 2.0, and 6.4 cm. The 10-hour dowels had a length of 50 cm while

the other three sizes had lengths of 41 cm. The three smaller sizes were weighed to the closest 0.1 g, while the 1000-hour fuel was weighed to the closest gram. The absolute accuracy of these measurements is therefore less than 1% moisture content. For the two smallest fuel sizes standard arrays of four connected dowels were weighed. An average weight across three separate dowels was used for the two largest sizes. To minimize the impacts of weathering on moisture measurements, the 1 and 10-hour dowels were replaced every three months while the 100-hour dowels were replaced every six months. The 1000-hour dowels were not replaced during the two years. Forcing data were taken from a nearby weather station run by Oklahoma Mesonet. Air temperature and humidity were measured at a standard screen height. Wind speed was measured at 10 m and was also interpolated to 30.5 cm.

The model was optimized by adjusting five parameters: A, B, K_m, m_{max}, and f. Based on work by Anderson (1990b), potential values ranged from 4.4 to 6.7 for A and -22 to -10 for B. Diffusivity values reported in the literature ranged from 0.1×10^{10} to 2×10^{10} m^2 s^{-1} (Fosberg, 1970; Deeming et al., 1977; Avramidis and Siau, 1987; Anderson, 1990a; Wadsö, 1993). This range was used as a starting point. However, as previously mentioned, d_s was not required to remain within this range. The value of m_{max} was allowed to vary between 30% and 150% and the value of f varied from 0.05 to 0.90. To find optimal parameter sets, a particle-swarm optimization routine (Clerc, 2010) implemented in R was used (cran.r-project.org/web/packages/pso/). Default values were used for all settings, except the swarm size was increased from the default of 13 to 32 as this was found to improve the stability of the search results.

Initial evaluation runs indicated that letting f vary across different stick sizes did not increase the optimal model skill but significantly reduced the ability of the model to predict moisture at different sites. A a single value of f was therefore used across all models. This was done by initially calibrating all models with an adjustable f. A final constant value of 0.22 was then calculated as the average of all optimal f values. The other four parameters were then optimized using this constant f value.

The Nash-Sutcliffe efficiency (NSE) was used to determine the skill of each model run. It is a measure of how close the modelled output is to a 1:1 agree-

61

ment with observations, and accounts for both bias and correlation. The *NSE* is computed as:

$$NSE = 1 - \frac{\Sigma_{t=1}^{N}(m_m^t - m_o^t)^2}{\Sigma_{t=1}^{N}(m_o^t - \bar{\ })^2} \qquad (4.25)$$

where m_m^t and m_o^t are the modelled and observed values, respectively, at time t, $\overline{m_o}$ is the mean of the observations, and N is the total number of time steps. *NSE* ranges from negative infinity to 1. A value of 1 indicates perfect agreement, while a negative value indicates that the average of the observations is more skillful than the model output. The optimal parameter set was assumed to be reached when the value of *NSE* did not improve by more than 10^{-4} over 20 consecutive iterations of the particle swarm algorithm.

In optimizing the model a priority was placed on accurate simulation of moisture values below the fibre saturation point of 30%. This was done for a number of reasons. Firstly, periods of low moisture are particularly important when estimating wildfire potential. Secondly, the accuracy of electronic fuel moisture sensors above the fibre saturation point has not been thoroughly determined, and manual moisture measurements decrease in reliability at higher moisture levels (Nelson, 2000). Therefore, a log transformation was applied to both the observations and model output before the NSE was calculated, creating a new NSE_{log}. This metric increases the influence of the dry periods and was used by the particle-swarm routine to find the optimal model.

Two approaches were used to test the transferability of the calibrated model across time and different sites. First, for each fuel size the model was calibrated using just the 1997 Oklahoma data and then evaluated using the 1996 Oklahoma data. In the second approach individual models were calibrated at all three sites (the two BC sites and the Oklahoma site) and then evaluated at the other sites. As well, in order to assess the influence of measurement height, predictions were made at BS using both the near-surface and screen-level temperature and humidity measurements.

During both calibration and evaluation the model was initialized using the first observed moisture value. Consequently, the first portion of the model output is not truly independent of the observations. However, analysis not shown here indicated

that for all but the 1000-hour fuel the choice of initial value has an negligible impact on the model output because the model quickly comes to equilibrium with the forcing data. For the 1000-hour model the impact of the initial value was felt for the first 20 days of the simulation. Therefore, the initial 20 days were used as a spin-up period in the 1000-hour simulations and were removed before model statistics were calculated.

4.3.1 Model sensitivity analysis

To determine the sensitivity of the model to each forcing variable, a series of model runs were undertaken in which each variable was randomized in turn and then input, along with the other, non-randomized, variables into the model. If the model was relatively insensitive to a forcing variable, then there should be little difference between the original model output and the output generated when the individual variable was randomized. Diffuse and direct downwelling shortwave radiation, downwelling longwave radiation, relative humidity, air temperature, and wind speed were all randomized. Precipitation was not included in this analysis as the discrete nature of the variable and its lack of a consistent diurnal trend does not lend itself to a comparison with the other forcing variables.

In detail, the time series of the variable to be randomized was divided into days, and those days were randomized across the season. In this way, the randomized variable still had realistic diurnal trends and the correlation structure across the variables was maintained. The sensitivity of the model to each forcing variable was quantified by calculating the bias and coefficient of determination between the randomized model runs and the original, non-randomized model run.

4.4   Results

Before evaluating the model, the accuracy of the fuel moisture sensors used at the BC sites were examined. The BC sensors were installed at the same site, both 30.5 cm above the ground, for 20 days at the beginning and 15 days at the end of the field season. A comparison of the observations from these two periods is presented in Figure 4.3. The root mean square error between the two sensors was larger than the accuracy reported by the manufacturer (Section 4.3): 2.56% for moisture levels

below 10%, $\pm$ 3.58% for moisture between 10% to 20%, $\pm$ 3.55% for moisture between 20% and 30% and $\pm$ 5.00% for values above 30%. However, at the lower moisture values the sensors were strongly correlated and much of the error was due to a consistent bias. As moisture levels increased, the spread increased and the bias changed sign.
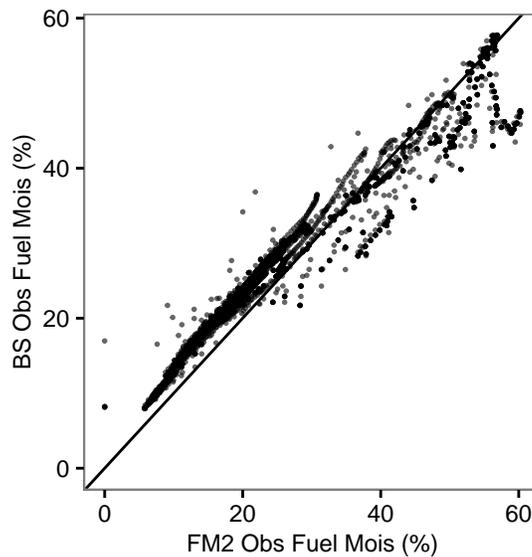
Figure 4.3: Comparison of co-located fuel moisture observations by the sensors used at sites BS and FM2. A 1:1 line is provided as a reference.

The optimal parameter values for all site and size combinations are presented in Table 4.1. The diffusivity coefficient, d_s, increased with increasing fuel size from 2.61 $\times 10^{-10}$ m^2 s^{-1} for the 1-hour model to 3.45 $\times 10^{-9}$ m^2 s^{-1} for the 1000-hour model. The optimal d_s values were above the range of values provided in the Methods section. This is not unexpected as a "bulk" approach was used to calculate diffusion in which the two layers are assumed to have constant temperature and moisture. The maximum allowable moisture content, m_{max}, was smaller for the larger fuel sizes. Parameters A and B did not show any apparent relationship to fuel size.

Model performance during calibration is summarized in Table 4.2. Although the model was optimized using NSE_{log}, the coefficient of determination, R^2, the

Table 4.1: Optimal parameter values for all calibration site/size combinations

Calibration Size (hour)	Calibration Site	A	B	d_s (m^2 s^{-1})	m_{max} (%)	f
1	OK	4.00	-12.00	2.61e-10	79.3	0.22
10	BS	4.98	-18.80	3.01e-10	76.8	0.22
10	FM2	4.70	-22.00	2.92e-10	90.6	0.22
10	OK	4.96	-20.10	5.39e-10	66.3	0.22
100	OK	5.11	-22.00	5.46e-10	48.6	0.22
1000	OK	4.81	-18.40	3.45e-09	44.0	0.22

root mean square error, and the model bias were also provided. Here the model bias is calculated as the mean difference between the modelled and observed values. A positive bias indicates that the model was, on average, wetter than the observations. At the Oklahoma site, model skill increased with increasing fuel size, while the model was more skillful in simulating the BC sites than the Oklahoma site. The models had a dry bias across all sites and sizes.

Table 4.2: Skill of optimal models applied to calibration data. Comparison statistics used are: the Log-transformed Nash-Sutcliffe efficiency, coefficient of determination, root-mean-square error, bias, and bias for all data with observed moisture below 30%. The units of Bias and RMSE are percent moisture content.

Calibration Size (hour)	Calibration Site	NSE_{log}	R^2	RMSE (%)	Bias (%)	Bias (<30%) (%)
1	OK	0.28	0.78	7.50	-0.04	0.58
10	BS	0.90	0.92	3.19	-0.38	0.07
10	FM2	0.93	0.94	2.86	-0.09	0.22
10	OK	0.85	0.85	4.01	-0.30	-0.05
100	OK	0.84	0.85	1.86	-0.08	-0.03
1000	OK	0.87	0.89	1.18	-0.07	-0.07

Results of calibrating using the 1997 Oklahoma data and evaluating on the 1996 data are presented in Table 4.3. Compared to the optimal results in Table 4.2, the model lost little predictive skill when applied to an independent time period.

Again, model skill generally increased with fuel size. Most of the reduction in skill from the optimal results was seen in the biases. Scatter plots for this model evaluation are presented in Figure 4.4, while example time series are presented in Figure 4.5. In particular, high moisture levels for the 1-hour fuel were poorly simulated.

Table 4.3: Model evaluation with independent time period: models are calibrated on 1997 Oklahoma data and evaluated using 1996 data. The units of Bias and RMSE are percent moisture content.

Evaluation Size (Hour)	NSE_{log}	R^2	RMSE (%)	Bias (%)	Bias ($<30\%$) (%)
1	0.14	0.72	9.37	0.83	1.94
10	0.84	0.90	3.18	0.80	1.01
100	0.82	0.84	1.98	0.53	0.58
1000	0.89	0.90	1.21	-0.44	-0.44
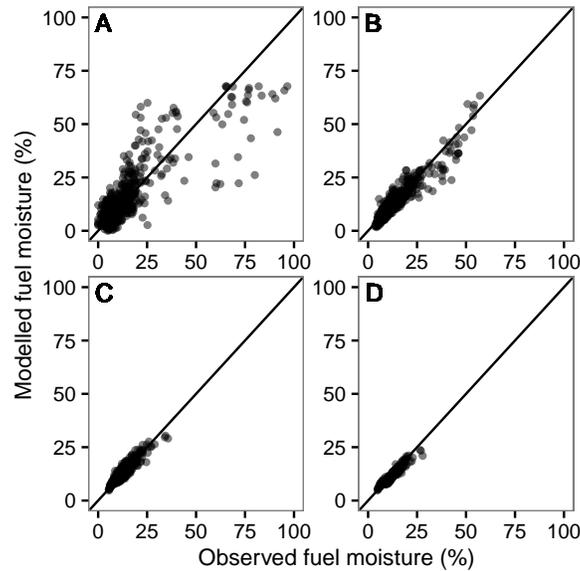
Figure 4.4: Comparison of modelled and observed fuel moisture at the Oklahoma site for 1996. The models used were calibrated for each size separately using the 1997 data. A) 1-hour fuel size, B) 10-hour fuel size, C) 100-hour fuel size, and D) 1000-hour fuel size.
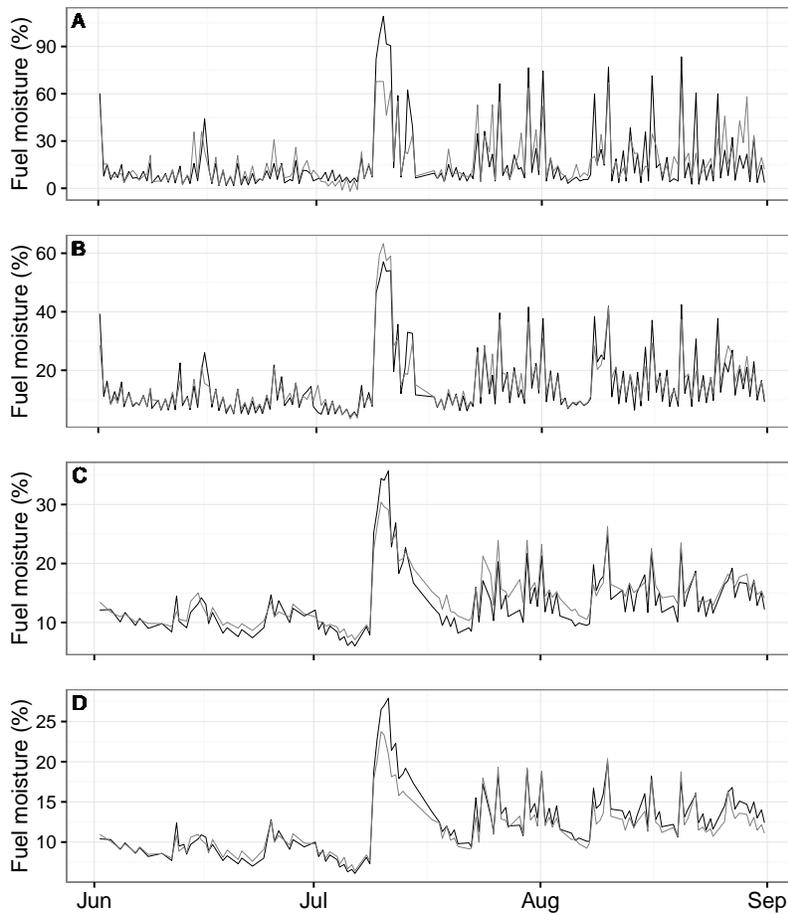
Figure 4.5: Example time series of modelled fuel moisture (*grey lines*) generated by 1997 Oklahoma models and observed fuel moisture (*black line*) at the Oklahoma site during 1996 for the A) 1-hour fuel size, B) 10-hour fuel size, C) 100-hour fuel size, and D) 1000-hour fuel size. Note the varying y-axis limits.

The second evaluation approach found optimal models for the 10-hour fuel size at all three sites and evaluated those models at the other sites. The models for 10-hour sticks, calibrated using the BC data set, were applied to the 10-hour and the 1-hour Oklahoma data to mirror the methods of Carlson et al. (2007). These results are presented in Table 4.4. As expected, model skill was high between the

two BC sites. Significantly, compared to the calibration results (Table 4.2), the skill of the Oklahoma model was not substantially reduced when applied to the BC sites. Indeed, it achieved higher R^2 values when modelling the independent data. This is in contrast to the BC model, which, when applied to the Oklahoma site, produced poorer predictions than during the calibration runs.

Table 4.4: Model evaluation with independent sites: models calibrated at one site are evaluated at the other two sites. All models are trained using the 10-hour fuel size. The units of Bias and RMSE are percent moisture content.

Calibration Site	Evaluation Site	Evaluation Size (hour)	NSE_{log}	R^2	RMSE (%)	Bias (%)	Bias (<30%) (%)
BS	FM2	10	0.75	0.94	3.90	1.96	2.79
BS	OK	1	0.22	0.77	7.47	0.53	1.67
BS	OK	10	0.79	0.82	4.49	1.15	1.42
FM2	BS	10	0.68	0.90	4.54	-2.48	-2.54
FM2	OK	1	0.26	0.76	8.05	-1.83	-1.26
FM2	OK	10	0.74	0.79	5.40	-1.16	-1.32
OK	BS	10	0.80	0.91	4.04	-2.26	-1.76
OK	FM2	10	0.83	0.93	3.70	0.29	1.15

Much of the reduction in skill was due to larger biases. The BS model produced a wet bias at the other two sites, while the Fuel Moisture 2 model produced dry biases when applied to the BS and OK sites. These biases are apparent in Figure 4.6, where scatter plots compare modelled moisture to observations. Figure 4.6B mirrors the results shown in Figure 4.3. That is, compared to the BS sensor, the Fuel Moisture 2 sensor had a dry bias for lower moisture and a wet bias during wetter conditions. Consequently, the Fuel Moisture 2 model had a similar bias when predicting at BS: the Fuel Moisture 2 model underpredicted fuel moisture at low moisture values and overpredicted at the highest levels. As was the case for the cross-time evaluation results (Figure 4.4), model error was highest when simulating higher moisture values at the Oklahoma site (Figure 4.6D).

Figure 4.7 presents sample time series of modelled and observed 10-hour fuel moisture at BS and Oklahoma sites. The model calibrated at FM2 overpredicted during precipitation events due to its higher m_{max} value (see Table 4.1). The dry bias of the Oklahoma model is apparent in Figure 4.7C. At the lower moisture lev-
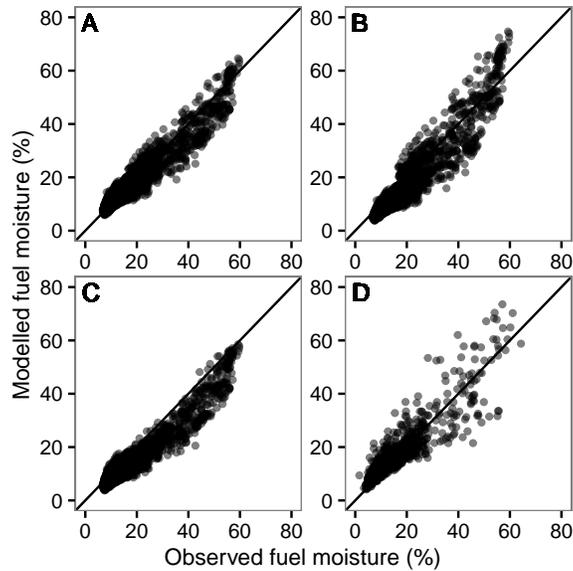
Figure 4.6: Comparison of modelled 10-hour fuel moisture with observations when the model is calibrated and evaluated at different sites. A) Calibrated at BS and evaluated at BS, B) Calibrated at FM2 and evaluated at BS, C) Calibrated at Oklahoma and evaluated at BS, D) Calibrated at BS and evaluated at Oklahoma.

els, this bias is due to larger diurnal cycles and excessive drying during the day, leading to daytime moisture minima that were almost always lower than the observations. The Oklahoma 10-hour model had a higher diffusivity value compared to BS model. Consequently, the model responded more quickly to the diurnal cycle leading to these larger amplitudes in moisture. The opposite is true in Figure 4.7D where the Oklahoma observations were modelled by the BS model.

To test the influence of measurement height, humidity and temperature were measured at the near-surface (0.305 m above the ground) as well as the screen-level (1.62 m) at BS and the 10-hour Oklahoma model was forced with both. When forced with the near-surface observations, the model generated consistently higher fuel moisture than when the screen-level data were used. In particular, diurnal cycles were larger and nocturnal maxima were noticeably higher during fair-weather conditions. Overall, the model output based on near-surface forcing data has a positive 1.1% bias compared to screen-level forced output. This bias is evident in
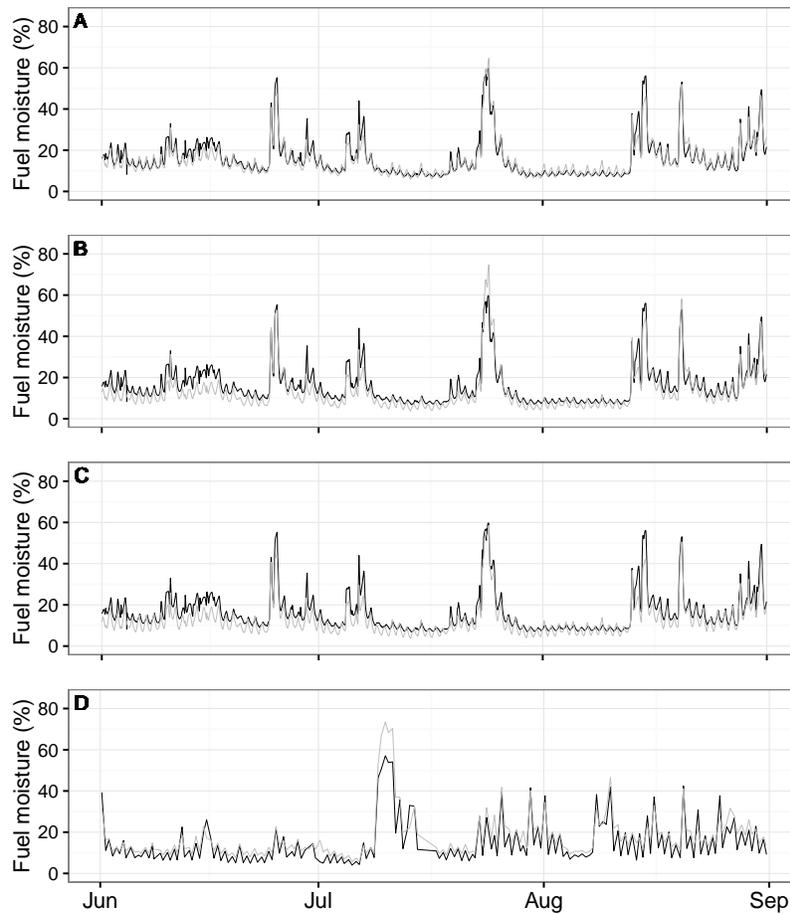
Figure 4.7: Example time series of observed (*black*) and modelled (*grey*) 10-hour fuel moisture when the model is calibrated and evaluated at different sites. A) Calibrated at BS and evaluated at BS, B) calibrated at FM2 and evaluated at BS, C) calibrated at Oklahoma and evaluated at BS, D) Calibrated at BS and evaluated at Oklahoma. Note that BS data are from 2014 while the Oklahoma data are from 1996.

the sample time-series presented in Figure 4.8. As well, the near-surface conditions were, on average, wetter than at screen level, with a 0.05 kPa bias in absolute humidity and a 2.9% bias in relative humidity.

The results of the model sensitivity analysis are presented in Figure 4.9. The fuel moisture model is substantially more sensitive to relative humidity than to any
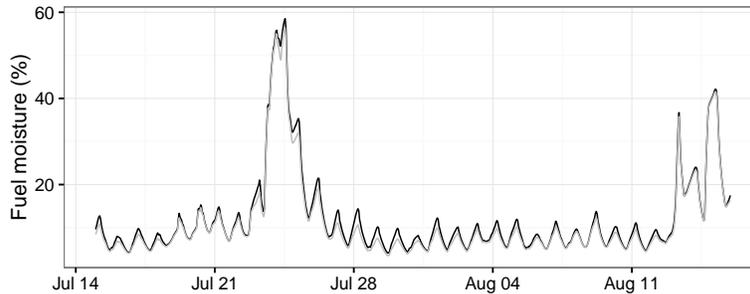
Figure 4.8: A comparison of modelled 10-hour fuel moisture generated at BS using the 10-hour Oklahoma model forced by screen-level observations (grey) and near-surface observations (black).

other variable. Air temperature and longwave radiation have a secondary impact on the model output. Significantly, this analysis suggests that diffuse shortwave radiation and wind speed have very little influence on the model output.

Table 4.5 provides a comparison of our model skill, given as R^2 values, with the results of Carlson et al. (2007), who used the same Oklahoma data to evaluate the Nelson model. As our model was trained at both BS and FM2, Table 4.5 includes two different R^2 values for the 1-hour and 10-hour fuels. The parameters used by Carlson et al. (2007) for the 1-hour and 10-hour sizes were identical and had previously been calibrated using a separate dataset. Therefore, their test of the 1-hour and 10-hour model mirrors our evaluation of the 10-hour model calibrated at the two BC sites using the Oklahoma data. For the Nelson model, the regressions of simulated against observed values had R^2 values of 0.64 and 0.79 for the 1-hour and 10-hour fuel sizes, respectively. When applied to the same data our model achieved higher R^2 values of 0.77 and 0.76 for the 1-hour fuel size. For the 10-hour fuel size our model improved or matched the skill of the Nelson model with R^2 values of 0.82 and 0.79. The biases produced by our model are dependent on the calibration site. The BS model produced a smaller bias for the 1-hour fuel size (0.53% compared to 1.4% reported by Carlson et al. 2007) while the FM2 model produced a larger bias of -1.83%. For the 10-hour fuel size, Both BC models produced a larger bias (1.15% and -1.16% compared to 0.1%).

Carlson et al. (2007) used the Oklahoma data set for both calibration and eval-

71
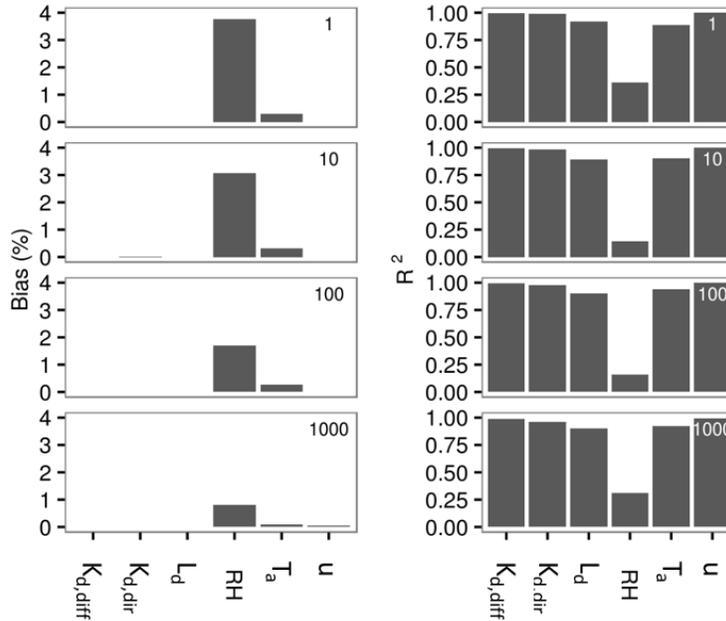
Figure 4.9: Comparison statistics when comparing original fuel moisture model output at BS with model output when one of the forcing variables (downwelling diffuse and direct shortwave, downwelling longwave, relative humidity, air temperature, and windspeed) is randomized across days. Mean bias is provided on the left and the coefficient of determination is provided on the right. Results for all four fuel sizes are provided.

uation of their 100-hour and 1000-hour models. In this case it is most appropriate to compare their results to the model skill achieved by our optimized models. The Nelson model achieved R^2 values of 0.77 and 0.56 for the 100-hour and 1000-hour fuel sizes, respectively. Our model improves on this, with optimal R^2 values of 0.85 and 0.89 for the same sizes. Additionally, our optimized models produced biases of -0.08% and -0.07 % for the 100-hour and 1000-hour fuel sizes, respectively. This is also an improvement on the Nelson model biases: 0.6% for the 100-hour model and -0.2% for the 1000-hour model.

The skill of the new model can also be compared to that of Resco de Dios et al. (2015), who developed a simple model for simulating daily minimum 1-hour

Evaluation	R^2		Bias (%)	
Size (hour)	Nelson	Current	Nelson	Current
1	0.64	0.77, 0.76	1.4	0.53, -1.83
10	0.72	0.82, 0.79	0.1	1.15, -1.16
100	0.77	0.85	0.6	-0.08
1000	0.56	0.89	-0.2	-0.07

Table 4.5: Comparison of model skill between the Nelson model and the model presented here when applied to the Carlson dataset. The unit for Bias is percent moisture content.

and 10-hour fuel moisture content. The authors evaluated their model using observations from a previous version of the Campbell Scientific 10-hour fuel moisture sensor (the CS505). When evaluating their model with an independent dataset they achieved an R^2 value of 0.67 and a bias of 0.73%. Our model improves on these results as well, with higher correlations and comparable biases. However, some of the sensors used for evaluation by Resco de Dios et al. (2015) were placed on the ground, while their calibration sensors were suspended 30.5 cm above the ground. This difference in placement could have led to a reduction in their model skill.

4.5 Discussion

The model presented here improved on the skill achieved by the Nelson model when applied to the same dataset and has additional features that allow for a more realistic treatment of canopy coverage and changes in sky conditions. Fuel moisture simulated by the new model had consistently higher correlations with observations compared to the Nelson model, suggesting that the new model would be better at simulating seasonal and diel trends in fuel moisture.

This study has demonstrated that when simulating the moisture of standard fuel sticks, more sophisticated treatments of internal moisture transport, precipitation interception, and the transfer of moisture to and from the atmosphere do not necessarily increase the skill of the model. If the model was intended to be applied to a range of fuel types with varying characteristics, then a more detailed process-based model may indeed be more appropriate. However, the simple characteristics of the moisture sticks lend themselves to a less complex formulation such as ours,

especially if it can be calibrated to observations.

A portion of the model bias seen in the evaluation results can be explained by intrinsic differences between individual sensors or sticks. That is, model skill was limited by inconsistent observations across sites. The comparison of co-located fuel moisture sensors (Figure 4.3) demonstrated that significant biases can exist even between sensors sourced from the same manufacturer. Even though Carlson et al. (2007) averaged over multiple sticks that were periodically replaced, the types of sticks used in that study may have exhibited a systematic bias compared to the BC sensors.

These results point to the importance of having co-located meteorological observations; small changes in local conditions could reduce the maximum achievable model skill. Overall, the BC sites, which had co-located weather observations, yielded better calibration results. When applied to the BC sites, the performance of the Oklahoma model was not significantly reduced from the calibration run. This finding suggests that the benefit of having co-located measurements at the BC sites compensated for the inevitable reduction when the model was applied to the independent dataset. Indeed, the opposite was not true; the BC models yielded larger reductions in skill when applied to the Oklahoma site.

The model had the most difficulty predicting high moisture levels. There are a number of reasons for this. Firstly, as previously mentioned, the reliability of standardized fuel moisture sticks is reduced during wet conditions. Consequently, the lack of dependable observations could have led to modelling error. Secondly, the rate at which the stick loses and gains moisture increases with increasing moisture. Therefore, any error in the modelled response time or differences in conditions between the weather station and the fuel sticks would be magnified at these higher levels of moisture.

These issues become particularly important for the smaller fuel sizes, which likely explains why the 1-hour model had the poorest results and high RMSE values: the rapid moisture changes are more difficult to predict, the stick is more often at elevated moisture levels, and the lack of co-located weather observations would be particularly detrimental in this case. However, this reduction in skill at higher moisture levels is less of a concern as it is the simulation of low-moisture conditions that is most important for fire management purposes.

Forcing the model with near-surface observations (0.305 m above the ground) led to a wet bias relative to the screen-level measurements (1.62 m). It was also shown that near-surface conditions were consistently wetter than at screen height. This vertical gradient likely explain the biases between the two tests.

As previously mentioned, our model is capable of including the impact of canopy cover on downwelling longwave radiation. However, because Carlson et al. (2007) only made measurements at open sites, and for the sake of brevity, the impact of canopy coverage was not assessed here, even though a closed canopy would likely increase the amount of downwelling radiation substantially and increase nocturnal stick temperature, especially during clear nights. Based on Equation 4.16, this would lead to increased stick moisture. Yet, it should be mentioned that the sensitivity analysis results suggest that, compared with relative humidity, longwave radiation has little impact on fuel moisture. The influence of canopy coverage on fuel stick moisture will be examined in Chapter 5.

In contrast to the Nelson model, our model requires wind speed as a forcing variable. However, the sensitivity analysis demonstrated that the model is insensitive to winds speeds. This lack of influence was expected, because at lower moisture levels the rate at which the stick exhanges moisture with the atmosphere is limited by sorption processes within the stick (that are not influenced by wind), as opposed to turbulent fluxes within the atmosphere (see Section 4.2.5). Consequently, using a constant aerodynamic resistance would remove wind speed from the list of required forcing variables and may do little to alter model skill, especially at lower moisture levels.

4.6   Conclusions

The model developed in this chapter differs from the Nelson model (Nelson, 2000) in a number of ways. It simplifies the treatment of the internal transport of moisture and heat, the capture of precipitation, and the transfer of moisture between the stick and the atmosphere, while its treatment of longwave and shortwave radiation is more sophisticated: it avoids linearising the net longwave component and allows for variations in sky condition and canopy coverage. As well, it does not assume that the stick acts like a wet bulb, as this assumption does not hold true when the

stick is exposed to direct sunlight. This model can be applied operationally using standard weather observations.

The model was evaluated to determine its transferability across different time periods and different sites. The model lost little skill when applied to an independent time period. It was also demonstrated that the 10-hour fuel model retains much of its predictive skill when it is calibrated at one site and evaluated at an independent site. However, in some cases the model did exhibit relatively larger biases when applied to the evaluation dataset. This could partly be due to intrinsic differences in the observation technique: one dataset used manually weighed fuel sticks while the other used automatic fuel moisture sensors. Our results also suggest that having co-located weather observations at the same height as the moisture stick improves model results. The skill of our model improved on the performance of the Nelson model (as presented by Carlson et al. 2007) when predicting the same set of fuel moisture measurements.

In the next chapter the model will be applied to the field observations described in Chapter 2, along with modelled below-canopy precipitation and radiation, to simulate fuel moisture and fire danger at all 24 sites. The modelled dataset will then be used to examine the spatial variability of fuel moisture and fire danger across a forested landscape. The model will also be used to examine the influence of canopy cover on simulated fire danger.

Chapter 5

Modelling the spatial variability of fuel moisture and fire danger across a heterogeneous forested landscape

5.1 Introduction

A number of studies have examined the influence of terrain on surface conditions and fuel moisture. Hayes (1941) measured the fuel moisture at open sites on nearby north-facing and south-facing slopes. Fuel moisture was always higher on the north slope. Conditions were wetter at lower slope positions where the average difference was 1.9% moisture content. Stambaugh et al. (2007) also found that deciduous litter was drier on south-facing slopes under most conditions, but the impact of aspect was absent during the wettest and driest conditions. Gibos (2010) examined the influence of aspect on fine fuel moisture within montane spruce stands. The absence of a significant difference between a north and south aspect was attributed to high canopy coverage at both sites, which reduced radiation levels by around 90%. Nyman et al. (2015b) reported that fuel moisture was higher on cooler aspects, although the cooler aspects also had increased canopy cover and understory

vegetation, and thicker organic soils which retained moisture.

Sullivan and Matthews (2012) modelled forest floor fuel moisture for different aspect and slope combinations. Differences in modelled fuel moisture mainly occurred during the morning on steep slopes due to lower morning sun angles. Holden and Jolly (2011) used a network of temperature and humidity sensors across a region of complex terrain to create high resolution maps of the estimated fire danger, which is strongly impacted by fuel moisture. There was significant variability in fire danger and these patterns changed over the fire season. Specifically, south facing slopes had drier fuels, due in part to increased radiation. As well, the distribution of early season fire danger was bi-modal, reflecting significantly different drying rates between different facets and elevations.

Others have examined the impact of stand structure on fuel moisture. Countryman (1977) demonstrated that within-stand variability in fuel moisture was dependent on the integrated amount of direct sunlight experienced by a particular location; more radiation led to decreased moisture. Observations by Whitehead et al. (2006) indicated that lower moisture content was found in thinned stands compared to unthinned stands. However, these differences diminished as the fuels dried out and were not significant during the driest periods of the season. In a similar study by Estes et al. (2012), moisture levels were measured for fuel sticks of various sizes placed on the forest floor of thinned and unthinned stands. Overall, the drying impact of a reduced canopy cover was small with the only significant influence occurring for large 10,000-hour fuels early in the season. Pook and Gill (1993) found that fine fuel moisture within *Pinus radiata* stands was most sensitive to canopy coverage and density during wetter periods. Both Banwell et al. (2013) and Faiella and Bailey (2007) could not identify any significant differences in fuel moisture across sites with differing canopy cover. A slightly different result was obtained by Tanskanen et al. (2006) who also observed increased drying rates in open stands as compared to mature closed stands. However, the differences between sites increased over the season, which the authors attributed to the enhanced light interception by the canopy with decreasing solar angle.

Rothermel et al. (1986) created a model that simulates the impact of both canopy cover and aspect on fuel moisture. Their model uses empirical relationships between radiation levels, wind speed, and fuel moisture developed by Byram

and Jemison (1943). These relationships were established using a "weather simulator" whereby surface fuels were encompassed in a large box in which radiation levels and wind speeds were controlled by lights and fans. Changing light levels were used to simulate the impact of changing radiation loads with aspect and slope. These empirical relationships suggested that radiation load has a significant impact on fuel moisture. However, their model underestimated moisture levels at high radiation levels, possibly because the authors did not include the impact of evaporative cooling or resistance due to sorption processes in their calculations. Rothermel et al. (1986) also developed a canopy shading algorithm that directly calculated shading cast by the canopy, taking into account canopy height, tree type, aspect and slope. They found that their model was more accurate than the FFMC (see Chapter 1) when predicting fuel moisture in direct sunlight.

There are a number of gaps in the literature that will be addressed in this chapter. Firstly, when examining the spatial patterns of fuel moisture, most studies used observations with approximately a weekly resolution. Some studies made daily measurements, but this is still too coarse to resolve diurnal trends. As well, to my knowledge, the relative impact of canopy coverage and aspect on fuel moisture has not been examined. As mentioned in Chapter 1, aspect can impact fuel moisture directly through changes in radiation, but it also has an indirect effect by affecting understory and overstory vegetation cover and soil type. In order to accurately predict fuel moisture patterns across the landscape, it will be important to disentangle these direct and indirect effects, especially if disturbance history decouples the relationship between radiation load and vegetation. To my knowledge, only one other study (Nyman et al., 2015a) has attempted to separate the effects of radiation load and canopy cover on fuel moisture. Their results suggested that the impact of aspect was primarily an indirect effect due to increased vegetation on cooler slopes.

This study will examine the spatial patterns and temporal trends of observed and modelled fuel moisture and fire danger across a heterogeneous forested landscape and address these knowledge gaps. Using hourly resolution data will allow for an analysis of diurnal trends, nocturnal conditions, and the impact of synoptic weather variability on fuel moisture. This chapter will isolate the direct impact of radiation load on fuel moisture. In this study, the isolation of the direct effect of radiation load will be accomplished by (1) choosing sites with homogenous un-

derstory vegetation, (2) sampling across the entire parameter space described by canopy cover and radiation load (see Chapter 3), and (3) focusing on elevated fuel sticks that are not impacted by underlying soil moisture.

As a fire moves across a landscape, the speed and intensity of the propagating front of the fire is dependent, not just on fuel moisture, by also on wind speed, fuel amount, and the slope of the terrain (Rothermel, 1972). Consequently, spatial patterns in fire intensity (the amount of heat released by the fire), and the fire severity (the resulting impact of the fire) will not be entirely dictated by patterns in fuel moisture. For instance, a fire may burn more intensely as it moves up slope, and local wind fields can have a significant impact on patterns as well (McKenzie et al., 2011). However, this chapter will focus on the contribution of fuel moisture to fire danger. To this end, the Energy Release Component (ERC) of the US National Fire Danger Rating System Cohen and Deeming (1985) will be used here as a metric for potential fire danger. The ERC is strongly dependent on fuel moisture, and does not account for the impact of wind speed or the influence of slope on the propagating fire. The ERC is related to the total available energy per unit area that could potentially be released by the fire front and provides an indication of seasonal wetting and drying cycles.

The results from Chapters 3 and 4 suggest a number of possible outcomes for this chapter. (1) It was shown in Chapter 3 that relative humidity, which is the main driver of fuel moisture, was relatively homogeneous during the day, regardless of weather conditions, while the opposite was true at night. One would therefore expect similar homogeneous fuel moisture during the day, with elevated variability at night. (2) During days without rain, open sites had, on average, higher levels of relative humidity, suggesting that open sites may have wetter fuels. (3) It is likely that conditions will be anomalously wet at the outlying Site 22 where there was an elevated water table throughout the season. (4) Given its strong performance as a predictor of near-surface climate, one would expect that canopy gap fraction will be a better predictor of patterns in fuel moisture than radiation load. (5) Model sensitivity analysis in Chapter 4 demonstrated that modelled fuel moisture was primarily driven by relative humidity. Longwave and shortwave radiation had a much smaller secondary influence, suggesting that the impact of the canopy on fuel moisture is primarily an indirect one. That is, changes in canopy cover will

impact near-surface conditions, which, in turn, will impact fuel moisture. Changes in the radiation budget of the stick with a changing canopy will only be a secondary driver of changes in fuel moisture.

This chapter will pursue the following research questions and accompanying hypotheses:

- Research Question #1: How much variability in fuel moisture and fire danger is seen at the landscape scale and how does that variability change with the time of day and with weather conditions?

    - Hypothesis #1a: During the day, fuel moisture and fire danger will be homogeneous. Heterogeneity will increase at night, while Site 22 will be significantly wetter relative to the other sites.

    - Hypothesis #1b: During the day, variability will decrease with increasing solar radiation. Nocturnal spatial variability will be highest during dry, clear-sky conditions with low winds.

- Research Question #2: How do modelled changes in precipitation and/or radiation absorbed by the moisture stick impact fire danger and fuel moisture?

    - Hypothesis #2a: Changes in radiation amounts absorbed by the moisture sticks will have little impact on fire danger.

    - Hypothesis #2b: Changes in precipitation amounts will have a large initial impact, but this influence will recede over the course of around a week.

- Research Question #3: What are the relative impacts of canopy coverage and radiation load on spatial patterns in fuel moisture and fire danger?

    - Hypothesis #3a: Canopy coverage is the dominant factor influencing fuel moisture and fire danger, and this influence is strongest for nocturnal conditions.

    - Hypothesis #3b: Open sites will see wetter fuels relative to closed-canopy sites.

This chapter begins with a description of the methods in Section 5.2, which includes an overview of the data analysis (Section 5.2.1), and a description of both the precipitation and shortwave radiation interception models (Sections 5.2.2 and 5.2.3). Results are presented in Section 5.3, followed by a discussion (Section 5.4) and concluding remarks (Section 5.5)

5.2 Methods

5.2.1 Analysis overview

The fuel moisture model described in Chapter 4 was forced with meteorological observations described in Chapter 2 to model 1-hour, 10-hour, 100-hour, and 1000-hour fuel moisture at all 24 sites. For the 1-hour, 100-hour, and 1000-hour fuel sizes parameter sets optimized to the Oklahoma dataset (Carlson et al., 2007) were used. The 10-hour fuel size was modelled using the parameter set optimized to the Base Station (see Chapter 4).

The model requires relative humidity, temperature, precipitation, shortwave radiation, and wind speed and a sky view factor for each site. Relative humidity and temperature were measured using the LogTag sensors. The influence of the canopy on precipitation, shortwave radiation, and longwave radiation was also modelled. The precipitation and shortwave components of the canopy model are described in the next two sections. These models were forced using observations from the Base Station, which assumes that above-canopy conditions are homogeneous across the sites. As the furthest sites were 1.8 km apart with no significant elevation differences, this estimation should be reasonable. Details of the longwave component of the canopy model were provided in Chapter 4. In order to evaluate the full suite of models, below-canopy fuel moisture simulated at the closed-canopy Fuel Moisture 1 site was compared to observation.

Wind speed was only measured at the Base Station. Although wind speed is reduced within denser canopy (Graefe, 2004), it was shown in Chapter 4 that the fuel moisture model is only weakly sensitive to wind speed. Indeed, at lower moisture levels, wind speed had no discernible impact. Because of this fact, and because there were no below-canopy wind observations to evaluate a potential wind

speed model, wind speed was assumed not to spatially vary across sites.

Potential fire danger was estimated using the ERC, which is a component of the American National Fire Danger Rating System (Cohen and Deeming, 1985) and is an estimate of the maximum amount of heat that could be potentially released by the propagating fire front. The ERC is not dependent on slope, wind speed, or fuel amount and is strongly related to the moisture of all four fuel sizes. In the context of this study the term "potential fire danger" is used synonymously with ERC, and can be considered as the contribution of fuel moisture to potential fire behaviour, independent of the impacts of weather, fuel amounts, or the impact of slope on fire propagation.

The ERC was used by Holden and Jolly (2011) for assessing the heterogeneity of potential fire danger over a large mountainous region. The "G" fuel model was used to calculate the ERC. This choice, which was also made by Holden and Jolly (2011), was based on maps of fuel models provided by www.landfire.gov, which categorized similar forest types within the states of Washington and Oregon as "G" type fuels. As was mentioned in Chapter 4, a 20 day spin-up period was used when modelling 1000-hour fuel moisture to remove any sensitivity to initial conditions. Consequently, modelled ERC presented here begins 20 days after the start of the field season.

To address the first research question regarding spatial variability in fuel moisture and potential fire danger, an analysis similar to that of Chapter 3 was used. Daily anomalies from the intersite mean were calculated for daily maximum and minimum modelled fuel moisture (all sizes) and ERC. Daily standard deviations and maximum ranges were calculated to quantify the spatial variability. Spatial variability in fuel moisture was also assessed using fuel moisture observations at the Base Station, Fuel Moisture 1, and Fuel Moisture 2 sites.

In order to assess the influence of weather conditions, the daily standard deviations were correlated against air temperature, relative humidity, wind speed, shortwave radiation, and Days Since Precipitation. The weather variables were then combined in a multiple regression to create an optimal model of ERC variability. Analysis of Variance was used to determine whether the inclusion of additional variables improved the model. In order to isolate the impact of these weather variables, only days without precipitation were used, as the impact of rain dominates

variability during wet days. As well, the outlier Site 22 was removed from this analysis.

To address the second research question, precipitation interception, shortwave radiation interception, and the impact of the canopy on longwave radiation were removed from the canopy model one at a time before modelling fuel moisture. A fourth simulation removed all three components from the model. These resulting fuel moisture time series were then compared to the original simulation to determine the relative influence of each component. This analysis was performed using Site 4, which had one of the densest canopies. It is important to note here that the same relative humidity and temperature observations were used as inputs into the model. These observed near-surface conditions were, of course, influenced by the canopy as well. Therefore, this analysis separates the direct impact that the canopy has on the fuel moisture stick through changing the incident precipitation and net radiation at its surface, from the indirect impact of the canopy through its influence on near-surface conditions.

The third research question was addressed using a similar analysis to that used in Chapter 3. Longer term averages of fuel moisture and ERC anomalies were calculated over the entire field season for days with and without rain, and for each month. Optimal linear regression models were then developed using canopy gap fraction, radiation load, and their interaction as possible predictors of these average anomalies (see Chapter 3 for further details).

The influence of canopy gap fraction and radiation load was also explored using a Principal Component Analysis (PCA). PCA was applied to the 24 column matrix composed of the ERC time-series from all sites, resulting in 24-element component loading vectors for 24 principal components (PC). Sites with similar component loading values were assumed to have similarly varying ERC time-series. The component loading values of the four leading PCs were then regressed against canopy gap fraction and radiation load to determine if either of those variables were able to isolate similarly varying sites.

5.2.2 Precipitation interception model

Below-canopy precipitation was modelled using a simplified sparse-canopy Rutter model based on the approach of Valente et al. (1997). This model uses a "water-bucket" approach wherein canopy storage is the net result of incident precipitation minus evaporation from the canopy, drainage to the stems, and drainage directly to the forest floor. The canopy is modelled as a water-bucket with a maximum storage capacity. Any additional precipitation above this capacity drains out of the canopy. Above-canopy incident precipitation was assumed to equal the amount measured at the Base Station. Here precipitation is assumed to fall vertically.

Figure 5.1 provides a schematic of the model. Before any interception occurs, a certain amount of the incident precipitation, P_g, falls directly to the forest floor through gaps in the canopy. Once the incident precipitation has entered the canopy, evaporation from the canopy, E_c is calculated as:

$$E_c = \begin{cases} (1-\varepsilon)E\frac{C_c}{S_c} & : C_c < S_c \\ (1-\varepsilon)E & : C_c \geq S_c \end{cases}$$

where E (mm) is the potential evaporation, C_c (mm) is the current amount of canopy storage per unit area of covered area, ε is the fraction of total forest stand evaporation that occurs from the trunk and stems, and S_c (mm) is the canopy storage capacity per unit of covered area, which is calculated as $S_c = S/c$, where S is the canopy storage capacity (in mm) and c is the canopy cover fraction. Both S and ε are adjustable model parameters.
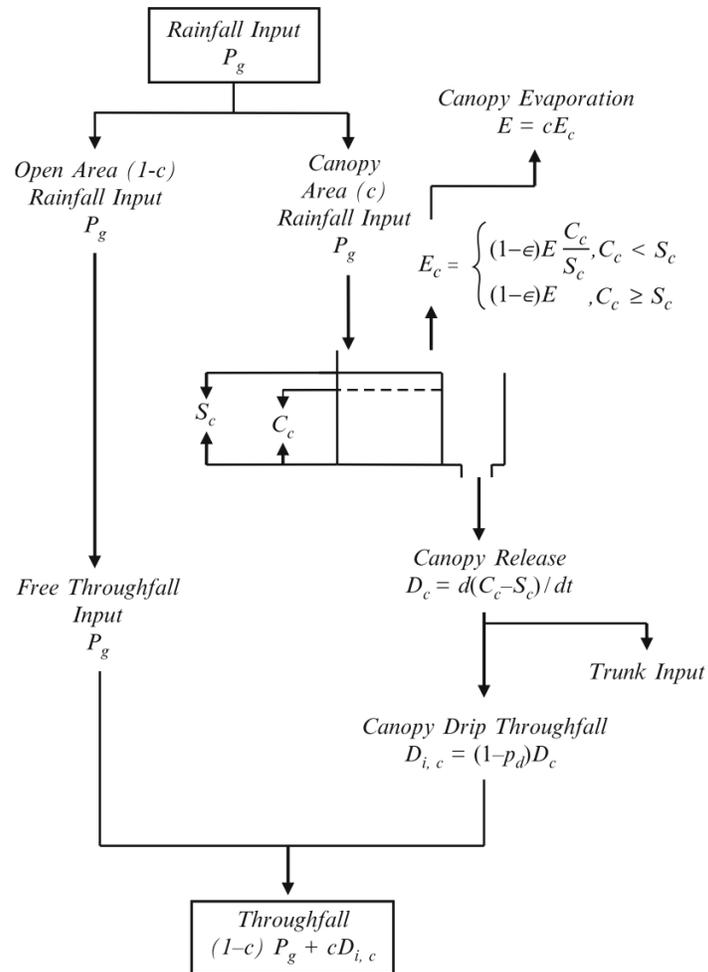
Figure 5.1: Schematic of the rutter precipitation interception model. Adapted from Valente et al. (1997)

The portion of canopy drainage, D_c (mm), that is diverted to stemflow is determined by the stemflow fraction parameter, p_d, which is also an adjustable model parameter. The final precipitation rate at the forest floor, P_f (mm), is the average of the free throughfall and the canopy drip throughfall, $D_{i,c}$ (mm), weighted by the canopy cover fraction:

$$P_f = (1-c)P_g + cD_{i,c} \tag{5.1}$$

The canopy cover fraction, c, was estimated at each site using hemispherical photo analysis described in section 5.2.3. For this application, the canopy coverage was estimated using a minimum angle above the horizon of 85 degrees. That is, it was assumed that only the canopy directly above the gauge contributed to the precipitation at a specific point.

Following Carlyle-Moses and Gash (2011), potential evaporation from the canopy, E, which assumes a saturated canopy, is modelled using a Dalton-type equation:

$$E = \frac{\rho_a c_p}{\lambda \gamma r_a}[e_s^* - e_a] \tag{5.2}$$

where ρ_a (1.225 kg m^{-3}) is the density of air (which is assumed to be constant), c_p (1.00467 $\times$ 10^{-3} MJ kg^{-1} K^{-1}) is the specific heat of air, λ (2.45 MJ kg^{-1}) is the latent heat of vaporisation, γ (0.0665 kPa K^{-1}) is the psychrometric constant, r_a (s m^{-1}) is the aerodynamic resistance, e_s^* is the saturation vapour pressure (kPa), e_a is the ambient vapour pressure (kPa), and $e_s^* - e_a$ is the vapour pressure deficit (kPa) between the saturated canopy and the ambient air. In lieu of direct measurements above the canopy, screen height measurements from the Base Station were used as a replacement for above-canopy conditions.

Aerodynamic resistance is calculated following Rutter et al. (1975):

$$r_a = \frac{1}{k^2 u}\left(ln\frac{z-d}{z_o}\right)^2 \tag{5.3}$$

where k (0.4) is the von Kármán constant, u (m s^{-1}) is the windspeed at height z (m), which is 2 m above the canopy, d is the displacement height, which is taken to be 75% of the canopy height, and z_o is the aerodynamic roughness length, which is taken to be 10% of the canopy height. Canopy height at each site was estimated using the Vegetation Resource Inventory database (https://www.for.gov.bc.ca/hts/vri). The average canopy height of 20 m was used in all cases.

The screen-height wind speed measured at the Base Station, u_{screen}, was interpolated to the above-canopy height, z, using the approach of Rutter et al. (1975):

$$u = ln\left(\frac{z-d}{z_o}\right)\left(0.818 + ln(a+4.75)\right)^{-1} u_{screen} \qquad (5.4)$$

where a is the anemometer height (1.62 m).

There are three adjustable parameters in this model: the maximum canopy storage capacity, S, the proportion of canopy drainage diverted to stemflow, p_d, and the proportion of total stand evaporation that comes from stems and trunks, ε. Average values for S (1.54 mm), p_d (0.05), and ε (0.02) were calculated from values reported by the literature for forest types similar to the study site (Rutter et al., 1975; Whitehead and Kelliher, 1991; Loustau et al., 1992; Klaassen et al., 1998; Spittlehouse, 1998; Iroume and Huber, 2002; Link et al., 2004; Pypker et al., 2005) and used here. Parameter calibration was not attempted as there was only one site with below-canopy precipitation measurements and therefore not enough data to perform accurate model calibration.

Modelled precipitation was compared to observations at Fuel Moisture 2, Site 8, Site 1, and Fuel Moisture 3. The first three sites were assumed to be open locations as there was no canopy coverage for altitudes of 85° above the horizontal at these rain gauges. Consequently, the model assumed that there was no canopy interception, and these sites therefore tested the assumptions that above-canopy precipitation was homogeneous across all sites and that precipitation at a given point on the forest floor is determined only by the amount of canopy directly above. The rain gauge at Fuel Moisture 1 was below the canopy and was used to evaluate the interception model.

Because only one closed-canopy site was used, the skill with which the model predicts spatial patterns in below-canopy precipitation cannot be tested here. However, the sparse-canopy Rutter model is a widely accepted approach and the parameters values used are based on optimal values taken from the literature. Moreover, as will be seen in the results, fuel moisture is relatively insensitive to precipitation amounts, especially during dry periods.

5.2.3 Shortwave radiation interception model

The canopy interception of shortwave radiation was modelled by combining the hemispherical photos described in Chapter 2 with solar geometry calculations following the technique of Moore et al. (2005). As a first step, above canopy radiation is assumed to equal measured radiation at the Base Station and is divided into its direct, (K_{dir}) and diffuse (K_{diff}) components using the procedure detailed in Appendix B. To generate gap fraction as a function of zenith angle, θ, and azimuth, ψ, each hemispherical photo was converted to grayscale and a brightness threshold was chosen to demarcate pixels of open sky from pixels of canopy. The image was then divided into 5° by 5° segments, which were each assigned a gap fraction from the proportion of open sky pixels to total pixels. Figure 5.2 provides examples of both original and processed hemispherical photos.

Time series of the solar zenith and azimuth angle were calculated using the equations of Iqbal (1983). At each time step this information was used to place the sun within a particular 5° by 5° segment of the hemispherical photo. The above-canopy direct radiation was then reduced by that segment's gap fraction to generate a time series of below-canopy direct radiation, $K_{bc,dir}(t)$.

Below-canopy diffuse radiation was modelled using a sky-view factor calculated by integrating $f(\theta, \psi)$ over the the half sphere:

$$f_v = \frac{1}{\pi} \int_0^{2\pi} \int_0^{2\pi} f(\theta, \psi) \cos\theta \sin\theta \, d\theta \, d\psi \qquad (5.5)$$

This integral was estimated numerically using the 5° resolution gap fraction.

The total below-canopy downwelling shortwave radiation was calculated as:

$$K_{bc}(t) = K_{bc,dir}(t) + f_v K_{diff}(t) \qquad (5.6)$$

where $K_{bc}(t)$ is the time series of total below-canopy solar radiation at the forest floor.

The model was evaluated by comparing modelled K_{bc} at Fuel Moisture 1 and 2 to the measured below-canopy shortwave radiation at those two sites. Daily values were used for the evaluation. This choice of resolution was made for a number of reasons. Firstly, hourly values of modelled shortwave radiation are impacted by
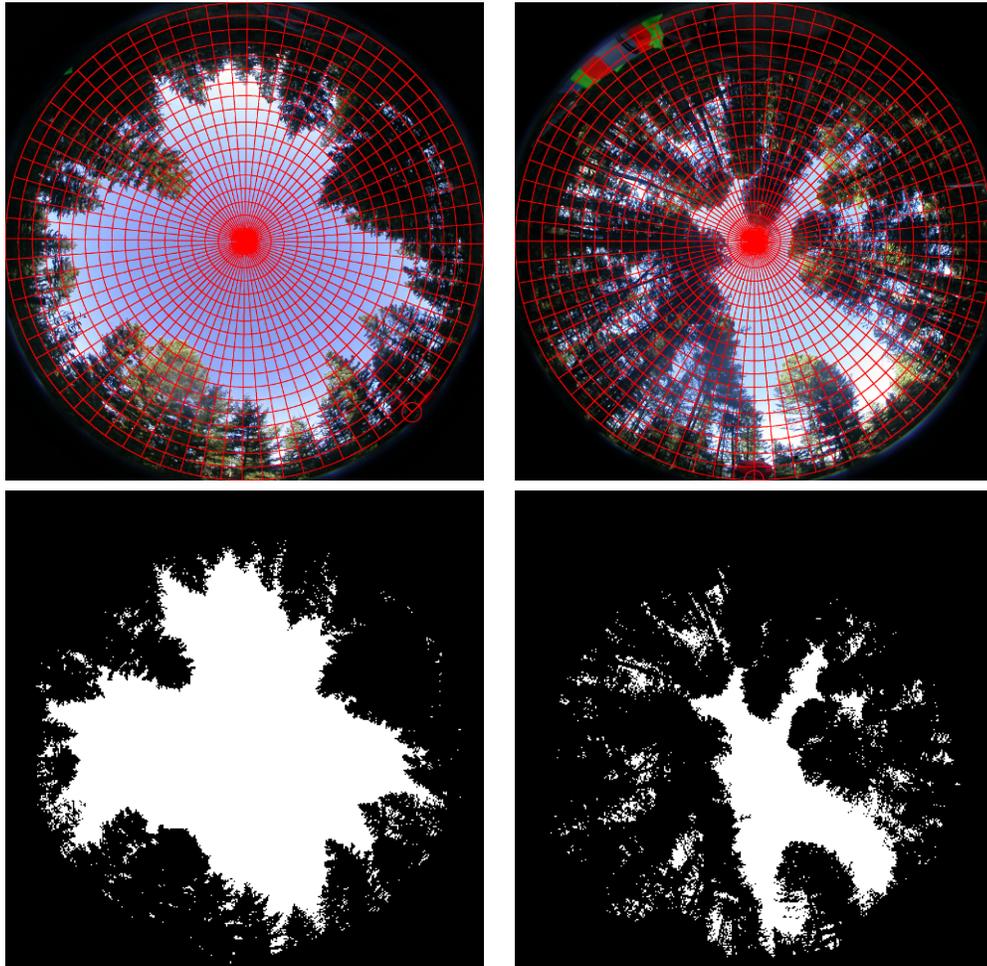
Figure 5.2: Hemispherical photos overlayed with radial grids with a 5 degree resolution (*top row*), and thresholded hemispherical photos (*bottom row*). Examples provided are from Sites 15 (*left column*) and 23 (*right column*).

the location of individual sun flecks and are therefore sensitive to the exact position that the hemispherical photo was taken. In this case, the hemispherical photos were taken directly above the Logtag sensors rather than the pyranometers. Therefore, at the hourly scale, there was a significant amount of model error. However, this model error was reduced at the daily time scale. Secondly, given the slow response time of fuel moisture, it is less important to model hourly variations in radiation than it is to simulate daily and seasonal variability.

The one adjustable parameter in the model is the brightness threshold used to demarcate open sky pixels from canopy pixels. The modelled radiation was found to be sensitive to this threshold. Therefore, for the two evaluation sites, the brightness threshold was adjusted to obtain the lowest model bias, following the procedure of Leach and Moore (2010).

5.3 Results

5.3.1 Model evaluation

Below-canopy precipitation model

Modelled below-canopy precipitation was compared to observations at Fuel Moisture 1, Fuel Moisture 2, Site 8, and Site 1. Model skill statistics are presented in Table 5.1. Scatter plots of modelled versus observed precipitation are shown in Figure 5.3. Both Fuel Moisture 2 and Site 1, which had gauges below open canopy, showed low model biases with RMSE values less than 1 mm, supporting the assumption that precipitation was relatively uniform across the study area. However, the other open site, Site 8, had a large negative model bias. It is not likely that this error was due to an intrinsic bias of the rain gauges, as they were calibrated in the lab. It is also unlikely that the bias was due to a spatial gradient in rainfall intensity, as Site 8 was located within 250 m of Fuel Moisture 2, which did not experience the same bias. It is possible that there was wind-induced undercatch of precipitation at the Base Station (Mekonnen et al., 2015), which was more exposed than Site 8 and consequently likely experienced higher wind speeds. At Fuel Moisture 1, which had a canopy coverage of 57% directly above the rain gauge, the simulated

precipitation had a bias of 0.04 and an RMSE of 0.6 mm. This model accuracy is comparable to the open sites Fuel Moisture 2 and Site 1.

Table 5.1: Precipitation interception model statistics: Coefficient of determination, model bias and root mean square error.

Site	R^2	Bias (mm)	RMSE (mm)
Fuel Moisture 1	0.93	-0.04	0.60
Fuel Moisture 2	0.94	-0.01	0.66
Site 1	0.99	0.01	0.34
Site 8	0.91	-0.36	1.12

Shortwave interception model

The optimal brightness threshold that minimized the error in modelled below canopy shortwave radiation at Fuel Moisture 1 was 210. For Fuel Moisture 2, model bias decreased as the brightness threshold increased. However, once the brightness threshold was increased beyond 141, portions of the open sky began to be incorrectly masked out as "canopy." Therefore, 141 was used as the optimal brightness threshold for Fuel Moisture 2. For all other sites, 210 was used as the optimal brightness threshold unless the same incorrect masking of the open sky occurred. If this erroneous masking did occur, the optimal threshold was taken to be the highest possible value before the masking of open sky occurred.

Modelled below-canopy shortwave radiation was compared to observations at Fuel Moisture 1 and Fuel Moisture 2. Model skill statistics are presented in Table 5.2. Time series and scatter plots of modelled and observed shortwave radiation are shown in Figures 5.4 and 5.5, respectively. The model accuracy was high for Fuel Moisture 2. The bias was -3.4 Wm^{-2}, or 2% of the seasonal average, while the RMSE was 9.9 Wm^{-2}. Model bias at Fuel Moisture 2 became more negative as the season progressed. Figure 5.5 demonstrates that, as previously discussed, the model did a substantially better job at simulating daily data than hourly data. The larger scatter of hourly observations is likely due to the fact that the hemispherical photos were taken above the LogTag sensors, and not the pyranometer. The two locations would have experienced slightly different insolation at short time scales
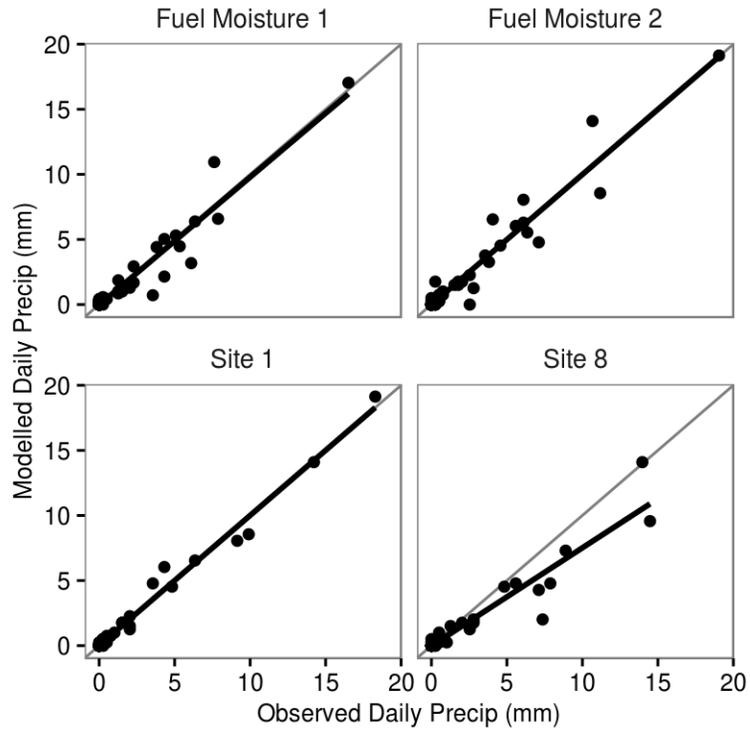
Figure 5.3: Scatter plots of daily modelled and observed precipitation. Regression lines are provided (*Black Lines*), and 1:1 lines are provided for reference (*grey lines*).

as sun flecks moved across the forest floor. The model was less accurate for Fuel Moisture 1. However, the model bias of -7.0 Wm^{-2}, was still only 9% of the seasonal average.

Table 5.2: Shortwave interception model statistics: Coefficient of determination, model bias and root mean square error.

Site	R^2	Bias (Wm^{-2})	RMSE (Wm^{-2})
Fuel Moisture 1	0.86	-7.03	12.87
Fuel Moisture 2	0.99	-3.44	9.88
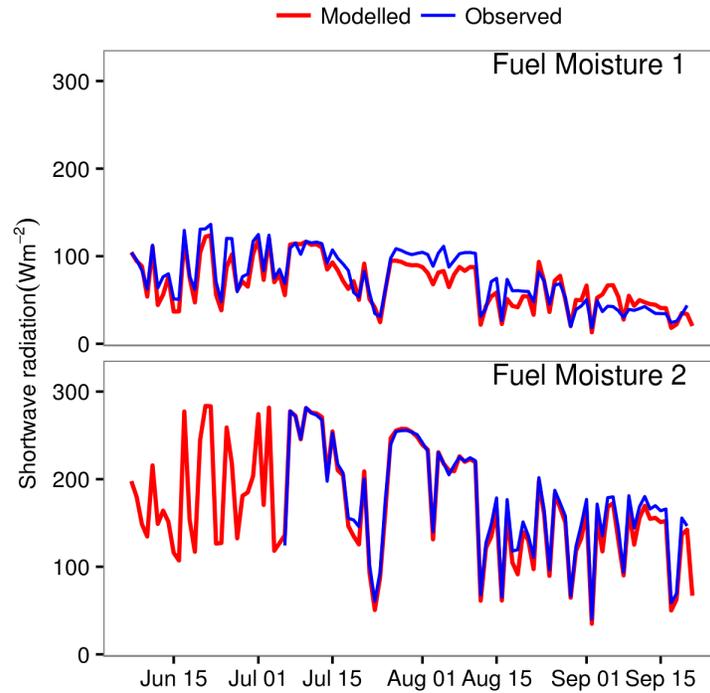
Figure 5.4: Time series of modelled and observed daily shortwave radiation at Fuel Moisture 1 and Fuel Moisture 2.

Combined model of below-canopy fuel moisture

A two-month sample of modelled and observed fuel moisture at Fuel Moisture 1 is presented in Figure 5.6, while a scatter plot of the entire season's data is provided in Figure 5.7. Overall, the model accurately simulated the seasonal pattern of fuel moisture. Model accuracy improved with decreasing moisture content. The model had a bias of -1.4%, an RMSE of 4.3% and an R^2 of 0.88. For moisture below 30% the bias and RMSE decreased to -0.5% and 2.1%, respectively, while the R^2 decreased to 0.85. Much of the error during the drier periods was due to larger simulated diurnal cycles, particularly during early August.
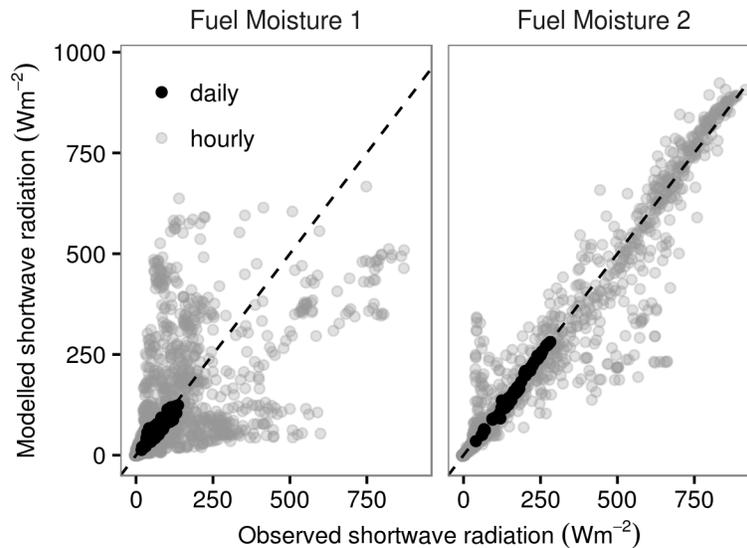
Figure 5.5: Scatter plots of modelled and observed hourly and daily short-wave radiation at Fuel Moisture 1 and Fuel Moisture 2. A 1:1 line is included for reference (*dashed line*).

5.3.2 Spatial variability of fuel moisture and fire danger

Observed 10-hour fuel moisture from the Base Station, Fuel Moisture 1, and Fuel Moisture 2 is presented in Figure 5.8 as hourly (5.8A), daily maximum (5.8B), and daily minimum values (5.8C). Overall, the three stations maintained similar moisture levels throughout the season, particularly during the day when conditions were dry. However, Fuel Moisture 1 had a dry nocturnal bias and smaller diurnal variability during dry conditions. Consequently, the fuel sticks were, on average, wetter at the the open sites.

A sample of hourly modelled 1-hour fuel moisture, 1000-hour fuel moisture, and ERC is presented in Figure 5.9. The same sites highlighted in Chapter 3 are also highlighted here: the south-facing open canopy Fuel Moisture 2 site, the north-facing closed-canopy Site 4, and the anomalously wet Site 22. Similar to observed fuel moisture, all 24 sites had similar seasonal trends in modelled fuel moisture as well as ERC, and nocturnal differences were larger than during the day. The open canopy south-facing Fuel Moisture 2 site exhibited wetter fuels and lower

ERC at night than the closed-canopy Site 4. As the sites dried out during the day, the 1-hour fuel moisture responded quickly and became drier at the open site during the day, while the more slowly varying 1000-hour remained consistently wetter at the open site; the nocturnal cooling overwhelmed the daytime heating for the larger fuel size. Although not shown here, daytime 10-hour and 100-hour fuel moisture were also higher at open sites. Consequently, daytime ERC was often similar between the open and closed sites. Finally, the moist Site 22 had a consistently low ERC, particularly during the day. Site 22 and Fuel Moisture 2 experienced similar nocturnal conditions, despite the large differences in canopy cover.

Spatial heterogeneity across stations is explored in more detail in Table 5.3. Fuel moisture and ERC were consistently more homogeneous during the day than at night, and larger fuels were less variable than smaller fuels. Precipitation increased variability, particularly for the smaller fuels.

Table 5.3: Daily standard deviation (SD) and maximum range (Range) of daily minimum and maximum 1-hour fuel moisture (1-h_{min} and 1-h_{max}), 1000-hour fuel moisture (1000-h_{min} and 1000-h_{max}), and ERC (ERC_{min} and ERC_{max}) averaged across each month and across all days with and without rain.

Period	ERC_{max} Range	SD	ERC_{min} Range	SD	1-h_{max} (%) Range	SD	1-h_{min} (%) Range	SD	1000-h_{max} (%) Range	SD	1000-h_{min} (%) Range	SD
May					21.4	5.4	5.8	1.6				
June	9.4	2.1	18.0	4.5	17.0	4.4	2.3	0.6	2.0	0.5	1.6	0.4
July	11.8	2.6	15.5	4.0	10.8	2.7	3.8	0.9	1.9	0.5	1.7	0.4
Aug.	12.9	2.6	18.1	4.8	19.7	5.0	3.5	0.8	2.1	0.5	2.0	0.4
Sept.	14.9	3.6	20.1	5.1	21.9	5.0	5.7	1.3	2.6	0.7	2.3	0.6
Dry Days	11.9	2.6	17.9	4.6	14.2	3.6	2.8	0.7	2.0	0.5	1.9	0.4
Rain Days	12.5	2.8	17.3	4.5	24.4	6.0	6.3	1.5	2.3	0.7	1.9	0.4
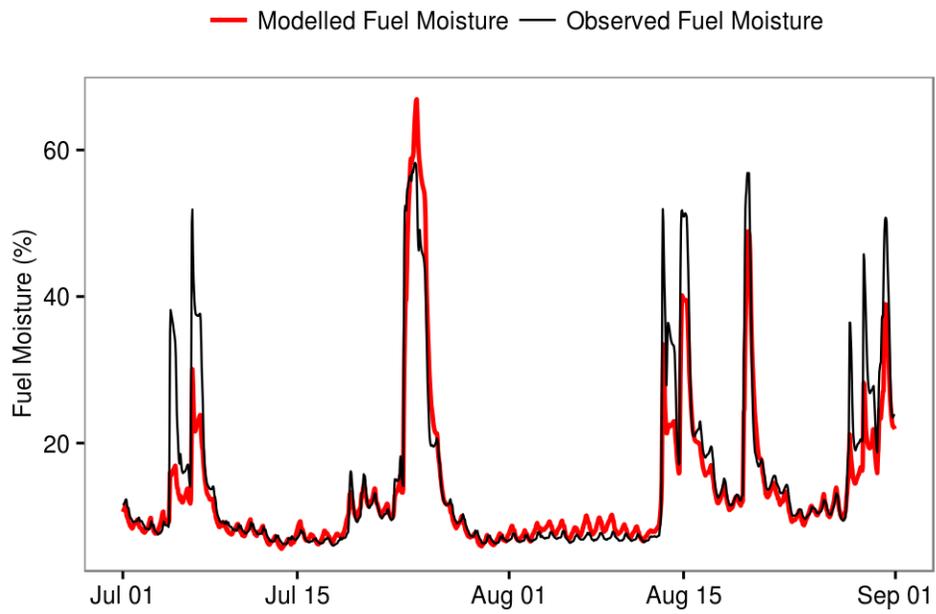
Figure 5.6: Two months of modelled and observed fuel moisture for the Fuel
Moisture 1 site using the precipitation and radiation canopy interception
models and the fuel moisture model.
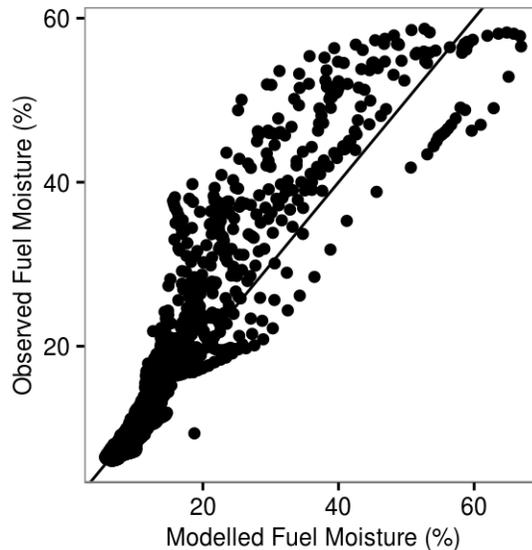
Figure 5.7: Scatter plot of modelled and observed fuel moisture for the Fuel Moisture 1 site using the precipitation and radiation canopy interception models. Data from the entire season are used here. A 1:1 line has been added for reference (*black line*).

Afternoon and early morning ERC time-series are shown in Figure 5.10 and are compared to the ERC climatology for Sparks Lake, which was located at a standard open site. The reduced variability in daytime ERC is evident here. Daytime fuel moisture at Site 22 decreased at a slower rate than the other sites. During the driest periods, the nocturnal spread across sites was comparable to the difference between the median and 95th percentile modelled at the open Sparks Lake site. Again, apart from Site 22, there is less spread in daytime ERC.

Daily standard deviations of minimum and maximum ERC are plotted against weather variables in Figure 5.11. Changes in the spatial variability of daytime potential fire danger were correlated only with wind speed at the 95% confidence level; higher wind speeds led to a more homogeneous landscape. Nocturnal fire danger variability was most strongly correlated with wind speed and relative humidity. At night the landscape was more homogeneous during days with high relative humidity and low wind speed. Temperature, shortwave radiation, and Days Since Rain were all negatively related to nocturnal ERC variability, although these

correlations are weak. Modelling the standard deviation of nocturnal ERC with maximum relative humidity and wind speed resulted in an R^2 value of 0.46. The addition of the remaining variables did not improve model performance at the 95% confidence level.

5.3.3   Influence of canopy cover on below-canopy fuel moisture

The impact of removing components of the canopy model on fuel moisture is presented in Figure 5.12. When the canopy did not absorb or emit longwave radiation, fuel moisture increased. In contrast, removing shortwave canopy interception led to dry biases. As would be expected, removing precipitation interception led to wet biases. Overall, the largest biases occurred during and immediately after rain, particularly for the smaller fuel sizes. For the 1-hour fuels, these biases disappeared almost immediately after rain, but the 1000-hour fuel remained anomalously wet for at least ten days following rain. When the canopy was removed entirely, the influence of the increased shortwave radiation was generally larger than both the decreased longwave and increased precipitation, leading to a dry bias overall. An exception was during periods of rain or low amounts of shortwave radiation.

The impact of canopy removal on ERC is presented in Figure 5.13. The removal of shortwave interception from the model increased the ERC by 7.0 on average, which is a mean relative bias of 13.1%. During periods of high ERC the bias decreased to around 5. Removing the canopy impact on longwave radiation decreased ERC on average by -4.0 (-7.4%). Removing precipitation interception decreased the ERC on average by -2.0 (-3.6%). The decrease in ERC due to increased precipitation was only comparable to the radiation terms during and immediately following periods of rain. When the influence of the canopy was removed entirely, the ERC bias was almost always positive with an average ERC bias of 1.9 (3.5%). The one exception was during a period of persistent rain in late August and early September.

5.3.4 Modelling spatial patterns in fuel moisture and potential fire danger with canopy cover and radiation load

The results of the model selection procedure are provided in Table 5.4. Canopy gap fraction was almost always the best single predictor and the addition of radiation load as a second predictor only improved the model (at the 95% confidence level) for daytime 1-hour fuel moisture. Daytime ERC and 1000-hour fuel moisture were not significantly related to either canopy gap or radiation load. Overall, the strongest models were for daytime and nocturnal 1-hour fuel moisture. Nocturnal ERC was also relatively well predicted. Spatial patterns were generally poorly predicted during periods of rain.

Conditions were wetter at more open sites during the night. Daytime 1-hour fuel moisture was lower at open sites, while canopy gap did not impact daytime 1000-hour fuel moisture. Although not shown in Table 5.4, both 10-hour and 100-hour fuel moisture had weak positive relationships with canopy gap during the day, suggesting that only the smallest fuel size dried quickly enough to recover from the wetter nocturnal conditions. Daytime 1-hour fuel moisture was also lower on south-facing slopes. This relationship was particularly strong at the end of the fire season in September. Daily mean fuel moisture was generally higher and ERC lower at open sites.

The first PC of the ERC time series reflected the average seasonal trend in ERC. Canopy gap fraction was weakly correlated with the loading values of the first PC ($R^2 = 0.31$). Loading values of the second PC were strongly correlated with canopy gap fraction with an $R^2 = 0.84$ (Figure 5.14). Radiation load was weakly correlated with the second PC ($R^2 = 0.31$), but did not improve predictive skill (at the 95% confidence level) when added as a second predictor along with canopy gap fraction. The two predictors were not significant predictors of any of the higher PCs.

Apart from the outlier Site 22, the sites with the three lowest and three highest PC2 loading values also had the highest and lowest canopy gap fraction. These six sites are highlighted in Figure 5.15, in which two months of ERC data are presented. The closed-canopy sites (high PC2) saw smaller changes in ERC over the day compared to the open canopy sites (low PC2).

5.4 Discussion

Overall, daytime fuel moisture and potential fire danger exhibited low spatial variability, regardless of weather conditions, and daytime ERC was not related to either radiation load or canopy cover. Fuel moisture and fire danger were more variable at night and that variability increased during cool, moist periods with low wind speeds. Patterns in fuel moisture and fire danger were dominated by differences in nocturnal longwave cooling due to changes in canopy cover. Consequently, open sites had lower daily minimum and daily mean fire danger, and radiation load did not have a significant impact on ERC.

As mentioned in the introduction of this chapter, the ERC, which is used here as a metric for fire danger, does not include the impact of slope, wind speed, or fuel amounts on fire behaviour. Rather, the ERC represents the seasonal cycle of fire danger due to the drying and wetting of fuels. Consequently, patterns in the fire behaviour and resulting fire effects of an individual fire will also be dictated by variability of the wind field, and patterns in fuel amounts. For instance, wind speeds are generally lower below dense canopy (Oke, 1990), which may counteract the elevated ERC found under denser stands. As well, even though ERC was not related to aspect, warmer, south facing aspects may experience increased upslope flows and more intense fire behaviour. Landscape patterns in fuel type and amount are also impacted by stand density, slope, and aspect, and can also impact patterns in fire behaviour (McKenzie et al., 2011). However, fuel moisture is an important driver of fire behaviour (Rothermel, 1972), and the patterns in ERC that have been presented here will likely play an important role in determining both the behaviour of an individual fire, as well as the pattern of long-term fire potential or burn likelihood.

5.4.1 Spatial variability of fuel moisture and potential fire danger

Nocturnal variability was higher than daytime variability, consistent with Hypothesis #1a. Excluding Site 22, variability in daytime conditions was small relative to the interannual variability recorded at the Sparks Lake fire weather station (see Figure 5.9). These results suggest that, apart from areas with an additional source of moisture due to a higher water table (such as Site 22), the study landscape dries

out during the day at a similar rate following rain, regardless of canopy cover or aspect.

During dry periods, open canopy sites had moist nocturnal conditions similar to median conditions modelled at Sparks Lake, while nocturnal conditions at the dry closed canopy sites were comparable to the station's most extreme years (see Figure 5.10). The average difference in ERC between the driest and wettest site ranged from 15 to 20, depending on the time of year. This range can be compared to the results of Holden and Jolly (2011) who modelled daily ERC over a larger mountainous region (>400 km^2) with an elevational range of over 1400 m. In their study, the range of ERC across the study region was comparable to what was found here. Therefore, the current study demonstrates that, at the landscape scale, variability in nocturnal fire danger can be significant for areas with a mosaic of canopy cover.

Hypothesis #1a also correctly predicted the wet conditions exhibited by Site 22. These results suggest that locations with a supply of subsurface moisture will have a relatively cool, wet near-surface climate that, in turn, will lead to reduced potential fire danger relative to surrounding areas. Previous work supports this conclusion. Duff moisture is generally higher at the bottom of hillslopes (Samran et al., 1995; Keith et al., 2010b; Vo, 2001), and Camp et al. (1997) found that fire refugia were most likely to occur in regions with a large contributing upslope area, such as regions of confluence, over perched water tables, and within valley bottoms.

Overall, variability in modelled daytime ERC was not strongly related to weather variables (Figure 5.11). This is not unexpected, as the spatial variability across sites during the day is low (see Table 5.3. Wind speed was the one variable with a significant but weak impact on the spatial variability of ERC: variability was lower on windier days. Based on the results of Chapter 3, Hypothesis #1b incorrectly predicted that increased solar radiation would lead to increased daytime ERC variability. However, it is possible that increased modelling accuracy would have revealed such a relationship.

The low variability in daytime fuel moisture and ERC reiterates what was found in previous studies (e.g., Chrosciewicz 1989; Whitehead et al. 2006; Faiella and Bailey 2007; Estes et al. 2012; Banwell et al. 2013). These studies also sug-

gested that daytime variability is higher during moist conditions and following rain. In contrast, the results of the current study suggest that, during the day, the spatial variability of ERC is relatively insensitive to weather conditions.

Hypothesis #1b predicted that, as was found for relative humidity and temperature in Chapter 3, ERC would also become less variable during cool and moist conditions. However, these results found the opposite: nocturnal ERC variability is highest during cool, moist conditions. Unlike near-surface climate, the amount of below-canopy precipitation directly impacts fuel moisture and ERC. From Figure 5.13 it is clear that the impact of precipitation on ERC persists for around a week. Therefore, it is likely that variations in canopy interception across sites led to higher nocturnal variability in ERC. Indeed, when precipitation interception was removed from the model, relative humidity lost much of its impact on nocturnal ERC variability and the negative relationship with Days Since Rain disappeared completely.

Increased wind speed reduces nocturnal variability in ERC. It is likely that this relationship was not due to the direct impact of wind speed on the fuel stick, as Chapter 4 demonstrated that this impact was small. Rather, wind speed primarily influences fuel moisture and ERC indirectly though its impact on near-surface conditions. Indeed, nocturnal relative humidity was also more homogeneous during days with high wind speeds (see Chapter 3).

5.4.2   Influence of canopy cover on below-canopy fuel moisture

Setting the canopy to be transparent to longwave radiation decreased the energy absorbed by the stick. When the stick was saturated immediately following rain, this reduction in net radiation reduced the amount of energy available for evaporation, leading to wet fuels. When the stick was below the fibre saturation point and sorption processes dominated, the decreased longwave radiation led to lower stick temperatures, which, in turn, led to higher equilibrium moisture content and higher moisture overall (see Figure 5.12). The opposite was true for shortwave radiation; removing shortwave interception led to a dry bias relative to the full model. It is clear from Figure 5.12 that biases due to changes in radiation interception were much larger during wet periods following precipitation. Resistance to moisture re-

moval increases as the stick dries out. Consequently, changes in the energy budget have the most impact on fuel moisture during wetter periods.

Removing shortwave radiation interception by the canopy led to an average ERC bias of 7.0, which is comparable to, or larger than, the average spatial anomalies reported in Table 5.3. Therefore, in contrast to what was predicted in Hypothesis #2, the impact of changing a stick's radiation budget is not negligible. However, it is still of secondary importance compared to the impact of near-surface relative humidity (See Chapter 4).

It was hypothesized that precipitation would have a large impact during rain events, but that this impact would recede over the course of a week after rain ceased. It was indeed the case that the wet bias due to increased precipitation was largest during rain events and that this bias decreased over the course of a week. However, in most cases increased precipitation had a smaller impact than changes to the radiation components, and the ERC was lowered by less than 5 units, or on the order of a few percentage points of relative change. The impact of changing below-canopy precipitation was largest during a period of moderate but persistent rain in late July and early August, suggesting that the duration of a rain event is more important than rain amount. This is because persistent low-intensity precipitation will readily be intercepted and evaporated from the canopy.

The simulated removal of the dense canopy from Site 4 increased daily precipitation by, on average, 1.0 mm, which, in turn, decreased the average ERC at the site by 3.6% but had little impact on ERC during dry periods. The average error for the precipitation interception model was less than 0.66 mm (Table 5.1). Therefore, the accuracy of the model was high enough for the purpose of simulating potential fire danger, especially during extended dry periods. The same reasoning extends to the shortwave interception model. Removing the canopy from Site 4 increased the average shortwave radiation by 180 W m^{-2}, leading to an ERC bias of 13%. The much smaller errors of the interception model (Table 5.2) would therefore result in only minor errors in ERC. Based on these comparisons, it is likely that the complexity of both interception models could be reduced without diminishing the accuracy of modelled potential fire danger, especially during dry conditions, and if observations of near-surface humidity and temperature are available.

5.4.3 Modelling spatial patterns in fuel moisture and potential fire danger with canopy cover and radiation load

Based on the results from Chapter 3, it was predicted in Hypothesis #3a that canopy cover would be the dominant factor in determining spatial patterns in fuel moisture and potential fire danger. This hypothesis has been confirmed here. Apart from 1-hour fuel moisture, canopy gap fraction was the best single predictor, and radiation load did not improve the models when added as a second predictor. The dominant impact of canopy cover was reiterated by the PCA. Canopy cover is the most important determinant of diurnal variability in ERC. These results demonstrate that the direct impact of aspect on fuel moisture through changes in radiation load is likely secondary to the indirect impact of increased canopy cover. This conclusion was also reached by Nyman et al. (2015a), who found that the impact of aspect was primarily an indirect effect due to increased vegetation on cooler slopes.

It was also hypothesized that predictive skill would be larger during the night. This prediction was true for the 1000-hour fuel moisture and ERC, neither of which were related to either factors during the day. However, the daytime and nocturnal 1-hour fuel moisture models were equally skillful.

Only the 1-hour fuel size was drier at open sites and south-facing slopes during the day. In fact, daytime 10-hour and 100-hour fuel moisture was higher at open sites. Consequently, as predicted in Hypothesis #3b, open sites had, on average, higher modelled fuel moisture and lower potential fire danger, although the relationships were weak with relatively low R^2 values. Observed 10-hour fuel moisture was also wetter at open sites.

There are a number of possible reasons why ERC was lower at open sites. Firstly, an examination of Figure 5.9 suggests that, because of their longer response times, the larger fuel sizes were not able to dry out quickly enough at open sites to reverse the nocturnal pattern when fuels were wetter at open sites. In contrast, 1-hour fuel moisture responded quickly enough so that it mirrored the daytime relative humidity patterns seen in Chapter 3, with drier conditions at open sites and south-facing slopes. Secondly, Chapter 3 demonstrated that canopy gap fraction had a much larger impact on relative humidity patterns at night, and that daily mean absolute humidity was also higher at open sites. Thirdly, Figure 5.12 demonstrated that 100-hour and 1000-hour fuel moisture were elevated for a few days follow-

ing rain. Consequently, precipitation patterns may have counteracted patterns in daytime solar radiation and enhanced patterns in nocturnal cooling for these larger fuels. It is possible that previous results pointing to a small or insignificant impact of canopy cover on fuel moisture (Faiella and Bailey, 2007; Estes et al., 2012; Banwell et al., 2013) could be explained by this counteracting effect of solar heating and nocturnal cooling.

5.5 Conclusions

Canopy interception models of precipitation and shortwave radiation were reasonably accurate, especially for the purpose of modelling below-canopy fuel moisture. The suite of models developed here was able to accurately simulate the observed seasonal trends in below-canopy fuel moisture. The models produced a bias of 1.4%, and RMSE of 4.3% and an R^2 of 0.88, although these results improved during dry periods.

Compared to longwave radiation and precipitation, shortwave radiation had the strongest direct impact on fuel moisture. Precipitation interception had the smallest impact on fuel moisture and ERC, especially during dry periods. The impact of precipitation became negligible around a week following rain. As previously mentioned, it is important to note this analysis separates the direct impact that the canopy has on the fuel moisture stick through changing the incident precipitation and net radiation at its surface, from the indirect impact of the canopy through its influence on near-surface conditions.

Both observed and modelled fuel moisture and potential fire danger were relatively homogeneous across the landscape during the day; daytime variability in modelled fuel moisture was comparable to the model error. This lack of daytime variability agrees with previous studies and may be a result of the counteracting effects of nocturnal cooling and increased precipitation versus daytime solar heating. Daytime ERC variability was not strongly influenced by weather conditions. This result is in contrast to previous studies, which generally concluded that the impact of canopy cover on fuel moisture is diminished during dry periods. While daytime 1-hour fuel moisture was related to canopy cover and radiation load, patterns in daytime ERC were not related to either canopy cover or radiation load. At

the anomalously moist Site 22, an elevated water table likely contributed to low ERC throughout the season.

Fuel moisture and potential fire danger were more variable at night. Compared to a climatology of ERC modelled at a nearby long term station, the wettest sites were comparable to a median season, while the driest sites had ERC levels similar to the 95th percentile. The variability in nocturnal ERC was comparable to the variability in average ERC found across a much larger mountainous region (Holden and Jolly, 2011), suggesting that a mosaic of canopy cover can lead to significant variability in nocturnal ERC at the landscape scale.

Nocturnal fire danger was also more strongly influenced by weather conditions. Specifically, the landscape became more variable during cool and moist periods, and during periods with low wind speeds. This is in contrast to the near-surface climate which was relatively homogeneous during cool and moist conditions. The difference is likely due to variations in below-canopy precipitation, which has a stronger, direct impact on fuel moisture. Spatial patterns in nocturnal ERC and fuel moisture were correlated with canopy cover but not radiation load. These correlations were strongest for the smaller fuel sizes.

Overall, open sites saw significant nocturnal longwave cooling and increased precipitation. Because these impacts persisted within the slowly varying larger fuels, fuel moisture and ERC patterns were dictated by canopy cover with wetter average conditions at open sites. Only the 1-hour fuel size reacted quickly enough to mirror the drier and warmer daytime conditions at open sites and south-facing slopes. Finally, these results demonstrate that the direct impact of aspect on fuel moisture through changes in radiation load is likely secondary to the indirect impact of increased canopy cover.

The assessment of spatial patterns in potential fire danger presented here was limited to point measurements across a small field site. This analysis will be extended to a larger scale in the following chapter, where the suite of models presented here will be used to generate high-resolution rasters of ERC across a large (140 km^2) region with a significant elevational gradient. This approach will allow for a comparison of the relative influence of not just radiation load and canopy cover, but elevation as well. Moreover, simulating high-resolution rasters will allow for a more detailed analysis of patterns in ERC to determine if there are patches

within the landscape that remain moist relative to their surroundings.

Table 5.4: Results of model selection. Standardized regression coefficients are shown in the Canopy Gap and Rad Load columns. Bold values indicate the predictor with the strongest single variable model as determined by the coefficient of determination. Missing values indicate that the addition of the predictor did not substantially improve the model performance. The standard error of the estimate is also provided in units of the predictand (ERC: unitless, FMC: %).

Predictand	Period	Canopy Gap	Radiation Load	R^2	Std. Error
ERC_{min}	All Dry Days	**-0.86**		0.72	2.35
1-h FM_{max}	All Dry Days	**0.89**		0.78	1.40
1000-h FM_{max}	All Dry Days	**0.69**		0.46	0.30
ERC_{max}	All Dry Days				
1-h FM_{min}	All Dry Days	**-0.61**	-0.43	0.78	0.23
1000-h FM_{min}	All Dry Days				
ERC_{mean}	All Dry Days	**-0.7**		0.46	1.76
1-h FM_{mean}	All Dry Days	**0.84**		0.70	0.51
1000-h FM_{mean}	All Dry Days				
ERC_{min}	All Rain Days	**-0.68**		0.43	3.13
1-h FM_{max}	All Rain Days	**0.64**		0.39	3.74
1000-h FM_{max}	All Rain Days	**0.54**		0.25	0.52
ERC_{max}	All Rain Days				
1-h FM_{min}	All Rain Days	**-0.77**		0.58	0.56
1000-h FM_{min}	All Rain Days				
ERC_{mean}	All Rain Days	**-0.5**		0.21	2.53
1-h FM_{mean}	All Rain Days				
1000-h FM_{mean}	All Rain Days				
ERC_{min}	June	**-0.73**		0.51	2.96
1-h FM_{max}	June	**0.84**		0.68	2.05
1000-h FM_{max}	June				
ERC_{max}	June				
1-h FM_{min}	June	**-0.68**	-0.33	0.79	0.19
1000-h FM_{min}	June				
ERC_{mean}	June	**-0.45**		0.16	2.21
1-h FM_{mean}	June	**0.74**		0.53	0.80
1000-h FM_{mean}	June				
ERC_{min}	September	**-0.8**		0.63	3.25
1-h FM_{max}	September	**0.78**		0.58	3.10
1000-h FM_{max}	September	**0.67**		0.42	0.51
ERC_{max}	September				
1-h FM_{min}	September		**-0.75**	0.54	0.53
1000-h FM_{min}	September				
ERC_{mean}	September	**-0.66**		0.40	2.89
1-h FM_{mean}	September	**0.64**		0.39	1.50
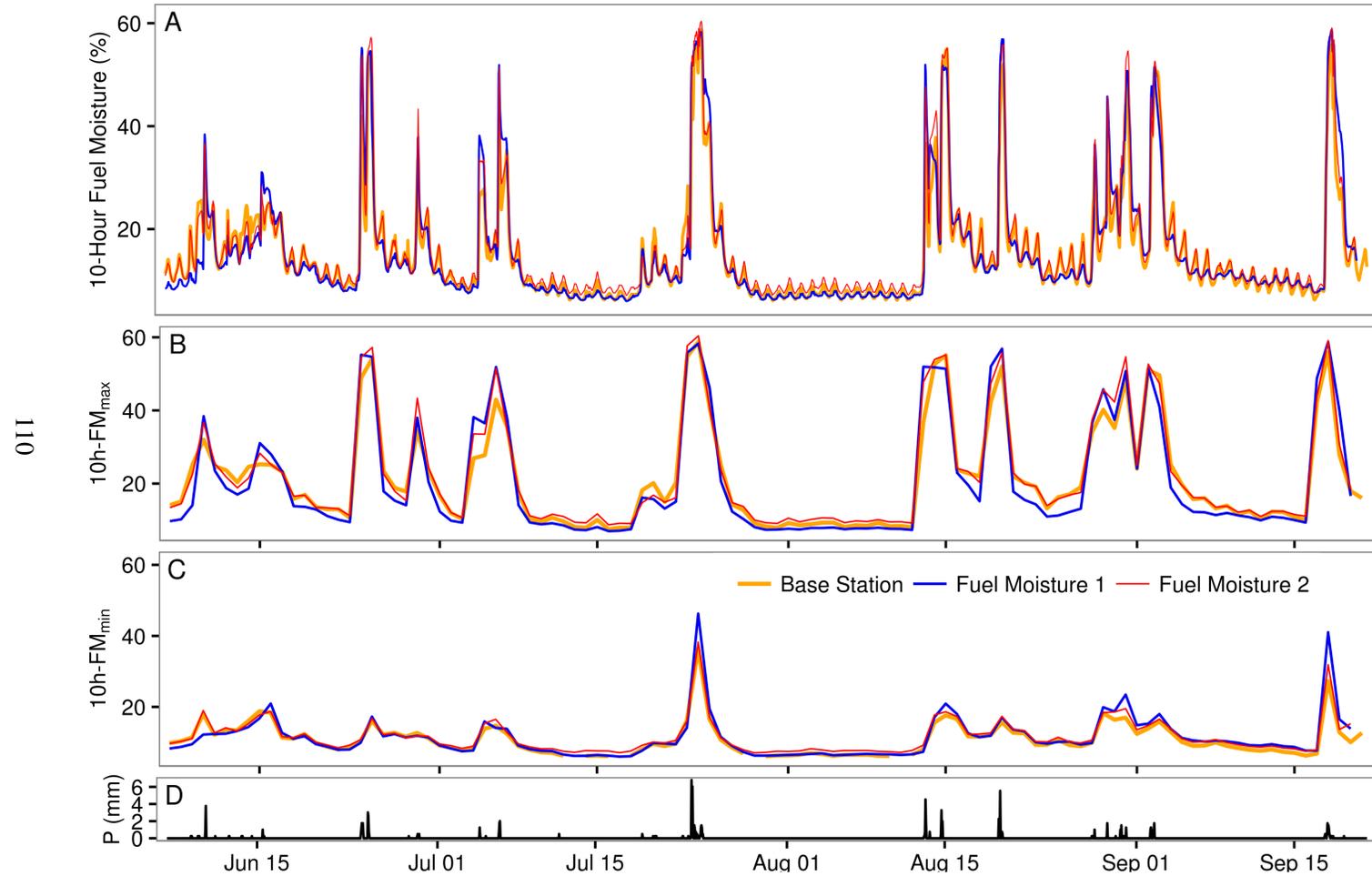
Figure 5.8: Observed hourly 10-hour fuel moisture at all three sites (*A*), along with daily maximum (*B*) and daily minimum (*C*) values. Observed precipitation at the Base Station is also provided (*D*).
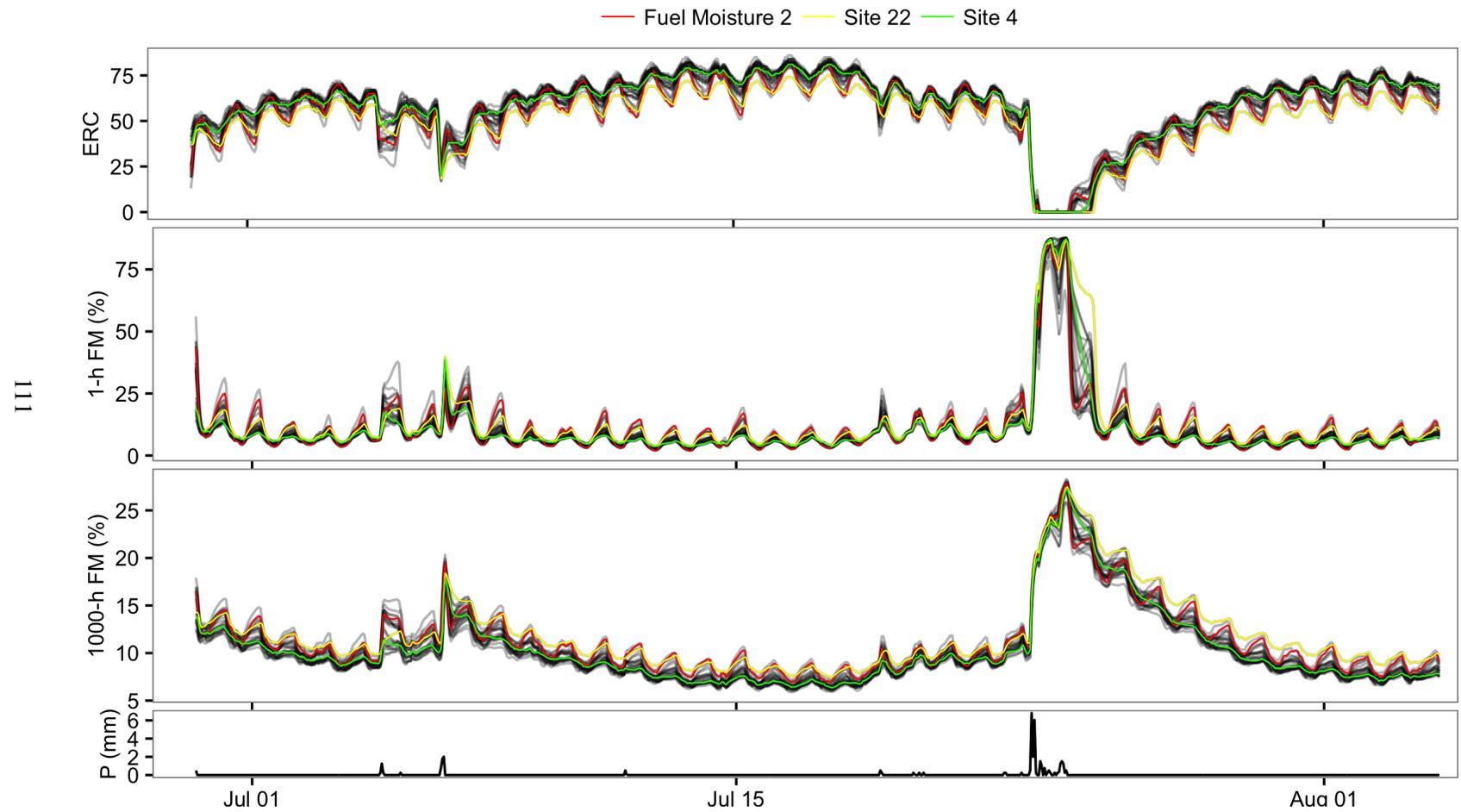
Figure 5.9: A sample of modelled hourly 1-hour and 1000-hour fuel moisture, modelled ERC for for all sites (*grey lines*), and observed precipitation at the Base Station. Fuel Moisture 2, Site 22, and Site 4 are highlighted.
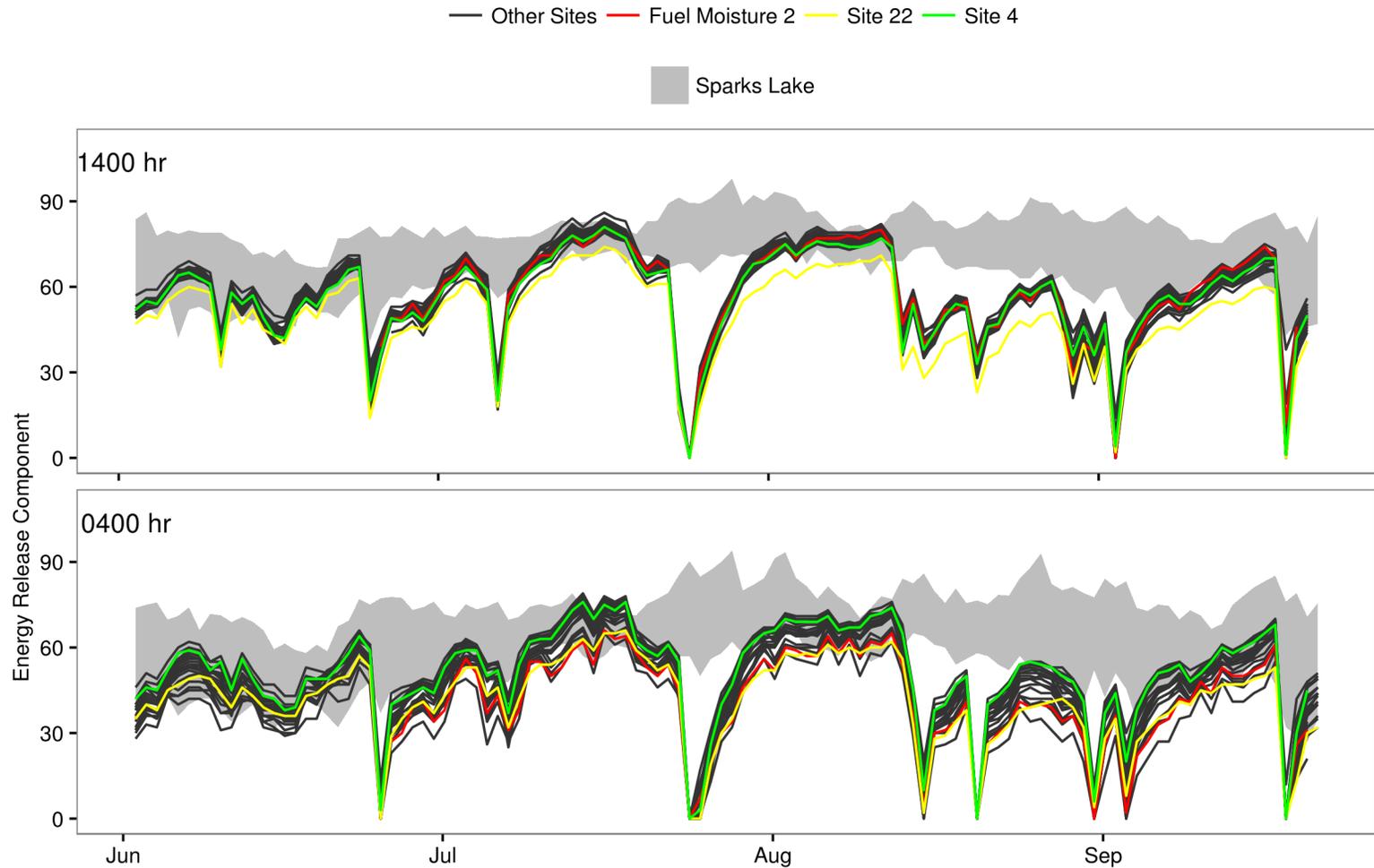
Figure 5.10: Daytime and night-time ERC for all sites. As in Figure 5.9, Fuel Moisture 2, Site 22, and Site 4 are highlighted. The *grey ribbon* indicates the range between the median and 95th percentile ERC calculated at the Sparks Lake station over 26 seasons.
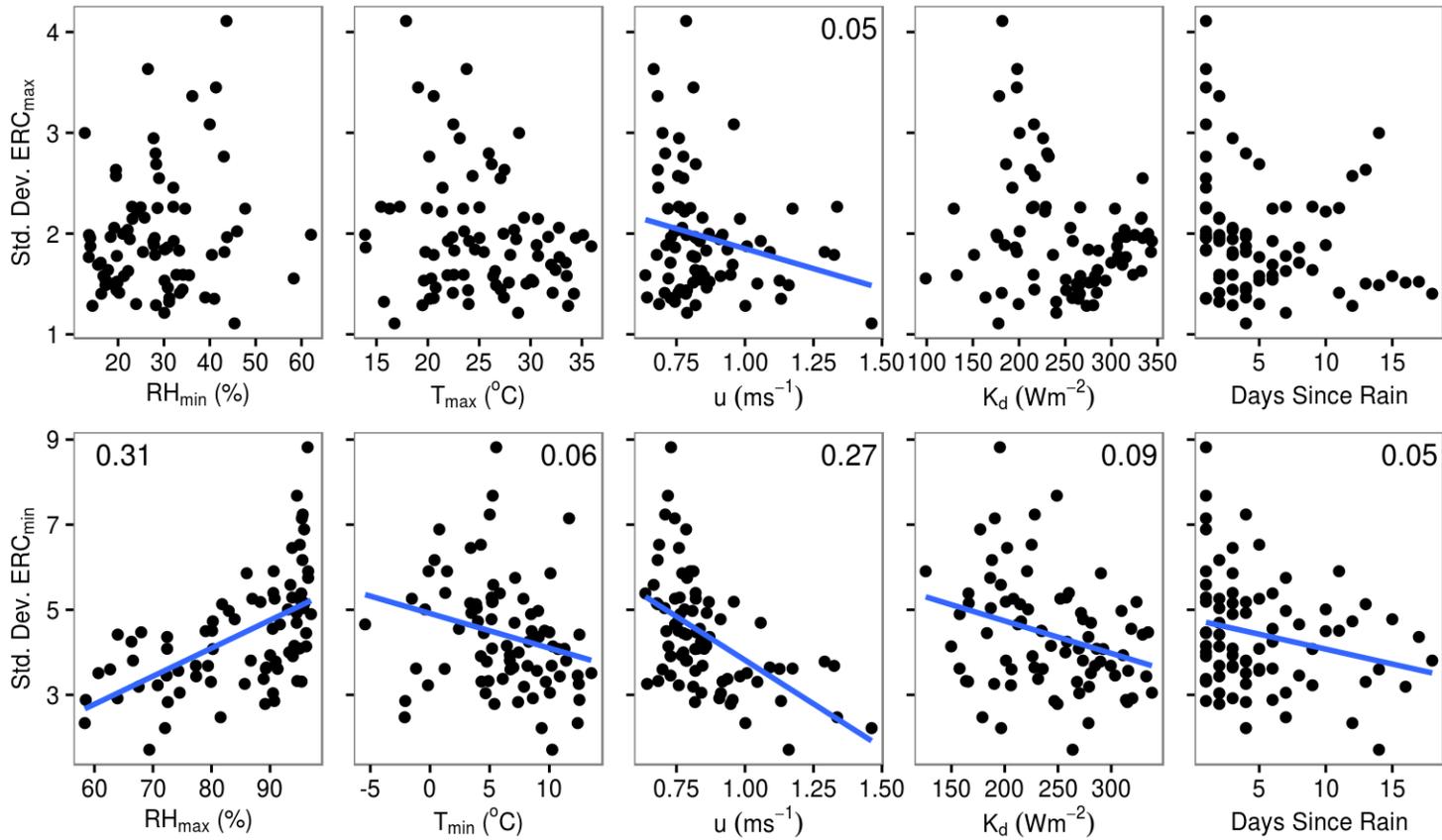
Figure 5.11: Daily standard deviation of maximum and minimum ERC plotted against daily minimum and maximum relative humidity and temperature, daily mean wind speed, daily mean sortwave radiation, and Days Since Rain. Regression lines and the coefficient of determination (R^2) are included for plots where null hypothesis that the regression coefficient is equal to zero was rejected at the 95% confidence level (*blue lines*).
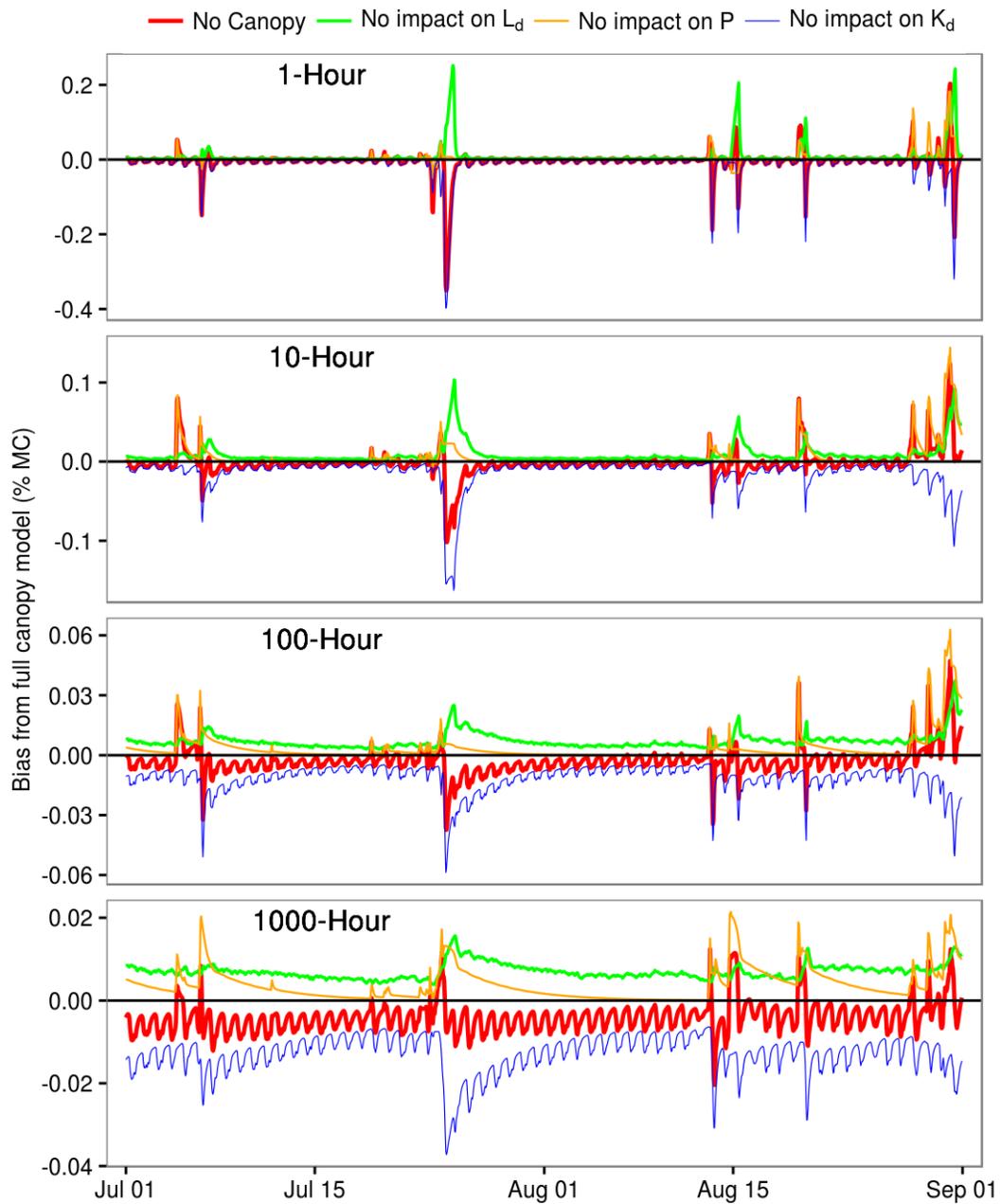
Figure 5.12: Modelled fuel moisture biases (compared to the original model) at Site 4 for all four sizes when removing one or all of the components of the canopy model: Longwave, shortwave, or precipitation. Note the varying scales of the y-axes.

114
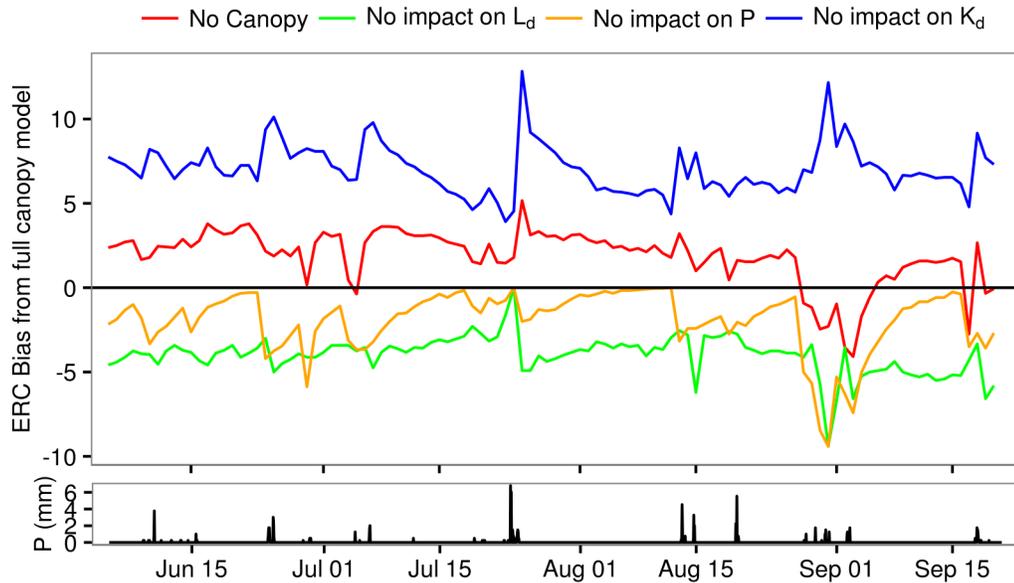
Figure 5.13: Daily mean ERC biases (compared to the original model) at Site 4 when removing one or all of the components of the canopy model: Longwave, shortwave, or precipitation. Hourly precipitation at the Base Station is included.
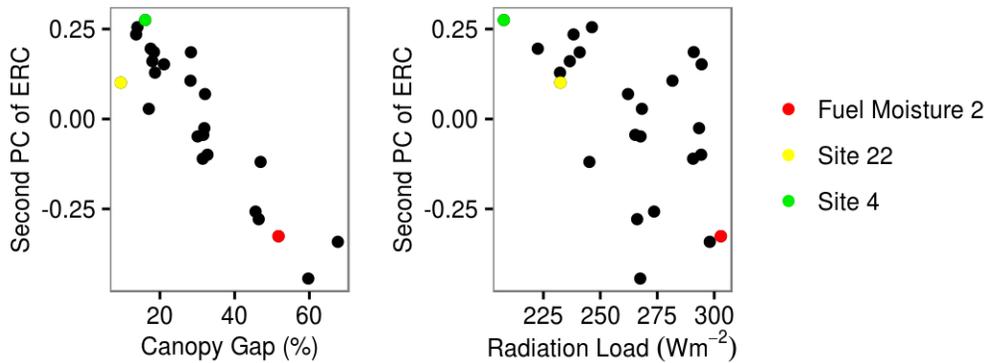
Figure 5.14: Second principal component of ERC for all 24 sites plotted against canopy gap fraction and radiation load. As in Figures 5.9 and 5.10, Fuel Moisture 2, Site 22, and Site 4 are highlighted.
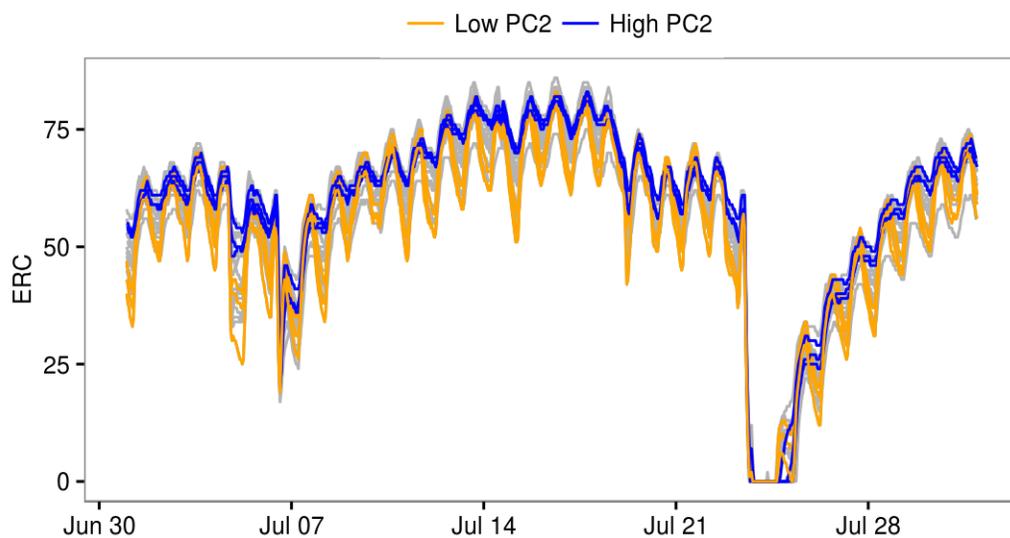
Figure 5.15: A month of ERC values for all 24 sites (*grey lines*). The sites with the three highest PC2 loadings (*blue lines*) and the sites with the three lowest PC2 loadings (*orange lines*) are highlighted.

Chapter 6

Modelling high resolution fire danger rasters across a large study region

6.1 Introduction

Wildfire behaviour depends on a complex combination of fuels, topography and weather, all of which vary at multiple scales. Consequently, the spatial pattern of wildfires and their ecological impact across the landscape is heterogeneous (McKenzie et al., 2011). Determining the drivers of this spatial behaviour will aid in predicting the spatial pattern of fire effects, which can, in turn, influence successional trajectories and ecological processes (Romme et al., 2011). Understanding what drives the spatial behaviour of fires is also significant from a fire management perspective if the goal is to create more resilient ecosystems in the face of a changing climate by introducing more fire onto the landscape (Holden et al., 2011a).

Patterns in fuel moisture likely influence fire spread (Littell and Gwozdz, 2011; Miller and Urban, 2000) and burn severity patterns (Alexander et al., 2006; Dillon et al., 2011; Arkle et al., 2012). It is therefore important to assess how fuel moisture varies at different spatial scales, and the relative influence of the factors driving

these patterns. In the extreme case where the landscape is homogeneously dry, a fire can spread unimpeded through a region, given ideal wind conditions. However, in moderate fire weather conditions, particular areas of the landscape may be susceptible to fire spread while others are not, and in this case the pattern of fuel moisture becomes important. If fuel moisture changes gradually across the landscape, i.e. there is a large spatial autocorrelation, a fire can easily spread across the drier portion of the region. Alternatively, if the fuel moisture pattern is patchier, and the scale of spatial autocorrelation decreases, a fire will be less likely to move across the entire landscape without patches of wetter fuels impeding its spread (Littell and Gwozdz, 2011).

Results from Chapter 5 suggest that in the dry Interior Douglas-fir forests studied here, daytime variability in fuel moisture and potential fire danger is low, apart from locations that are influenced by a high water table. That is, the whole landscape dries out at a similar rate. Moreover, spatial patterns in daytime fire danger were not significantly correlated with either canopy gap fraction or radiation load. Nocturnal fire danger is more variable and significantly impacted by canopy cover.

However, the above results were based on point measurements across a small area. These data provide limited information about actual landscape patterns or the potential for areas to remain persistently wet relative to their surroundings. As well, the previous chapters were restricted to a relatively small area (approximately 1 km^2) with little change in elevation. In this chapter the relationships identified in previous chapters will be extrapolated to a larger 140 km^2 area with a mosaic of canopy coverage and radiation load and a significant elevational gradient. Central to this analysis is the development of non-linear random forest models for predicting near-surface temperature and relative humidity across the landscape using meteorological data from a base station along with raster layers of canopy cover, radiation load, and elevation. The final product will be time-varying 30-m resolution rasters of temperature, humidity, and potential fire danger.

As described in Chapter 3, high resolution (<1 km) gridded maps of weather variables have been produced by a number of researchers (Holden et al., 2011a; Holden and Jolly, 2011; Ashcroft and Gollan, 2011; Bennie et al., 2010; Holden et al., 2015). However, much of this work has focused on temperature rather than relative humidity, which is an important driver of fuel moisture. Holden and Jolly

(2011) developed an empirical downscaling approach using Principal Component Analysis and a network of relative humidity sensors that generated 30-m resolution maps of relative humidity across a mountainous region. They found that elevation had a strong influence on relative humidity, while radiation load was a secondary predictor. However, this approach did not include the impact of canopy coverage and used measurements 2 m above the ground. Ashcroft and Gollan (2011) developed 25-m resolution grids of near-surface humidity and temperature that included the influence of canopy coverage. In their analysis, elevation and canopy cover were strong determinants of relative humidity patterns. However, the grids they produced were of long term extreme values; they did not produce time-varying maps. This chapter will build on the literature by developing high resolution maps of both near-surface temperature and relative humidity at a hourly time intervals that are dependent on canopy cover, aspect, and elevation.

Less work has been done on developing and analysing high resolution maps of fire danger. As mentioned in Chapter 5, high resolution fire danger maps developed by Holden and Jolly (2011) exhibited spatial patterns that changed over the fire season. The authors used the Energy Release Component (ERC) to represent potential fire danger. South facing slopes and lower elevations saw higher fire danger. This chapter will expand on these results by providing a novel examination of the relative influence of elevation, canopy cover, and radiation load on the variability and patterns of both nocturnal and daytime fire danger.

This study will pursue three research objectives:

- Objective #1: Develop and evaluate models to predict temperature and relative humidity across a forested landscape and use these models, along with models for precipitation and radiation canopy interception, to generate daily rasters of potential fire danger across a large study region (140 km^2).

- Objective #2: Examine the spatial variability of potential fire danger across the study region and determine the relative influence of canopy coverage, radiation load, and elevation on that variability. The following prediction will be tested:

    - Elevation is the most important factor driving the spread in potential

119

fire danger across the study region, followed by canopy gap fraction, and then radiation load.

- Objective #3: Examine the spatial patterns of potential fire danger across the study region and how it changes over the fire season. The following prediction will be tested:

  - The impact of canopy cover and radiation load on daytime fuel moisture and potential fire danger is not strong enough to create landscape patches that are significantly wetter than the surrounding area.

This chapter begins with a description of the methods and data used, including: an overview of the methods used to develop rasters of temperature, humidity, and fire danger (Section 6.2.1); a description of the required input rasters (Section 6.2.2), and a detailed description of the temperature and humidity random forest models (Section 6.2.3). The results section will provide: evaluation results for the humidity and temperature models (Section 6.3.1, Objective #1); an analysis of the relative influence of elevation, canopy cover and radiation load (Section 6.3.2, Objective #2); and an analysis of fire danger patterns across the study region (Section 6.3.3, Objective #3). This is followed by a discussion of results (Section 6.4) and conclusions (Section 6.5).

6.2 Methods

6.2.1 Overview

In this study I produced daily 30-m resolution rasters of the relative humidity, temperature, and ERC across a 140 km^2 study region centred around the study site described in the previous chapters (See Figure 2.1 for location). Figure 6.1 provides a schematic overview of the procedure. The ERC rasters were calculated by running the fuel moisture model (see Chapter 4) and the ERC model (see Chapter 5) at each 30-m grid cell. This required time-varying input rasters of below-canopy precipitation, below-canopy shortwave radiation, near-surface relative humidity and temperature, and wind speed. It also required a raster of canopy gap fraction (de-

scribed in Section 6.2.2). As mentioned in Chapter 5, ERC represents the potential heat released by a propagating fire front and, as such, does not include the impact of wind speed or slope fire danger. Instead, it can be viewed as representing the contribution of fuel moisture to fire danger.
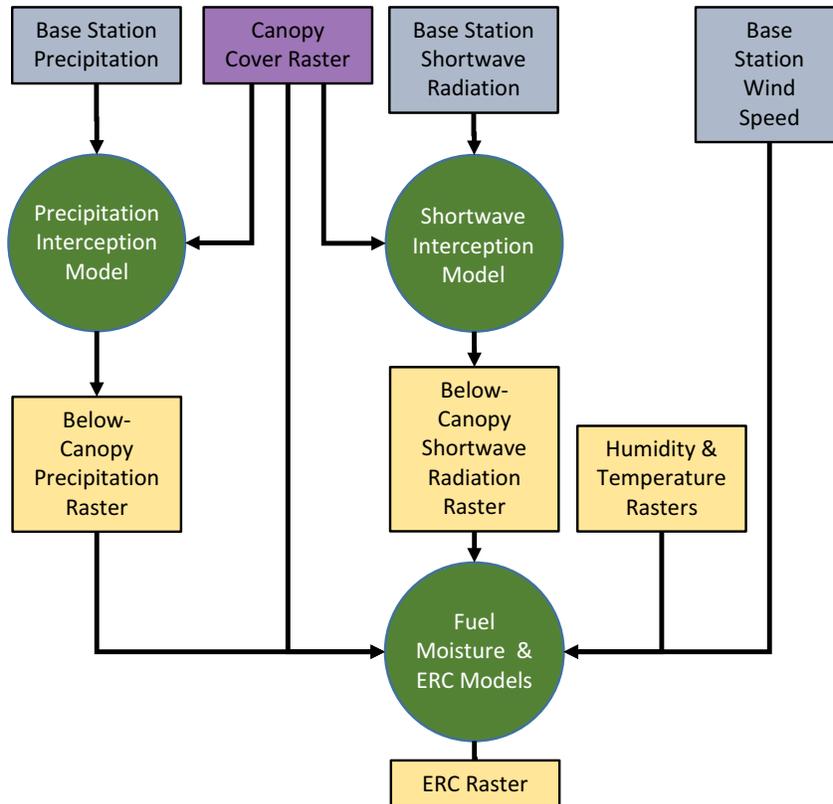
Figure 6.1: Procedure used to generate fire danger rasters. Variables are shown as *squares* and models are shown as *green circles*. Variables are either time-varying spatial rasters (*yellow squares*), constant spatial rasters (*purple squares*), or non-spatial time series (*grey squares*).

The weather rasters were generated using weather observations from the Base Station (described in Chapter 2) and rasters of canopy gap fraction and elevation. Specifically, the below-canopy precipitation raster was generated by running the precipitation interception model described in Chapter 5 at each grid cell, forced

with Base Station precipitation data and using the canopy gap fraction value at each cell. This approach assumes that above-canopy precipitation is constant across the study region. The below-canopy shortwave radiation raster was generated by running a simple empirical shortwave interception model (described below in Section 6.2.3) at each grid cell, which was forced with Base Station shortwave radiation observations and the canopy gap fraction at each cell.

Wind speed was assumed to be constant across the study region and was set to be equal to the wind speed observed at the Base Station. This is a significant simplification as wind speed would be expected to vary significantly across a mountainous landscape.However, this simplification was considered to be reasonable because, as shown in Chapter 4, modelled fuel moisture was relatively insensitive to wind speed. This finding was supported by additional analysis, in which ERC was calculated at the Base Station after wind speeds were adjusted by a constant factor, and then compared to the original ERC. Results for this analysis are shown in Appendix C, Figure C.1. Significant adjustments in wind speed did little to impact ERC, especially during dry periods. Moreover, estimating below-canopy wind speeds across a mountainous landscape would substantially increase the complexity of the study.

As mentioned in the introduction, rasters of near-surface relative humidity and temperature were generated by running non-linear random forest models at each grid point. A schematic of the procedure used is presented in Figure 6.2. The required inputs for these models are: rasters of canopy gap fraction, seasonally averaged above-canopy radiation load, and precipitation amount; shortwave radiation, temperature, relative humidity, hours since precipitation, and wind speed observed at the base station; as well as the hour of the day and the day of year. Before the Base Station temperature and relative humidity were input into the model, they were adjusted to the elevation of each grid cell using a time-varying lapse rate. The temperature and humidity lapse rates were calculated every hour using observations from the Kamloops Airport, which is at an elevation of 345 m above sea-level, compared to the Base Station's elevation of 1170 m (See Figure 2.1 for location). The Kamloops Airport data were acquired from Environment Canada and Climate Change via the Pacific Climate Impact Consortium's Data Portal (https://pacificclimate.org/data).
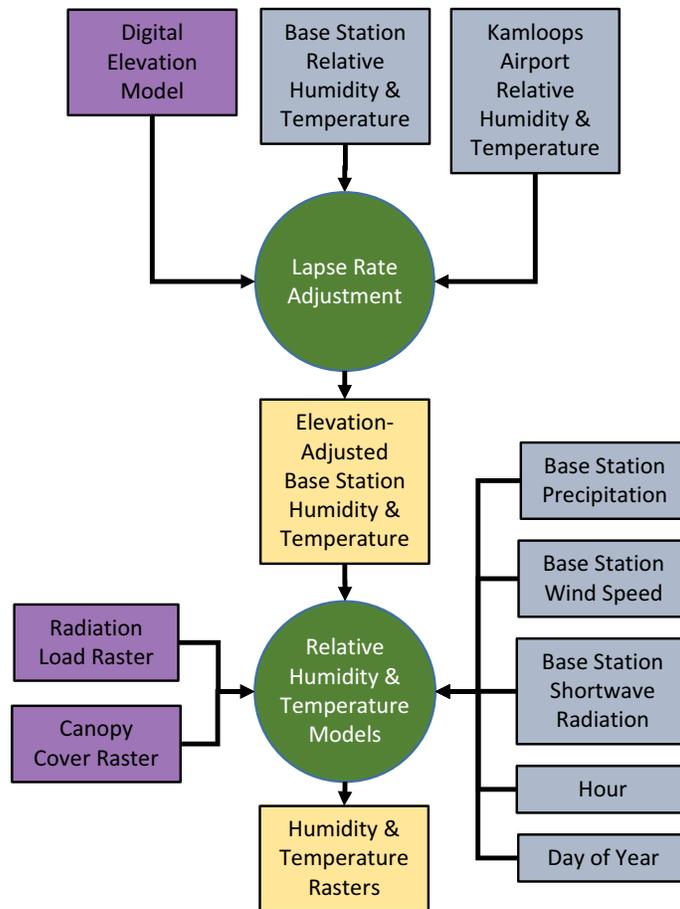
Figure 6.2: Procedure used to generate relative humidity and temperature rasters. Variables are shown as *squares* and models are shown as *green circles*. Variables are either time-varying spatial rasters (*yellow squares*), constant spatial rasters (*purple squares*), or non-spatial time series (*grey squares*).

To evaluate the relative influence of canopy coverage, radiation load, and elevation on the variability and patterns of potential fire danger across the study landscape, rasters of ERC were generated while setting all but one of the these three factors to be constant and equal to its average value across the study region.

Variogram analysis was used to quantify the spatial autocorrelation of ERC

patterns across the study region. Specifically, the variogram of ERC was calculated across the entire study region for each day. A spherical variogram model was then fit to the experimental variogram, as analysis not shown here indicated that it was the most appropriate model in this instance. The variogram range was then extracted from the spherical model for each day. The variogram range represents the maximum distance of spatial autocorrelation in ERC. Larger ranges indicate a slowly varying pattern, while patterns with smaller ranges vary at smaller scales and are more "patchy."

6.2.2 Spatial input data

The three required input rasters, shown in Figure 6.3, were elevation, canopy gap fraction, and seasonally averaged above-canopy radiation load (indicated as purple squares in Figure 6.2). Elevation data were taken from a 30-m resolution digital elevation model (DEM) of BC developed by Rosin (2010). The canopy gap fraction raster was derived from the Vegetation Resource Inventory Database (https://www.for.gov.bc.ca/hts/vridata/), which contains numerous GIS layers providing information on vegetation type, stand structure, and logging history. To generate the canopy gap fraction raster the "Crown Closure" layer was cropped to the study region and converted to a 30-m resolution raster with the same geometry as the DEM. The seasonally averaged above-canopy radiation load raster was calculated from the DEM using the Potential Incoming Solar Radiation tool available within the SAGA-GIS software. The radiation load raster was calculated as the mean potential incoming solar radiation averaged across the length of the field season (May 10 to September 22).

6.2.3 Modelling details

The random forest machine learning approach (Breiman, 2001) was used to model near-surface temperature and relative humidity across the landscape. Random forest models are an extension of classification and regression tree (CART) models. A CART model uses an iterative approach in which the set of training observations are split into smaller and smaller subsets based on threshold predictor values. At each iteration the split is made that generates the most homogenous subsets.

CART models have a number of advantages in that they do not make any assumptions about variable distributions, they can identify non-linear relationships, and are not susceptible to over-fitting. Random forest models generate a "forest" of trees using a bootstrapping approach in which an ensemble of trees are trained on random subsets of the training data and then validated against the remaining data. The results from the ensemble of trees are then aggregated. Random forest models have been increasingly used to predict spatial variables where there are non-linear and hierarchical relationships present (Dillon et al., 2011). The R package "randomForest" (Liaw and Wiener, 2002) was used with 120 random trees grown for each model.

As previously mentioned, there are three categories of predictor variables: hourly meteorological observations from a single site (precipitation amount, hours since precipitation, wind speed, temperature, relative humidity, and shortwave radiation); spatially varying site characteristics (seasonally averaged above-canopy radiation load, and canopy gap fraction); and two time variables (hour of day and day of year). Because different processes are more or less important depending on the time of day, separate models were developed for daytime hours and nighttime hours demarcated by sunrise and sunset. As well, seasonally averaged radiation load was not used as a predictor in the nighttime model.

The models were trained using the observational dataset described in Chapter 2. Near-surface relative humidity and temperature were simulated at the individual Logtag sites and compared to observations. The hourly meteorological input variables were taken from the Base Station. The same site-specific canopy gap fraction and average above-canopy radiation load values used in Chapters 3 and 5 were used as model inputs here. Due to its outlying behaviour, Site 22 was excluded from this analysis.

Although the random forest method uses cross validation to test each tree, the observations are divided randomly, ignoring site and time of year. However, it is important to examine how the models performed at independent sites and time periods not used for training. Therefore, two additional cross-validation approaches were developed. In one case the models were trained at a random subset of half the sites and evaluated using the remaining sites, and in the other case the models were trained on the first half of the field season, and evaluated on the remaining portion.

As mentioned above, the precipitation interception model, fuel moisture model, and ERC model were all taken, unchanged, from the previous chapters. However, estimating below-canopy shortwave radiation using hemispherical photos as was done in Chapter 5 is not feasible when a raster across the whole study region is required. Therefore, a simple shortwave interception model was created whereby the fraction of radiation intercepted by the canopy was modelled as a linear function of canopy gap fraction. The model was developed using three steps. Firstly, the simulated shortwave radiation that was generated in Chapter 5 was taken as a proxy for observations. Secondly, a seasonal average of below-canopy shortwave radiation was calculated for each site and divided by the average at the Base Station site. Finally, this ratio of below-canopy radiation to open-site radiation was regressed against canopy gap fraction. This linear regression was then combined with the canopy gap fraction raster and the hourly time-series of shortwave radiation measured at the Base Station to generate a time-varying raster of below-canopy shortwave radiation.

6.3 Results

6.3.1 Temperature/humidity model

Table 6.1 provides cross-validation model skill statistics for both the relative humidity and temperature models. Model skill was highest when the evaluation and training subsets were split across sites, rather than time. Cross-site model skill was highest for minimum relative humidity and minimum temperature. Example comparisons of modelled and observed daily relative humidity and temperature are shown in Figure 6.4 using data from site 10, which is one of the evaluation sites. The models are able to simulate the seasonal trends well. The large wet bias in maximum relative humidity seen in Table 6.1 is also apparent in this figure.

Modelled relative humidity and temperature, along with modelled below-canopy precipitation and shortwave radiation, were then used to model fuel moisture and ERC. The resulting ERC values were compared to the ERC values generated using observations (see Chapter 5) at the evaluation sites. Comparison statistics are provided in Table 6.2. Model root mean square errors were 5.06 and 5.70 for ERC_{max}

126

Table 6.1: Skill of models applied to evaluation data. Comparison statistics used are: root-mean-square error, bias, and coefficient of determination. Results are provided for evaluation across both time and sites.

	RH_{max} (%)		RH_{min} (%)		T_{max} (°C)		T_{min} (°C)	
	Time	Site	Time	Site	Time	Site	Time	Site
RMSE	7.23	5.71	4.54	3.50	1.47	1.42	1.74	0.99
Bias	2.94	1.03	-2.42	1.45	0.53	-0.36	-0.78	-0.03
R^2	0.88	0.88	0.95	0.96	0.95	0.95	0.88	0.94

and ERC_{min}, respectively, model bias was 1.51 and 3.26, and R^2 values were 0.90 to 0.95. Example scatter plots comparing ERC forced by both observed and simulated relative humidity and temperature are shown in Figure 6.5. Only sites not used for model training are shown. The correlations are strong especially at higher values, although some cases exhibited either negative or positive biases, depending on the site and time of day.

Table 6.2: Comparison statistics between modelled ERC forced by observed meteorology and modelled ERC forced by simulated meteorology. Comparison statistics used are: root-mean-square error, bias, and coefficient of determination. Results are provided for evaluation using both independent time-period and independent sites.

	ERC_{max}		ERC_{min}	
	Time	Site	Time	Site
RMSE	5.51	5.06	5.43	5.70
Bias	3.26	2.68	1.77	1.51
R^2	0.91	0.90	0.95	0.93

6.3.2 Relative impact of factors influencing the spatial variability of potential fire danger

The full suite of models shown in Figures 6.1 and 6.2 was applied to all 30-m grid cells within the study region to generate time-varying rasters of nighttime (0400 h) and afternoon (1600 h) ERC. These specific hours were used instead of daily maximum and minimum values for the sake of consistency across the study region. To show both the seasonal trend and spatial variability of ERC across the study

region, time-series from all grid cells are shown in Figure 6.6. To provide context, an ERC value of 60 was highlighted in the plots. Conditions above this threshold are often associated with extreme fire behaviour (Raymond and Peterson, 2005). As was seen in Chapter 5, afternoon ERC was less spatially variable than nighttime ERC. Nightitme ERC was most variable during moderately dry conditions at the beginning and end of the fire season.

The spatial variability of ERC across the study region is examined in more detail in Figure 6.7, where the standard deviation of nighttime and afternoon ERC is shown for the entire field season. Also included is the standard deviation of ERC maps generated when only one of the three influencing factors: canopy gap, elevation, or above-canopy radiation load, is allowed to vary across the study region (the other two factors are set to their average values). This isolation of factors allows for an analysis of the relative influence of these factors, addressing Objective #2 of this chapter.

Overall, ERC variability was enhanced by precipitation events, although this relationship was not as consistent at night as it was during the day. The spatial variability of afternoon ERC also was consistently reduced during dry periods. In contrast, the spatial variability of nighttime ERC was much noisier, and the influence of weather conditions was less obvious. For instance, in some cases rain acted to increase variability, while in other cases the opposite was true.

ERC was consistently more variable across the study region when all three factors were allowed to vary. As hypothesized, patterns in radiation load had the least amount of impact, while much of the spatial variability in afternoon ERC can be attributed to changes in elevation. One exception was during large rain events, when the variability driven by patterns in canopy cover was equal to or larger than the influence of elevation. Another exception was during the driest periods (mid-July, Early August, and Late August) when variability was low and all three factors had a similar influence. Canopy cover had a much larger influence on the spatial variability of nighttime ERC. Indeed, during the driest periods elevation had little influence on nighttime conditions, and a large majority of the variability was driven by canopy cover.

6.3.3 Spatial patterns of potential fire danger across the study region

Examples of ERC rasters are provided in Figures 6.8 and 6.9. Two days were chosen: the first day immediately following a large rain event, and 8 days later, after the landscape was able to dry out (both days are indicated in Figure 6.7).

Elevation had a dominant influence on the spread of ERC during the first day, but as conditions became drier the impact of elevation was diminished and canopy cover became more dominant, especially at night. As the landscape went from an elevation-dominated pattern to a canopy-dominated one, ERC transitioned from a slowly varying pattern with a large spatial autocorrelation scale, to a pattern dominated by the smaller scale variability of the canopy mosaic and a small spatial autocorrelation scale. This shift in spatial patterns can be seen in Figure 6.10 where the change in the semi-variogram range of both afternoon and nighttime ERC are presented. Between the two example days shown in Figures 6.8 and 6.9, the range transitioned from around 5 km to around 1 km, indicating that the spatial autocorrelation of ERC was substantially reduced as elevation, which has a large autocorrelation scale, lost influence. There were a number of other cases, generally during dry periods, where the range in ERC was significantly diminished, indicating a transition to a canopy-dominated pattern. In general, there was a trend towards lower variogram ranges during the middle of the season.

The relationship between the mean of ERC across the study region, the standard deviation of ERC, and the variogram range is presented in Figure 6.11. The variability in ERC across the study region decreased as the landscape dried out. It is also evident from Figure 6.11 that most days with a small autocorrelation scale were also relatively dry with little variability in ERC, especially during the day.

There were a few instances in which the region exhibited large variability during relatively dry periods. Two such days are highlighted in Figure 6.11 and presented as rasters in Figure 6.12. In both cases there was a large amount of spatial heterogeneity in potential fire danger, especially at the higher elevations where there is a mosaic of canopy coverage. In the daytime example (June 11th) the largest fire danger at higher altitudes was in areas with an open canopy, while the opposite was true during the nighttime example (July 15th). However, these instances of dry, variable conditions did not persist for multiple days.

Figures 6.7, 6.8, and 6.9 were repeated for both temperature and relative humidity and included as supplementary material in Appendix C.

6.4 Discussion

6.4.1 Temperature / humidity model

Chapter 3 demonstrated that spatial patterns in near-surface conditions were strongly dependent on canopy cover, radiation load, and weather conditions. The random forest models developed in this chapter were able to capture much of those relationships. When applied to independent sites, the models produced errors that were comparable to the accuracy of the LogTag sensors themselves (See Appendix A), especially for minimum relative humidity and minimum temperature. The nonlinearity of the random forest models was important for this application, as it was able to simulate the interaction between weather patterns and site characteristics seen in Chapter 3 (specifically, Figure 3.3). It is also interesting to note that model skill was highest when applied to independent sites, rather than an independent time period. This result suggests that the relationship between weather conditions and near-surface conditions changes over the course of the fire season.

Even though the modelled relative humidity and temperature had strong R^2 values when compared to observations, the model did not capture the full observational variability. When comparing the modelled standard deviation of relative humidity across the entire study region in Figure C.2 to the standard deviation of ERC generated from observations at just the 24 observation sites (Chapter 5, Table 5.3), it is clear that the modelled variability is lower than observations, especially for afternoon RH. This diminished variability in model output is unavoidable when a model is fit to observational data.

Moreover, model variability was also reduced because the field observations described in Chapter 2 did not sample as wide a range of radiation load as was found across the study region used in this chapter. Specifically, some steep, north-facing facets had average radiation loads lower than what was sampled. The random forest models interpolated to these lower values by maintaining a constant relationship between radiation load and near-surface conditions beyond the lowest

radiation load sampled by the field observations. Consequently, the models likely underestimated the variability of relative humidity and temperature across the study region that is driven by changes in radiation load. These results should therefore be examined with the understanding that actual variability in near-surface conditions is larger than what was produced by the suite of models, especially during the day.

The unique modelling approach used in the chapter for generating high-resolution maps of temperature and relative humidity across a complex landscape has applications beyond the objectives of this thesis. Understanding how temperature and humidity change at the local scale is important for determining the location of microclimates or microrefugias that are suitable for particular species (Dobrowski, 2011; Ashcroft and Gollan, 2013a). This thesis has demonstrated that a host of factors can interact to determine near-surface conditions at a specific spot on the landscape. This chapter has shown that the suite of models developed in this chapter has the ability to capture some of these interactions in order to simulate changing patterns of relative humidity and temperature across a forested landscape.

6.4.2 Simulated potential fire danger maps

In addressing Objective #2, it was found that afternoon fire danger was relatively homogeneous during dry periods, even across the extended study region of 140 km^2 with an elevation difference of over 1200 m. ERC variability was particularly low during the peak of the fire season. One driver of these low variability periods in afternoon ERC was a reduced relative humidity lapse rate; there is a moderate (0.51) correlation between the standard deviation of afternoon ERC using all factors (blue line in Figure 6.7) and the standard deviation of afternoon RH driven with just elevation (red line in Figure C.2). It may also be the case that the fuel moisture model was not able to dry out the fuels below a certain minimum moisture level. Consequently, all grid points approached this minimum moisture level, even if there was variability in relative humidity across the study region. In contrast, nighttime variability is higher, mirroring the results of Chapter 5 where ERC variability across the observational sites was also higher at night (see Table 5.3).

A number of studies have demonstrated that during dry periods fuel moisture is homogenous across a range of canopy cover (Whitehead et al., 2006; Estes et al.,

2012; Banwell et al., 2013) and radiation load (Gibos, 2010), findings which were supported by the results of Chapter 5. The present analysis expands on those results and suggests that during dry conditions fuel moisture and potential fire danger are relatively homogenous over a large regions on the order of 100 km^2 with a wide range of canopy cover, radiation load and elevation.

It was determined that, as hypothesized, elevation generally had the largest impact on overall fire danger variability, and radiation load had the smallest impact. However, there were a number of exceptions. For instance, canopy cover had a large influence on afternoon ERC variability during significant precipitation events when precipitation interception became important, although this influence diminished quickly as the landscape dried out. As well, canopy cover played a much larger role during the night, reflecting the findings of Chapter 5 where canopy gap fraction was only predictive of the spatial patterns in minimum ERC and had no connection with daytime patterns. Canopy cover drove the largest amount of nighttime variability during dry, clear-sky conditions, when the role of the canopy in determining net longwave radiation was most prominent. It should be mentioned that there was a small amount of variability in nighttime ERC when only radiation load varied. This variability was present, even though radiation load was not included as a predictor variable in the nighttime temperature and humidity models, because the influence of the daytime models persisted into the night due to the "memory" of the fuel moisture model.

As mentioned in the previous section, the model underestimated fire danger variability due to canopy cover and radiation load. In contrast, the impact of elevation was not modelled; rather, the lapse rate was calculated directly from observations. Consequently, it is likely that these results overestimated the influence of elevation as compared to canopy cover and radiation load. However, it is still likely that elevation was the dominant factor influencing variability, at least for afternoon ERC.

As was mentioned in this chapter's introduction, patches of wet fuels within a landscape could act as impediments to fire spread or lead to heterogeneous burn severity patterns, which has implications for ecological processes and fire suppression practices. Of the three factors controlling fuel moisture patterns in this study, only canopy cover and radiation load vary at spatial scales small enough to gener-

132

ate such patches. However, as seen in Figures 6.7 and 6.11, these two factors had the strongest relative influence during dry periods when ERC variability is low and the entire landscape is burnable. Moreover, while fire danger variability is larger during moderately dry conditions, these periods were also characterized by more slowly varying patterns in fuel moisture (i.e., large variogram ranges) dominated by changes in elevation. Consequently, these results confirm the second hypothesis that changes in near-surface conditions due to variations in radiation load and canopy cover are not large enough to generate patches that are substantially wetter relative to their surroundings.

Of course, it is possible that factors other than radiation load and canopy cover could lead to patches of anomalously wet fuels. For instance, based on results from Chapters 3 and 5, it is likely that areas characterized by high water tables can remain wet throughout the fire season. As well, it should be re-iterated that these results likely underestimate the influence of radiation load on fire danger patterns.

6.5   Conclusions

The random forest models described in this chapter were able to accurately predict relative humidity and temperature at independent sites not used for model training. Model accuracy was on par with the accuracy of the LogTag sensors and was the highest for minimum temperature and minimum relative humidity. These results demonstrated that the random forest model was able to capture the complex interaction between site characteristics and weather seen in Chapter 3. One limitation of the model was that the observational sites did not cover the full range of radiation load within the study region, resulting in an underestimation of the influence of radiation load across the region. Another limitation was that the tests sites were at a similar elevation. As the suite of models included the impact of elevation, it would have been beneficial to have test sites located across a range of elevation.

The full suite of models produced simulated ERC at independent sites with root mean square errors ranging from 5.06 and 5.70, biases ranging from 1.51 to 3.26, and R^2 values ranging from 0.90 to 0.95. These values are for the entire independent evaluation dataset. However, the model exhibited larger biases at individual sites although these biases tended to decrease at higher ERC values.

The modelled rasters of afternoon potential fire danger were relatively homogeneous during dry periods, even across the extended study region of 140 km^2 and with a difference in elevation of over 1200 m. This low variability was partly due to low relative humidity lapse rates, as well as the fact that modelled fuel moisture had a lower moisture limit that all grid points reached during dry periods, regardless of site characteristics. Unlike afternoon ERC, variability in nighttime ERC was less impacted by weather conditions.

Elevation had the largest overall impact on spatial fire danger variability, especially during the day. Canopy cover had a relatively strong influence during large precipitation events and at night during fair-weather conditions. Radiation load had little impact on the spatial variability of fire danger across the study region.

During dry periods, afternoon ERC transitioned from an elevation-dominated spatial pattern with a large spatial autocorrelation scale to a "patchy" pattern with a small autocorrelation scale that was dictated by the mosaic in canopy cover. However, these dry periods with patchy patterns were also characterized by low variability in potential fire danger. These results suggest that radiation load and canopy cover do not have a large enough influence on potential fire danger to generate patches within the landscape that are significantly wetter than the surrounding landscape.
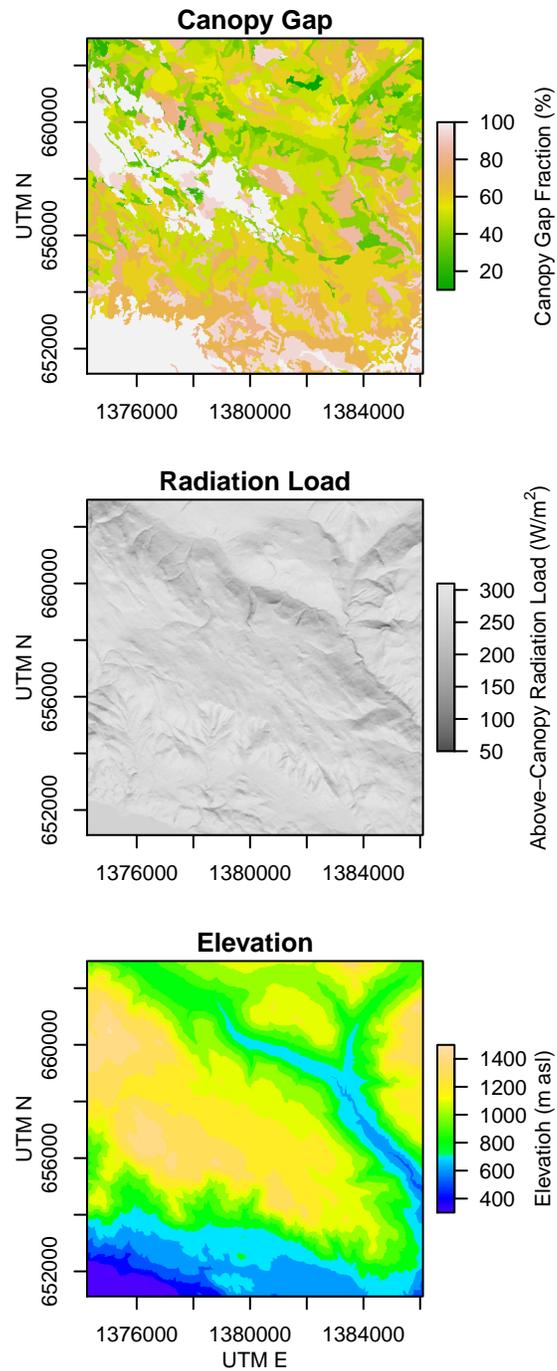
Figure 6.3: Canopy Gap, Radiation Load, and Elevation rasters used as input layers for relative humidity and temperature models.
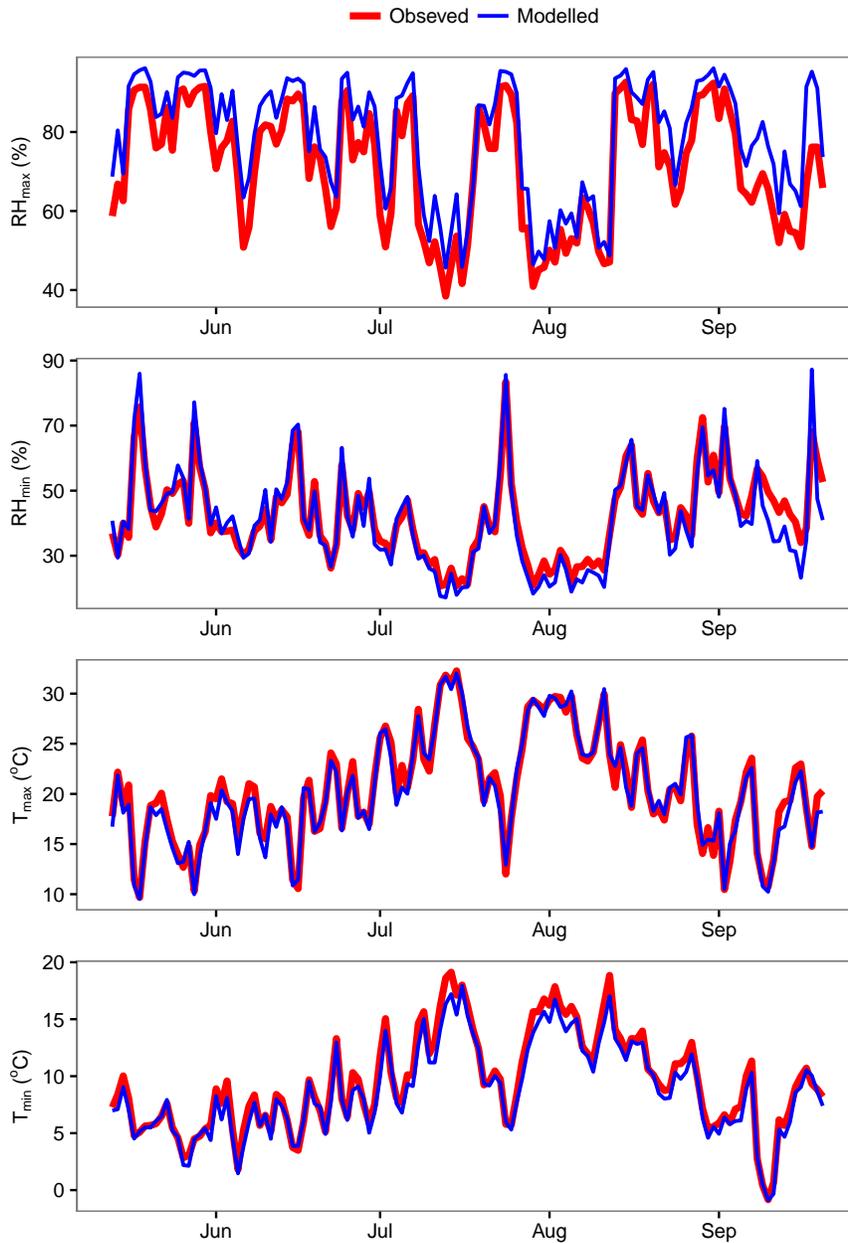
Figure 6.4: Both observed and modelled daily minimum and maximum relative humidity and temperature at Site 10, which was not part of the subset of sites used to train the model.
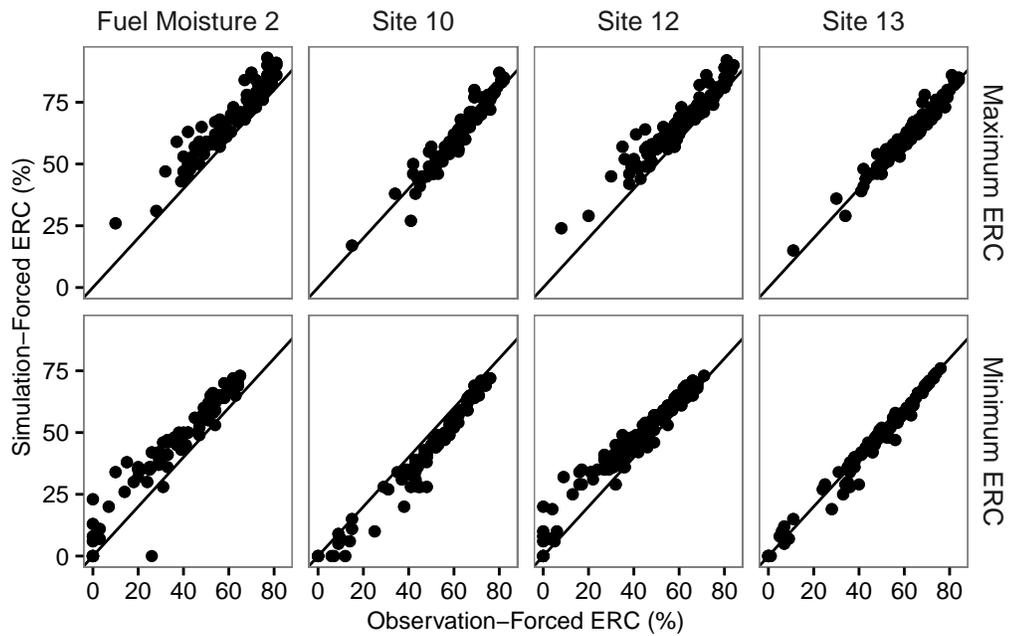
Figure 6.5: Example comparisons of ERC generated using observed mete-
orological conditions and ERC generated using simulated conditions.
Results for daily maximum and minimum ERC are shown. A subset of
four sites not used for training the humidity and temperature models are
shown here. 1:1 lines is provided for reference.
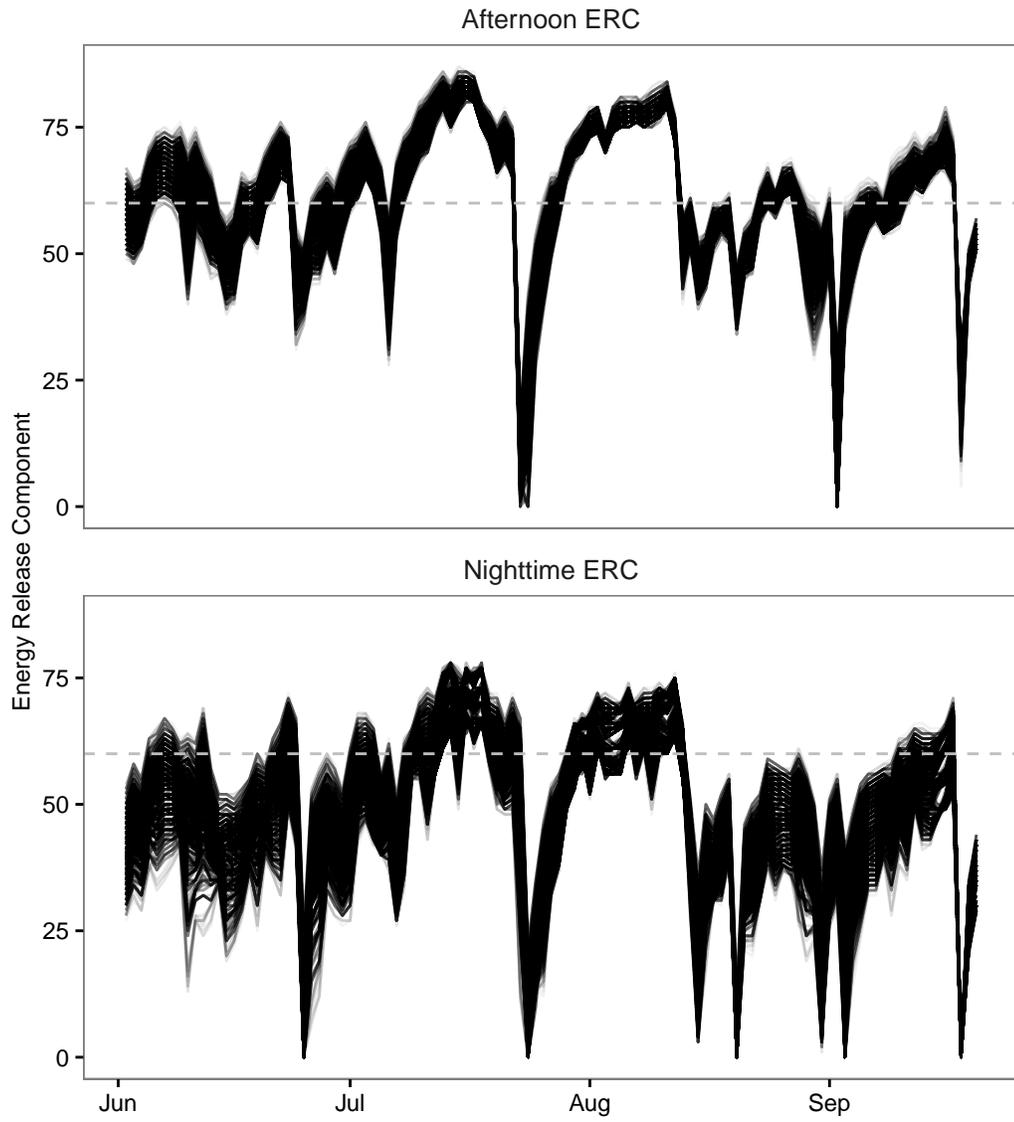
Figure 6.6: Afternoon and nighttime ERC for all grid points within the study region. The *dashed horizontal line* indicates an ERC value of 60.
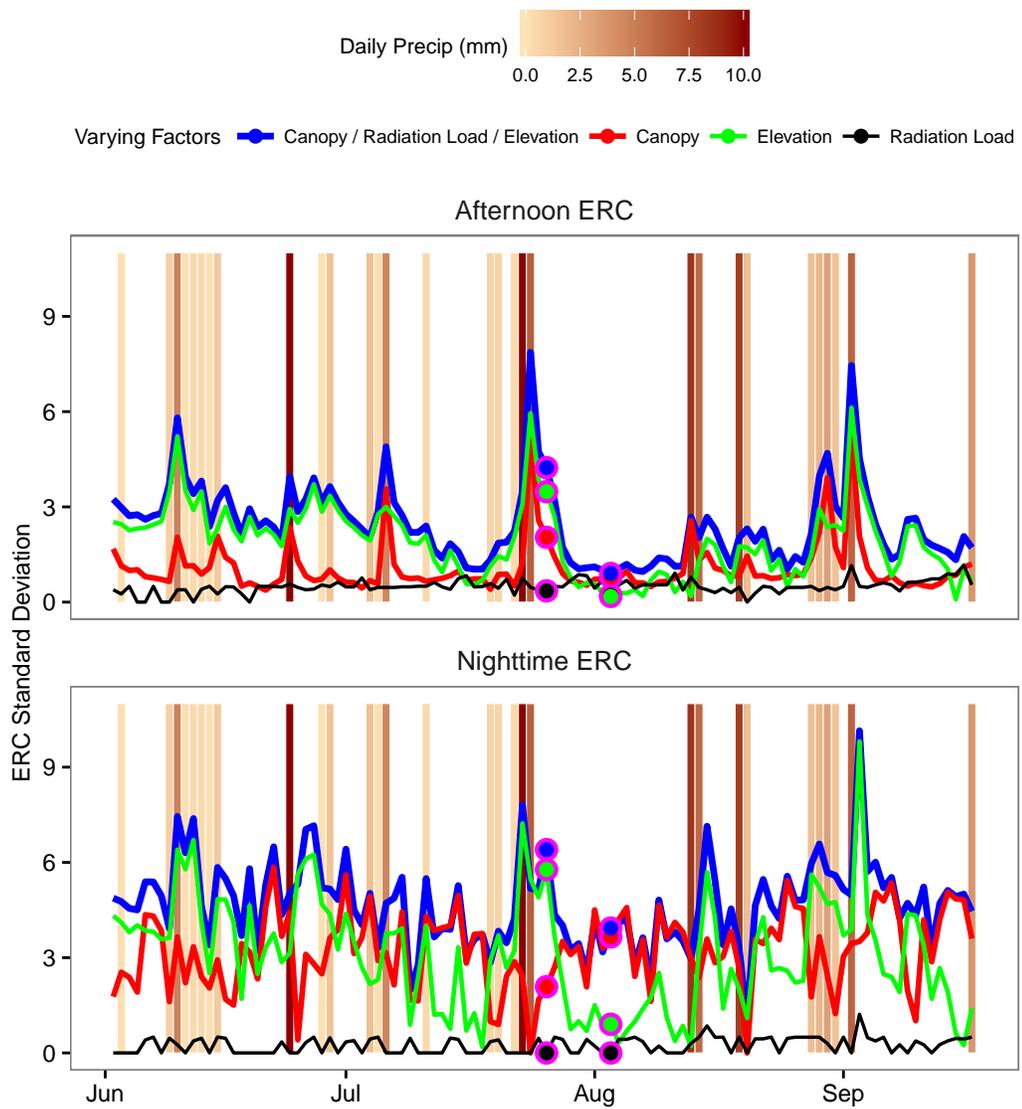
Figure 6.7: Standard deviations of nighttime and afternoon ERC across the entire study region. The results from four different simulations are shown here: three runs in which all but one of the three spatial factors were kept constant, and one when all three factors varied across the study region. The *magenta points* indicate the two days which are shown as rasters in Figures 6.8 and 6.9
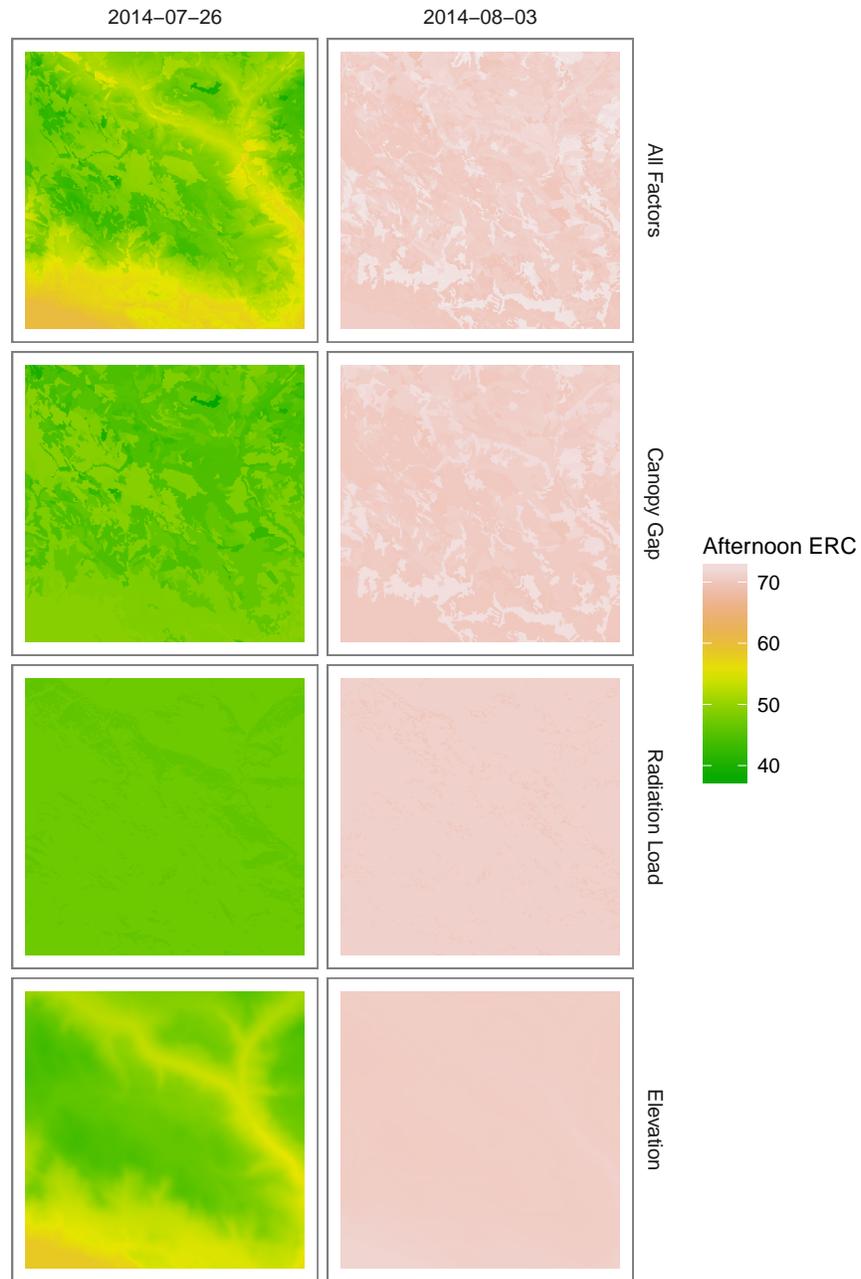
Figure 6.8: Rasters of afternoon ERC for two different days (*columns*, indicated in Figure 6.7). Rasters driven by all factors, and the three factors individually (*rows*) are provided.
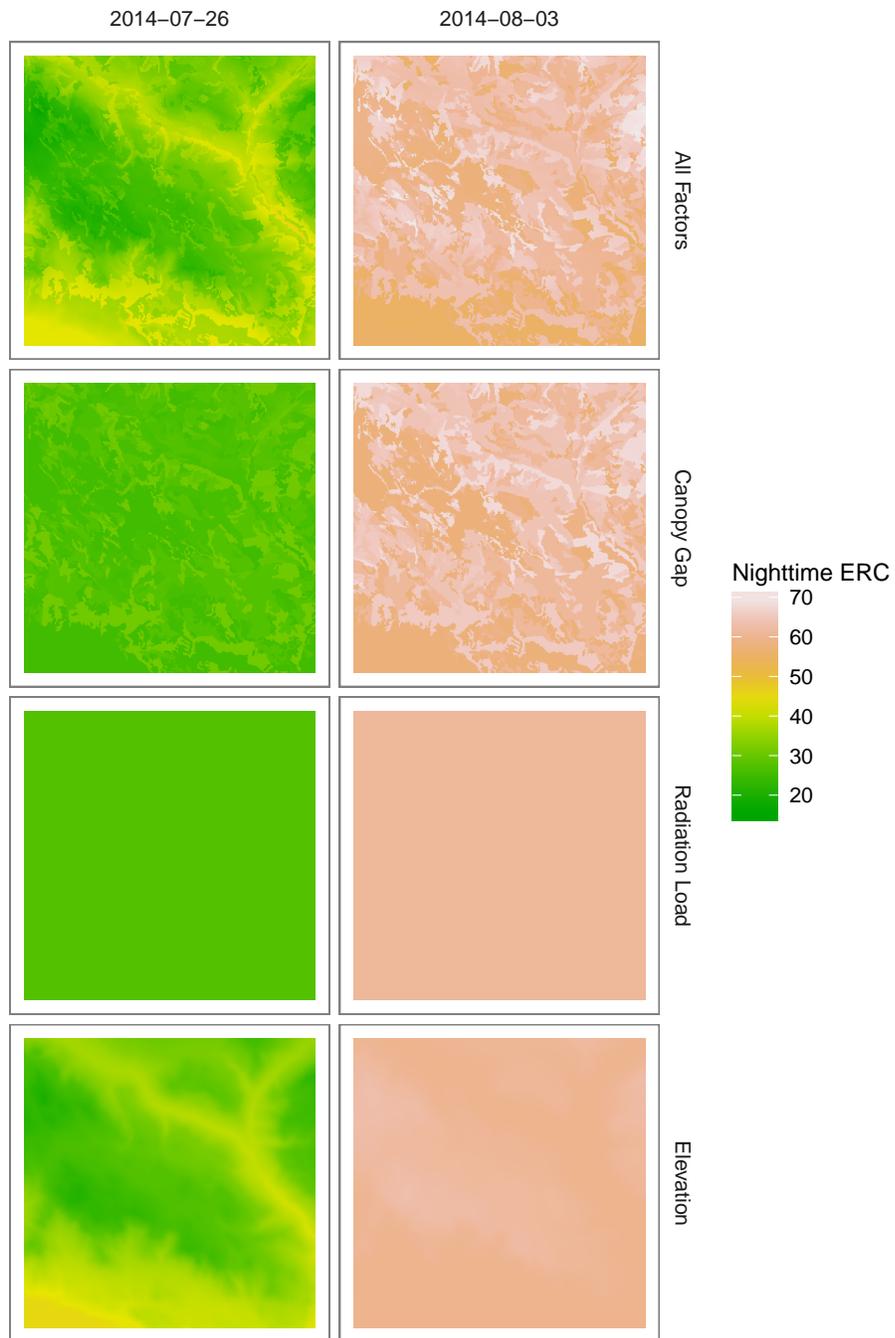
Figure 6.9: As in Figure 6.8, but for nighttime ERC.

141
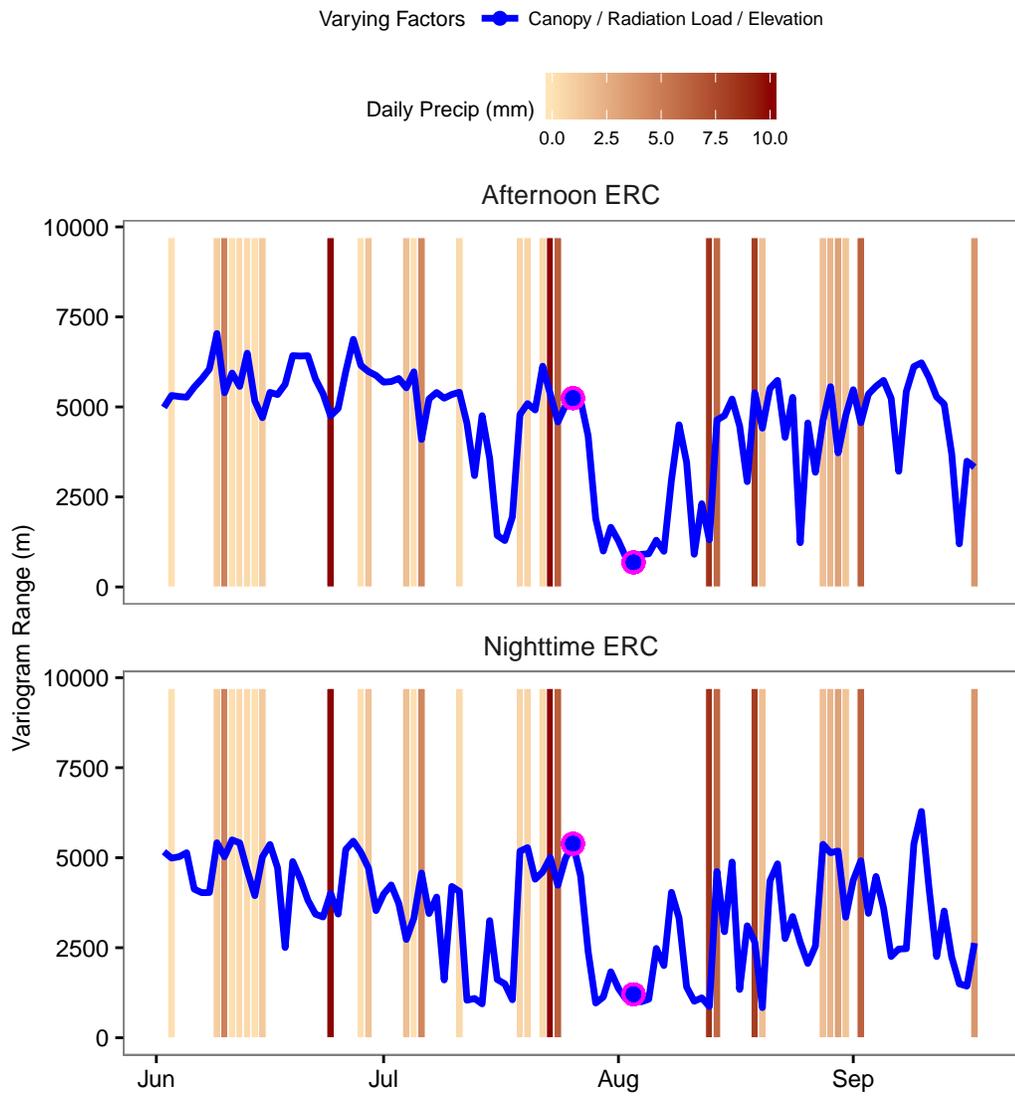
Figure 6.10: As in Figure 6.7, but for the variogram range of the ERC rasters.
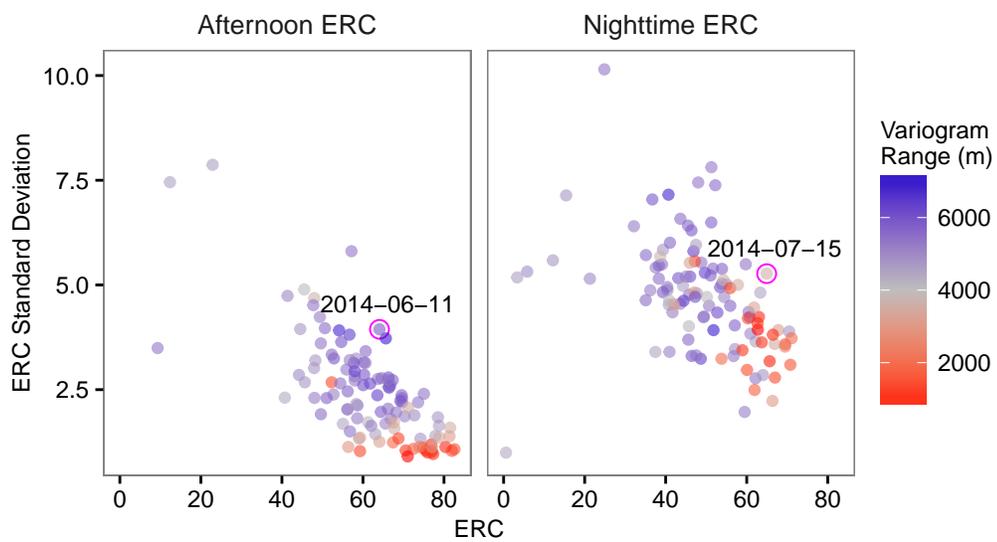
Figure 6.11: Relationship between the mean ERC, the standard deviation of ERC, and the variogram range of ERC across the landscape for both afternoon and nighttime ERC. Two example days when the fire danger was both high and variable are highlighted and the rasters for these two days are shown in Figure 6.12.

Afternoon ERC
2014−06−11

Nighttime ERC
2014−07−15

ERC
75
70
65
60
55
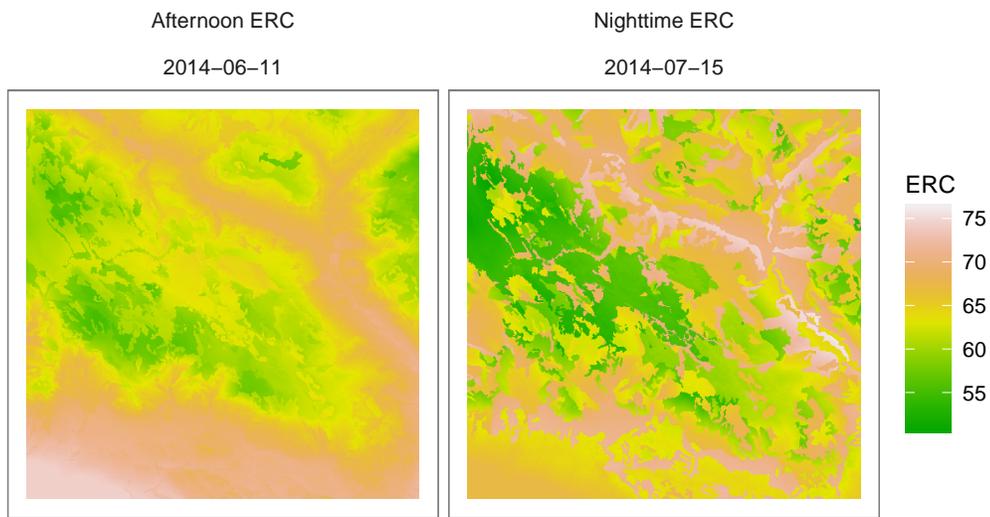
Figure 6.12: Example rasters for both an afternoon and nighttime case in which the fire danger is both high as well as variable. The two example cases are highlighted in Figure 6.11.

144

Chapter 7

Conclusions

This thesis quantified spatial patterns in near-surface atmospheric conditions, fuel moisture, and potential fire danger across a forested landscape, and examined how those patterns were impacted by weather conditions, canopy cover, radiation load, and elevation. It also identified the degree to which near-surface microclimates directly impact fuel moisture. Presented below are the key findings of the thesis, a discussion of their implications, and potential future research directions.

7.1 Summary of key findings

Chapter 3 examined spatial patterns in near-surface temperature and humidity across a forested landscape with complex terrain. The objective of the study was to quantify the amount of spatial variability in near-surface conditions, determine how weather conditions impact that variability, and determine the relative influence of canopy cover and radiation load on spatial patterns of near-surface conditions. Substantial variability was seen across the small (<4 km^2) study site. In general, near-surface conditions were more heterogeneous during during dry, clear-sky conditions, and spatial variability was reduced during, and for a few days following, precipitation. Weather conditions had the largest impact on nocturnal fuel moisture. An important finding was that the spatial variability in daytime relative humidity was low and relatively unaffected by weather conditions.

Spatial patterns in near-surface conditions were related to both canopy cover

and radiation load, with canopy cover being the more important predictor. Daytime conditions were drier and warmer on south-facing slopes. Canopy cover had a strong impact on nocturnal relative humidity, which was higher at open sites due to longwave cooling. Canopy cover had an opposite, but weaker effect on daytime humidity due to solar heating. Consequently, open sites experienced higher daily mean relative humidity. Finally, one site located near a draw with an inferred high water table remained anomalously cool and moist throughout the fire season.

Chapter 4 described a new model for simulating the moisture content of standardized fuel moisture sticks, which was subsequently used in Chapters 5 and 6 to simulate fuel moisture across the study landscape. The model included treatments of internal heat and moisture transport, radiation and turbulent heat fluxes, atmospheric moisture exchange, and precipitation absorption. Compared to the Nelson Model, which is used operationally by fire agencies, this novel model is relatively simple, apart from its treatment of radiation transfer, which is more sophisticated.

When evaluated using both an independent time period and an independent dataset, the optimized model was able to capture 72 to 94% of the variance in observations. Despite its simplified approach, the model improved on the skill achieved by the Nelson model. Moreover, the model allows for a more realistic treatment of canopy coverage and changes in sky conditions, features that are important for the simulation of fuel moisture patterns described in Chapter 5. Finally, sensitivity analysis suggested that relative humidity is the dominant driver of modelled fuel moisture. The model was relatively insensitive to wind speed and shortwave radiation, suggesting that treatment of these forcing variables could be further simplified.

In Chapter 5, fuel moisture and potential fire danger (represented by the Energy Release Component) were simulated across the field site using the new fuel moisture model, along with models of canopy interception of radiation and precipitation. This suite of models was able to accurately simulate the observed seasonal trends in below-canopy fuel moisture. Following model evaluation, the chapter's objective was to quantify the spatial variability of fuel moisture and potential fire danger, and determine the relative influence of canopy cover and radiation load. Daytime fuel moisture and fire danger exhibited low spatial variability, regardless of weather conditions, and daytime fire danger was not related to either factor.

Fuel moisture and ERC were more variable at night and that variability increased during cool, moist periods with low wind speeds. Overall, patterns in fuel moisture and ERC were dominated by differences in nocturnal longwave cooling due to changes in canopy cover. Consequently, radiation load only had a secondary impact on 1-hour fuel moisture, and open sites had lower daily minimum and daily mean fire danger. At the anomalously moist Site 22, an elevated water table likely contributed to low potential fire danger throughout the season.

Chapter 6 presented a method for producing high-resolution rasters of potential fire danger over a $140\,\text{km}^2$ region with a wide range of canopy cover, radiation load, and elevation. The study's objective was to assess the relative impact of these three factors on patterns in fire danger, and examine, in detail, the spatial patterns in fire danger. As part of this procedure a machine learning approach was used which accurately simulated spatial patterns in temperature and relative humidity.

During dry conditions fire danger was relatively homogenous over the region, which had a wide range of canopy cover, radiation load, and elevation. Change in elevation led to the most variability in potential fire danger across the landscape. While changes in radiation load and canopy cover sometimes led to "patchy" patterns in fire danger during dry conditions, these periods also saw little variability in fire danger. These results suggest that radiation load and canopy cover do not have a large enough direct influence on daytime fuel moisture to generate patches within the landscape that remain significantly wetter than the surrounding landscape.

7.2   Implications of findings

Increased radiation loads on warmer aspects can have a direct impact on fuel moisture by increasing drying rates on south-facing slopes. This direct impact is often cited as a significant factor dictating patterns in historical fire frequency (Heyerdahl et al., 2001) and burn severity (Holden et al., 2009; Birch et al., 2015; Kane et al., 2015; Dillon et al., 2011). However, results from this thesis suggest that in the Interior Douglas-fir forest type studied here the change in radiation load across terrain facets is likely a secondary factor in determining spatial patterns in fuel moisture, following canopy cover. Moreover, chapter 5 demonstrated that, across the study site, daytime ERC was not related to radiation load. Fine, 1-hour fuel

moisture was lower on warmer slopes, but canopy cover still played the dominant role. Therefore, it may be that indirect impacts of radiation load, though its impact on canopy cover and understory density, may play the larger role in determining fuel moisture patterns. Indeed, Nyman et al. (2015b) reached a similar conclusion.

Consequently, for the purpose of predicting the spatial pattern of fuel moisture across the landscape, it is as important to have accurate spatial vegetation data as it is to have terrain information. In many forest types aspect and canopy density are linked (Zou et al., 2007), so that both indirect and direct effects on fuel moisture work in concert and fuel moisture would reliably be lower on warmer aspects. However, there are many other factors that influence vegetation density, including soil properties, groundwater, and disturbance history, that weaken the aspect-vegetation relationship. Indeed, in wetter, energy-limited forests, stand composition is relatively unaffected by aspect (Ohmann and Spies, 1998). These results suggest that drier fuels will not necessarily be found on slopes with higher radiation loads.

Overall, there was a lack of variability in daytime fuel moisture and ERC across the landscape, supporting previous findings (Whitehead et al., 2006; Faiella and Bailey, 2007; Estes et al., 2012). However, this study built on the literature by examining not just the afternoon conditions, but the entire diurnal moisture cycle. This analysis determined that the lack of variability in afternoon fuel moisture is likely due to a balance between daytime solar heating and nocturnal longwave cooling. Moreover, this significant impact of nocturnal cooling meant that fuel moisture was, on average, lower at open sites, a result which was seen in both observed and modelled fuel moisture.

The important role that nocturnal cooling plays in determining fuel moisture is a significant finding, as many fuel moisture models ignore this process. For instance, the fire growth simulation model, FARSITE, which is used operationally, includes the impact of canopy cover on daytime solar radiation, but not nocturnal longwave cooling (Rothermel et al., 1986). However, this study suggests that changes in nocturnal longwave cooling can have a dominant impact on spatial patterns in fuel moisture, especially for the larger fuel sizes. Consequently, FARSITE may overestimate the differences in daytime fuel moisture between open and closed sites.

These results may have implications for the management of prescribed files or wildfires that burn for multiple days during moderate conditions. Understanding and predicting the spatial patterns of fire effects can help managers achieve their specific management objectives. For instance, even though fine fuels will likely be drier at open sites during the afternoon, the overall wetter fuels at open sites may mean that, all other things being equal, fires will be less intense and have less severe impacts at open sites. Brown et al. (1985) found that 1000-hour fuel moisture was a strong predictor of duff consumption by prescribed fires, which, in turn, can impact seedling establishment and post-fire recovery (Johnstone et al., 2010). Consequently, results from this thesis have a number of implications for prescribed fire management. Firstly, in the drier forest types examined here, and during moderate fire weather conditions, canopy cover and aspect may, on their own, have little impact on duff consumption during the day, and understory vegetation may be an important factor dictating burn patterns. Secondly, setting burns during cool moist conditions may lead to a more heterogenous burn pattern.

While there has been an effort to thin stands in drier forests in order to restore pre-settlement forest structure and reduce fire hazards, there is concern that these treatments will increase solar radiation penetration and decrease fuel moisture. However, results from this study and previous research suggest that these concerns may be overstated. In fact, it may be the case that thinning stands will decrease fuel moisture, especially for the larger fuel sizes.

The lack of variability in fuel moisture seen in Chapter 5 and the simulated fuel moisture patterns generated in Chapter 6 suggest that neither gradients in canopy cover nor radiation load have a large enough direct impact on fuel moisture to generate patches of wet fuels that persist into the field season. As long as sites are forced by the same above-canopy conditions, nocturnal recharge will balance daytime drying and not let sites diverge. In order for a site to remain wet, it requires a substantial source of additional moisture. Site 22 demonstrated that this moisture can come from an elevated water table that keeps an area moist throughout the season. Consequently, accurately predicting how fuel moisture changes across the landscape requires spatial information about subsurface flow and water table patterns.

7.3 Suggestions for future research

One limitation of this study was that it focused on observed and modelled moisture of elevated fuel sticks. Even though these fuel sticks are the basis of the American Fire Behaviour Prediction System, their moisture content may not represent the moisture of fuels on the forest floor. For instance, there may be differences between the microclimate immediately above the forest floor and at a height of 30.5 cm, as vertical gradients in temperature and humidity can be significant near the ground (Oke, 1990). Indeed, it was found in Chapter 4 that modelled fuel moisture is dependent on the height at which the temperature and humidity measurements are taken. Moreover, fuel elements on the forest floor may gain moisture from the underlying soils (Hatton et al., 1988; Samran et al., 1995), and elevated fuels have more exposed surface area and may be more efficient at exchanging moisture and heat with the atmosphere. Finally, there are number of methods of measuring fuel moisture, including destructive sampling of the litter layer (Gibos, 2010), weighing of dowels placed on the forest floor (Estes et al., 2012), or direct sensor measurements of the litter later (Nyman et al., 2015a). Consequently, it would be instructive to systematically compare the moisture of different types of fuels, measurement techniques, and measurement heights. Such comparison would allow us to compare results from different studies which use different measurement techniques.

As mentioned in Chapter 4, it would be useful to examine, in detail, the sensitivity of the fuel moisture model developed here to the different model parameters and forcing variables. Initial sensitivity analysis in Chapter 4 suggested that the model is strongly dependent on relative humidity and relatively insensitive to wind speed and shortwave radiation. Further analysis could identify elements of the model that could be simplified without sacrificing model skill. For instance, it is likely that using a constant aerodynamic resistance would not reduce model skill and remove the requirement for wind speed as an input. As well, the model's complex approach to calculating both shortwave and longwave radiation absorption could likely be reduced substantially. Such an analysis could result in an updated version of the model which would still be more sophisticated and skillful than most of the fuel moisture models reviewed in the Introduction, but also be simple

enough to be utilized by other researchers. For instance, when choosing a fuel moisture model to be used within a coupled fire-atmospheric model, Mandel et al. (2012) opted to use a relatively simple fuel moisture model rather than the model developed by Nelson (2000), which they deemed to be too complicated.

Another limitation of this study is its reliance on a single season of field observations taken across a relatively small area. Future studies could expand on this work by deploying new networks of near-surface measurements across different locations and different forest types. These new datasets could be used to test whether the relationships between near-surface conditions, radiation load, and canopy cover found here are applicable to other locations. Independent datasets such as these could also be used to evaluate the temperature and relative humidity random forest models developed in Chapter 6.

These networks could also be designed to examine the impact of factors other than radiation load and canopy cover on fuel moisture patterns. For instance, evidence from Chapters 3 and 5 suggested that relative humidity and fuel moisture likely increase in the vicinity of streams and regions with elevated water tables. A future field project could focus on quantifying gradients in fuel moisture and relative humidity near these wet regions. It would also be useful to determine the scale at which this influence occurs. That is, what amount of separation from a draw or stream is required before its effect becomes negligible? It is also possible that there would be a complex interaction between the distance from a saturated area, terrain, and canopy cover that could be explored. The impact of nocturnal katabatic flows and cold-air ponding on fuel moisture patterns would be another important area to study. Areas that are susceptible to cold-air ponding would likely see elevated relative humidity at night. It is unclear how pervasive this impact would be over a fire season, and if it is strong enough to impact daytime fuel moisture or generate patches of anomalously moist fuels. Finally, as mentioned above, atmospheric conditions immediately above the forest floor may be different than conditions at the 30.5 cm height used in this study. A network of sensors placed a few centimetres above the forest floor (similar to the measurements by Ashcroft and Gollan 2013b) may help identify those differences and be more applicable to surface fuels.

The sites used in this study were purposefully situated in similar areas with little understory growth and homogenous surface vegetation. Choosing sites with

consistent understory vegetation allowed for an examination of the direct impact of changes in microclimate on near-surface conditions and fuel moisture, rather than its indirect impact through changes in vegetation. However, as suggested by Nyman et al. (2015b), these indirect impacts are likely significant. It is important, then, to attempt to quantify these vegetation impacts on dead fuel moisture. For instance, a network of sites could be established where sites are chosen across gradients of understory and surface vegetation in a region with little variability in topography. Each site would be characterized by percent cover or density of forbs, mosses, dead litter, shrubs, and understory and overstory trees. The impact of these factors on fuel moisture could then be assessed. This analysis of vegetation impacts would provide complementary information to the results found in this study.

Networks of near-surface observations could also be used to assess the accuracy of modelling systems used operationally. For instance, the FARSITE (Finney, 2004) and FlamMap (Finney, 2006) models both estimate relative humidity, temperature, and fuel moisture across forested landscapes using a model developed by Rothermel et al. (1986). This model includes the impact of canopy, slope and aspect, and elevation on near-surface conditions, but does not include nocturnal longwave cooling. Fuel moisture is modelled using both the National Fire Danger Rating System (Cohen and Deeming, 1985) and the Nelson Model (Nelson, 2000). A network of near-surface observations could be used to evaluate these models. To my knowledge, no study has evaluated the ability of these models to accurately simulate spatial patterns in fuel moisture.

Finally, as was mentioned in Chapter 5, fuel moisture is one of a number of factors that will determine the behaviour of an individual fire. Others include wind speed, slope, and fuel amounts. Fire behaviour prediction tools such as FARSITE and FlamMap include treatments of all these processes, but could be improved by including some of the insights from this thesis. These tools could then be used to examine the sensitivity of spatial patterns in modelled fire behaviour to fuel moisture, wind speed, slope, and fuel amounts, and determine the most important determinant of spatial fire behaviour.

References

Alexander, J. D., Seavy, N. E., Ralph, C. J., and Hogoboom, B. 2006. Vegetation and topographical correlates of fire severity from two fires in the Klamath-Siskiyou region of Oregon and California. *Int. J. Wildland Fire*, 15(2):237–245. → pages 117

Alves, M. V. G., Batista, A. C., Soares, R. V., Ottaviano, M., and Marchetti, M. 2009. Fuel moisture sampling and modeling in Pinus elliottii Engelm. plantations based on weather conditions in Parana-Brazil. *iForest-Biogeosciences For.*, 2(3):99–103. → pages 5

Anderson, H. E. 1990a. Moisture diffusivity and response time in fine forest fuels. *Can. J. For. Res.*, 20(3):315–325. → pages 6, 61

Anderson, H. E. 1990b. Predicting equilibrium moisture content of some foliar forest litter in the northern Rocky Mountains. Research Paper INT-429. Technical report, US Department of Agriculture, Forest Service, Intermountain Research Station. → pages 6, 56, 61

Andrews, P. L. 2014. Current status and future needs of the BehavePlus Fire Modeling System. *Int. J. Wildland Fire*, 23(1):21–33. → pages 48

Arkle, R. S., Pilliod, D. S., and Welty, J. L. 2012. Pattern and process of prescribed fires influence effectiveness at reducing wildfire severity in dry coniferous forests. *For. Ecol. Manage.*, 276:174–184. → pages 117

Arnold, N. S., Willis, I. C., Sharp, M. J., Richards, K. S., and Lawson, W. J. 1996. A distributed surface energy-balance model for a small valley glacier. I. Development and testing for Haut Glacier d'Arolla, Valais, Switzerland. *J. Glaciol.*, 42(140):77–89. → pages 176

Ashcroft, M. B. and Gollan, J. R. 2011. Fine-resolution (25 m) topoclimatic grids of near-surface (5 cm) extreme temperatures and humidities across various

habitats in a large (200 x 300 km) and diverse region. *Int. J. Climatol.*, 32:2134–2148. → pages 25, 118, 119

Ashcroft, M. B. and Gollan, J. R. 2013a. Moisture, thermal inertia, and the spatial distributions of near-surface soil and air temperatures: Understanding factors that promote microrefugia. *Agric. For. Meteorol.*, 176:77–89. → pages 26, 131

Ashcroft, M. B. and Gollan, J. R. 2013b. The sensitivity of topoclimatic models to fine-scale microclimatic variability and the relevance for ecological studies. *Theor. Appl. Climatol.*, 114(1):281–289. → pages 151

Avramidis, S. and Siau, J. F. 1987. An investigation of the external and internal resistance to moisture diffusion in wood. *Wood Sci. Technol.*, 21(3):249–256. → pages 61

Banwell, E. M., Morgan Varner, J., Knapp, E. E., and Van Kirk, R. W. 2013. Spatial, seasonal, and diel forest floor moisture dynamics in Jeffrey pine-white fir forests of the Lake Tahoe Basin, USA. *For. Ecol. Manage.*, 305:11–20. → pages 3, 9, 78, 102, 106, 132

Barry, R. G. 2008. *Mountain Weather and Climate*. Cambridge University Press, Cambridge, UK, third edition. → pages 8, 23, 24, 41

Bennie, J. J., Wiltshire, A. J., Joyce, A. N., Clark, D., Lloyd, A. R., Adamson, J., Parr, T., Baxter, R., and Huntley, B. 2010. Characterising inter-annual variation in the spatial pattern of thermal microclimate in a UK upland using a combined empirical–physical model. *Agric. For. Meteorol.*, 150(1):12–19. → pages 118

Birch, D. S., Morgan, P., Kolden, C. A., Abatzoglou, J. T., Dillon, G. K., Hudak, A. T., and Smith, A. M. S. 2015. Vegetation, topography and daily weather influenced burn severity in central Idaho and western Montana forests. *Ecosphere*, 6(1):article 17. → pages 2, 3, 147

Bolstad, P. V., Swift, L., Collins, F., and Regniere, J. 1998. Measured and predicted air temperature at basin to regional scales in the southern Appalachian mountains. *Agric. For. Meteorol.*, 91:161–176. → pages 11, 24

Braithwaite, R. J. and Olesen, O. B. 1990. A simple energy balance model to calculate ice ablation at the margin of the Greenland ice sheet. *J. Glaciol.*, 36(123):222–228. → pages 176

Breiman, L. 2001. Random forests. *Mach. Learn.*, 45(1):5–32. → pages 124

Brooks, R. T. and Kyker-Snowman, T. D. 2008. Forest floor temperature and relative humidity following timber harvesting in southern New England, USA. *For. Ecol. Manage.*, 254(1):65–73. → pages 25

Brown, J., Marsden, M., Ryan, K., and Reinhardt, E. 1985. Predicting duff and woody fuel consumed by prescribed fire in the northern rocky mountains. Technical report, Research Paper INT-337. US Department of Agriculture, Forest Service, Intermountain Forest and Range Experiment Station. → pages 149

Byram, G. M. and Jemison, G. M. 1943. Solar radiation and forest fuel moisture. *J. Agric. Res.*, 67(4):149–76. → pages 78

Camp, A., Oliver, C., Hessburg, P., and Everett, R. 1997. Predicting late-successional fire refugia pre-dating European settlement in the Wenatchee Mountains. *For. Ecol. Manage.*, 95(1):63–77. → pages 10, 102

Campbell Scientific 2015. CS506 Fuel Moisture Sensor Instruction Manual. Technical report, Edmonton, AB. → pages 19

Canadian Council of Forest Ministers 2005. *Canadian Wildland Fire Strategy: a Vision for an Innovative and iItegrated Approach to Managing the Risks*. Natural Resources Canada, Edmonton. → pages 1

Carlson, J. D., Bradshaw, L. S., Nelson, R. M., Bensch, R. R., and Jabrzemski, R. 2007. Application of the Nelson model to four timelag fuel classes using Oklahoma field observations: model evaluation and comparison with National Fire Danger Rating System algorithms. *Int. J. Wildland Fire*, 16(2):204–216. → pages 60, 67, 71, 74, 75, 76, 82

Carlyle-Moses, D. E. and Gash, J. H. C. 2011. Rainfall interception loss by forest canopies. In *For. Hydrol. Biogeochem.*, pages 407–423. Springer. → pages 87

Catchpole, E. A., Catchpole, W. R., Viney, N. R., McCaw, W. L., and Marsden-Smedley, J. B. 2001. Estimating fuel response time and predicting fuel moisture content from field data. *Int. J. Wildland Fire*, 10(2):215–222. → pages 6

Chen, J., Franklin, J. F., and Spies, T. A. 1993. Contrasting microclimates among clearcut, edge, and interior of old-growth Douglas-fir forest. *Agric. For. Meteorol.*, 63(3-4):219–237. → pages 9, 25, 26, 39

Chen, J., Saunders, S. C., Crow, T. R., Naiman, R. J., Brosofske, K. D., Mroz, G. D., Brookshire, B. L., and Franklin, J. F. 1999. Microclimate in forest ecosystem and landscape ecology. *Bioscience*, 49(4):288–297. → pages 9, 23, 25, 43

Chrosciewicz, Z. 1989. Prediction of forest-floor moisture content under diverse jack pine canopy conditions. *Can. J. For. Res.*, 19(11):1483–1487. → pages 102

Chung, U. and Yun, J. I. 2004. Solar irradiance-corrected spatial interpolation of hourly temperature in complex terrain. *Agric. For. Meteorol.*, 126(1):129–139. → pages 24

Clerc, M. 2010. *Particle Swarm Optimization*. ISTE, Newport Beach, US. → pages 61

Cohen, J. D. and Deeming, J. E. 1985. The National Fire-Danger Rating System: basic equations. General Technical Report PSW-82. Technical report, US Department of Agriculture, Forest Service, Pacific Southwest Forest and Range Experiment Station. → pages 2, 7, 23, 47, 48, 80, 83, 152

Collins, B., Kelly, M., van Wagtendonk, J., and Stephens, S. 2007. Spatial patterns of large natural fires in Sierra Nevada wilderness areas. *Landsc. Ecol.*, 22(4):545–557. → pages 2

Countryman, C. 1977. Radiation effects on moisture variation in ponderosa pine litter. Research Paper PSW-126. Technical report, US Department of Agriculture, Forest Service, Berkeley, CA. → pages 78

Deeming, J. E., Burgan, R. E., and Cohen, J. D. 1977. The National Fire-Danger Rating System–1978. General Technical Report INT-169. Technical report, US Department of Agriculture, Forest Service, Intermountain Forest and Range Experiment Station. → pages 61

Denmead, O. T. and Bradley, E. F. 1985. Flux-gradient relationships in a forest canopy. In *For. Interact.*, pages 421–442. Springer. → pages 9

Dillon, G. K., Holden, Z. A., Morgan, P., Crimmins, M. A., Heyerdahl, E. K., and Luce, C. H. 2011. Both topography and climate affected forest and woodland burn severity in two regions of the western US, 1984 to 2006. *Ecosphere*, 2(12). → pages 2, 117, 125, 147

Dingman, J. R., Sweet, L. C., McCullough, I., Davis, F. W., Flint, A., Franklin, J., and Flint, L. E. 2013. Cross-scale modeling of surface temperature and tree seedling establishment in mountain landscapes. *Ecol. Process.*, 2(1):1–15. → pages 24, 25, 26, 42

Dobrowski, S. Z. 2011. A climatic basis for microrefugia: the influence of terrain on climate. *Glob. Chang. Biol.*, 17(2):1022–1035. → pages 11, 24, 26, 41, 131

Dobrowski, S. Z., Abatzoglou, J. T., Greenberg, J. A., and Schladow, S. G. 2009. How much influence does landscape-scale physiography have on air temperature in a mountain environment? *Agric. For. Meteorol.*, 149(10):1751–1758. → pages 24

Dwire, K. A. and Kauffman, J. 2003. Fire and riparian ecosystems in landscapes of the western USA. *For. Ecol. Manage.*, 178(1–2):61–74. → pages 10

Dyer, J. 2009. Assessing topographic patterns in moisture use and stress using a water balance approach. *Landsc. Ecol.*, 24(3):391–403. → pages 10

Eck, T. F. and Deering, D. W. 1992. Canopy albedo and transmittance in a spruce-hemlock forest in mid-September. *Agric. For. Meteorol.*, 59(3):237–248. → pages 53

Erbs, D. G., Klein, S. A., and Duffie, J. A. 1982. Estimation of the diffuse radiation fraction for hourly, daily and monthly-average global radiation. *Sol. energy*, 28(4):293–302. → pages 53

Estes, B. L., Knapp, E. E., Skinner, C. N., and Uzoh, F. C. C. 2012. Seasonal variation in surface fuel moisture between unthinned and thinned mixed conifer forest, northern California, USA. *Int. J. Wildland Fire*, 21(4):428–435. → pages 3, 9, 78, 102, 106, 131, 148, 150

Faiella, S. M. and Bailey, J. D. 2007. Fluctuations in fuel moisture across restoration treatments in semi-arid ponderosa pine forests of northern Arizona, USA. *Int. J. Wildland Fire*, 16(1):119. → pages 78, 102, 106, 148

Ferguson, S. A., Ruthford, J. E., McKay, S. J., Wright, D., Wright, C., and Ottmar, R. 2002. Measuring moisture dynamics to predict fire severity in longleaf pine forests. *Int. J. Wildland Fire*, 11(4):267–279. → pages 5

Finney, M. A. 2004. FARSITE, Fire Area Simulator–model development and evaluation. Research Paper RMRS-RP-4. Technical report, US Department of Agriculture, Forest Service, Rocky Mountain Research Station. → pages 48, 152

Finney, M. A. 2006. An overview of FlamMap fire modeling capabilities. In Andrews, P. L. and Butler, B. W., editors, *Fuels Manag. - How to Meas. Success*, pages 213–220, Rocky Mountain Research Station. U.S. Department of Agriculture, Forest Service. → pages 48, 152

Fosberg, M. A. 1970. Drying rates of heartwood below fiber saturation. *For. Sci.*, 16(1):57–63. → pages 61

Fosberg, M. A. and Deeming, J. E. 1971. *Derivation of the one-and ten-hour timelag fuel moisture calculations for fire-danger rating. Research Note RM-RN-207*. US Dept. of Agriculture, Forest Service, Rocky Mountain Forest and Range Experiment Station. → pages 7

Fosberg, M. A., Rothermel, R., and Andrews, P. L. 1981. Moisture content calculations for 1000-hour timelag fuels. *For. Sci.*, 27(1):19–26. → pages 6, 7

Frazer, G., Canham, C., and Lertzman, K. 1999. Gap Light Analyzer (GLA), Version 2.0: Imaging software to extract canopy structure and gap light transmission indices from true-colour fisheye photographs, users manual and program documentation. Technical report, Simon Fraser University and the Institute of Ecosystem Studies. → pages 16

Fridley, J. D. 2009. Downscaling climate over complex terrain: High finescale (less than 1000 m) spatial variation of near-ground temperatures in a montane forested landscape (Great Smoky Mountains). *J. Appl. Meteorol. Climatol.*, 48(5):1033–1049. → pages 9, 11, 26, 41

Geiger, R. 1965. *The Climate Near the Ground.* Harvard University Press, Cambridge, Mass. → pages 8, 24

Gibos, K. E. 2010. *Effect of Slope and Aspect on Litter Layer Moisture Content of Lodgepole Pine Stands in the Eastern Slopes of the Rocky Mountains of Alberta.* PhD thesis, University of Toronto. → pages 3, 8, 77, 132, 150

Graefe, J. 2004. Roughness layer corrections with emphasis on SVAT model applications. *Agric. For. Meteorol.*, 124(3):237–251. → pages 82

Hatton, T. J., Viney, N., Catchpole, E. A., and De Mestre, N. J. 1988. The influence of soil moisture on Eucalyptus leaf litter moisture. *For. Sci.*, 34(2):292–301. → pages 4, 10, 150

Hayes, G. L. 1941. Influence of altitude and aspect on daily variations in factors of forest-fire danger. Technical report, US Department of Agriculture, Forest

Service, Northern Rocky Mountain Forest and Range Experiment Station. →
pages 8, 77

Heyerdahl, E. K., Brubaker, L. B., and Agee, J. K. 2001. Spatial controls of
historical fire regimes: a multiscale example from the interior west, USA.
Ecology, 82(3):660–678. → pages 2, 147

Hille, M. and den Ouden, J. 2005. Fuel load, humus consumption and humus
moisture dynamics in Central European Scots pine stands. *Int. J. Wildland Fire*,
14(2):153–159. → pages 6

Hindmarsh, A. C. 1983. ODEPACK, a systematized collection of ODE solvers. In
Stepleman, R., editor, *Sci. Comput.*, pages 55–64. North Holland, Amsterdam.
→ pages 52

Holden, Z. A., Abatzoglou, J. T., Luce, C. H., and Baggett, L. S. 2011a. Empirical
downscaling of daily minimum air temperature at very fine resolutions in
complex terrain. *Agric. For. Meteorol.*, 151(8):1066–1073. → pages 117, 118

Holden, Z. A., Crimmins, M. A., Cushman, S. A., and Littell, J. S. 2011b.
Empirical modeling of spatial and temporal variation in warm season nocturnal
air temperatures in two North Idaho mountain ranges, USA. *Agric. For.
Meteorol.*, 151(3):261–269. → pages 23

Holden, Z. A. and Jolly, W. M. 2011. Modeling topographic influences on fuel
moisture and fire danger in complex terrain to improve wildland fire
management decision support. *For. Ecol. Manage.*, 262(12):2133–2141. →
pages 8, 10, 25, 78, 83, 102, 107, 118, 119

Holden, Z. A., Klene, A. E., F Keefe, R., and G Moisen, G. 2013. Design and
evaluation of an inexpensive radiation shield for monitoring surface air
temperatures. *Agric. For. Meteorol.*, 180:281–286. → pages 16

Holden, Z. A., Morgan, P., and Evans, J. S. 2009. A predictive model of burn
severity based on 20-year satellite-inferred burn severity data in a large
southwestern US wilderness area. *For. Ecol. Manage.*, 258(11):2399–2406. →
pages 2, 147

Holden, Z. A., Swanson, A., Klene, A. E., Abatzoglou, J. T., Dobrowski, S. Z.,
Cushman, S. A., Squires, J., Moisen, G. G., and Oyler, J. W. 2015.
Development of high-resolution (250 m) historical daily gridded air
temperature data using reanalysis and distributed sensor networks for the US
Northern Rocky Mountains. *Int. J. Climatol.*, 36(10):3620–3632. → pages 118

Iqbal, M. 1983. *An Introduction to Solar Radiation*. Academic Press, Toronto. →
pages 19, 89, 177

Iroume, A. and Huber, A. 2002. Comparison of interception losses in a
broadleaved native forest and a Pseudotsuga menziesii (Douglas fir) plantation
in the Andes Mountains of southern Chile. *Hydrol. Process.*,
16(12):2347–2361. → pages 88

Johnstone, J. F. and Chapin, F. S. 2006. Effects of soil burn severity on post-fire
tree recruitment in boreal forest. *Ecosystems*, 9(1):14–31. → pages 1

Johnstone, J. F., Chapin, F. S., Hollingsworth, T. N., Mack, M. C., Romanovsky,
V., and Turetsky, M. 2010. Fire, climate change, and forest resilience in interior
Alaska. *Can. J. For. Res.*, 40(7):1302–1312. → pages 149

Kane, V. R., Lutz, J. A., Alina Cansler, C., Povak, N. A., Churchill, D. J., Smith,
D. F., Kane, J. T., and North, M. P. 2015. Water balance and topography predict
fire and forest structure patterns. *For. Ecol. Manage.*, 338:1–13. → pages 2, 147

Keith, D., Johnson, E., and Valeo, C. 2010a. Moisture cycles of the forest floor
organic layer (F and H layers) during drying. *Water Resour. Res.*, 46:W07529.
→ pages 10

Keith, D. M., Johnson, E. A., and Valeo, C. 2010b. A hillslope forest floor (duff)
water budget and the transition to local control. *Hydrol. Process.*,
24(19):2738–2751. → pages 10, 102

Kim, H. J., Sidle, R. C., and Moore, R. D. 2005. Shallow lateral flow from a
forested hillslope: Influence of antecedent wetness. *Catena*, 60(3):293–306. →
pages 10

Klaassen, W., Bosveld, F., and Water, E. D. 1998. Water storage and evaporation
as constituents of rainfall interception. *J. Hydrol.*, 213:36–50. → pages 88

Latif, Z. A. and Blackburn, G. A. 2010. The effects of gap size on some
microclimate variables during late summer and autumn in a temperate
broadleaved deciduous forest. *Int. J. Biometeorol.*, 54(2):119–129. → pages 26

Leach, J. A. and Moore, R. D. 2010. Above-stream microclimate and stream
surface energy exchanges in a wildfire-disturbed riparian zone. *Hydrol.
Process.*, 24(17):2369–2381. → pages 91

Lertzman, K., Fall, J., Dorner, B., and Others 1998. Three kinds of heterogeneity
in fire regimes: at the crossroads of fire history and landscape ecology.
Northwest Sci., 72(4):23. → pages 2

Liaw, A. and Wiener, M. 2002. Classification and Regression by randomForest. *R News*, 2(3):18–22. → pages 125

Lin, C.-C. 2004. Modeling fine dead fuel moisture in Taiwan red pine forests. *Taiwan J. For. Sci.*, 19(1):27–32. → pages 5

Link, T. E., Unsworth, M., and Marks, D. 2004. The dynamics of rainfall interception by a seasonal temperate rainforest. *Agric. For. Meteorol.*, 124(3-4):171–191. → pages 88

Littell, J. S. and Gwozdz, R. B. 2011. Climatic Water Balance and Regional Fire Years in the Pacific Northwest, USA: Linking Regional Climate and Fire at Landscape Scales. In McKenzie, D., Miller, C., and Falk, D. A., editors, *Landsc. Ecol. Fire*, Ecological Studies, pages 117–139. Springer Netherlands. → pages 2, 117, 118

Liu, B. Y. H. and Jordan, R. C. 1960. The interrelationship and characteristic distribution of direct, diffuse and total solar radiation. *Sol. energy*, 4(3):1–19. → pages 21

Lookingbill, T. R. and Urban, D. L. 2003. Spatial estimation of air temperature differences for landscape-scale studies in montane environments. *Agric. For. Meteorol.*, 114(3–4):141–151. → pages 11, 23, 24

Loustau, D., Berbigier, P., and Granier, A. 1992. Interception loss, throughfall and stemflow in a maritime pine stand. II. An application of Gash's analytical model of interception. *J. Hydrol.*, 138(3):469–485. → pages 88

Lundquist, J., Pepin, N., and Rochford, C. 2008. Automated algorithm for mapping regions of cold-air pooling in complex terrain. *J. Geophys. Res.*, 113(D22):D22107. → pages 10

Mandel, J., Beezley, J. D., Kochanski, A. K., Kondratenko, V. Y., and Kim, M. 2012. Assimilation of perimeter data and coupling with fuel moisture in a wildland fire–atmosphere DDDAS. *Procedia Comput. Sci.*, 9:1100–1109. → pages 151

Marsden-Smedley, J. B. and Catchpole, W. R. 2001. Fire modelling in Tasmanian buttongrass moorlands. III. Dead fuel moisture. *Int. J. Wildland Fire*, 10(2):241–253. → pages 5

Matthews, S. 2006. A process-based model of fine fuel moisture. *Int. J. Wildland Fire*, 15(2):155–168. → pages 10, 56, 57

Matthews, S. 2013. Dead fuel moisture research: 1991–2012. *Int. J. Wildland Fire*, 23(1):78–92. → pages 5

McArthur, A. G. 1962. Control Burning in Eucalypt Forests. Commonwealth of Australia. → pages 5

McKenzie, D., Miller, C., and Falk, D. 2011. Toward a theory of landscape fire. In McKenzie, D., Miller, C., and Falk, D. A., editors, *Landsc. Ecol. Fire*, Ecological Studies, pages 3–25. Springer Netherlands. → pages 1, 2, 80, 101, 117

Mekonnen, G. B., Matula, S., Doležal, F., and Fišák, J. 2015. Adjustment to rainfall measurement undercatch with a tipping-bucket rain gauge using ground-level manual gauges. *Meteorol. Atmos. Phys.*, 127(3):241–256. → pages 91

Meyer, C. L., Sisk, T. D., and Covington, W. W. 2001. Microclimate changes induced by ecological restoration of ponderosa pine forests in northern Arizona. *Restor. Ecol.*, 9(4):443–452. → pages 25

Miller, C. and Urban, D. L. 2000. Connectivity of forest fuels and surface fire regimes. *Landsc. Ecol.*, 15(2):145–154. → pages 2, 117

Monteith, J. and Unsworth, M. 2008. *Principles of Environmental Physics: Plants, Animals, and the Atmosphere*. Academic Press, Amsterdam, 3 edition. → pages 53, 54, 55

Montgomery, D. C. and Peck, E. A. 1992. *Introduction to Linear Regression Analysis*. Wiley-Interscience, New York. → pages 38

Moore, R. D., Sutherland, P., Gomi, T., and Dhakal, A. 2005. Thermal regime of a headwater stream within a clear-cut, coastal British Columbia, Canada. *Hydrol. Process.*, 19(13):2591–2608. → pages 89

Nelson, R. M. 1984. A method for describing equilibrium moisture content of forest fuels. *Can. J. For. Res.*, 14(4):597–600. → pages 6, 56

Nelson, R. M. 2000. Prediction of diurnal change in 10-h fuel stick moisture content. *Can. J. For. Res.*, 30(7):1071–1087. → pages 4, 8, 48, 53, 54, 58, 59, 62, 75, 151, 152

Nyman, P., Baillie, C., Bovill, W., Lane, P., and Tolhurst, K. 2015a. Measurement of topographic controls on the moisture content of surface fuels in south east Australian forests. In *21st Int. Congr. Model. Simul.*, pages 264–269. → pages 8, 79, 105, 150

Nyman, P., Metzen, D., Noske, P. J., Lane, P. N. J., and Sheridan, G. J. 2015b. Quantifying the effects of topographic aspect on water content and temperature in fine surface fuel. *Int. J. Wildland Fire*, 24(8):1129–1142. → pages 3, 10, 24, 77, 148, 152

Ogée, J. and Brunet, Y. 2002. A forest floor model for heat and moisture including a litter layer. *J. Hydrol.*, 255(1):212–233. → pages 10

Ohmann, J. L. and Spies, T. A. 1998. Regional gradient analysis and spatial pattern of woody plant communities of Oregon forests. *Ecol. Monogr.*, 68(2):151–182. → pages 3, 148

Oke, T. R. 1990. *Boundary Layer Climates*. Routledge, New York, second edition. → pages 9, 19, 26, 60, 101, 150

Parks, S. A., Miller, C., Nelson, C. R., and Holden, Z. A. 2014. Previous Fires Moderate Burn Severity of Subsequent Wildland Fires in Two Large Western US Wilderness Areas. *Ecosystems*, 17(1):29–42. → pages 1

Pierce, A. D. and Taylor, A. H. 2011. Fire severity and seed source influence lodgepole pine (Pinus contorta var. murrayana) regeneration in the southern cascades, Lassen volcanic National Park, California. *Landsc. Ecol.*, 26(2):225–237. → pages 1

Pojar, J., Klinka, K., and Meidinger, D. V. 1987. Biogeoclimatic ecosystem classification in British Columbia. *For. Ecol. Manage.*, 22(1):119–154. → pages 15

Pook, E. W. and Gill, A. M. 1993. Variation of live and dead fine fuel moisture in Pinus radiata plantations of the Australian-Capital-Territory. *Int. J. Wildland Fire*, 3(3):155–168. → pages 5, 78

Prata, A. J. 1996. A new long-wave formula for estimating downward clear-sky radiation at the surface. *Q. J. R. Meteorol. Soc.*, 122(533):1127–1151. → pages 176

Pypker, T. G., Bond, B. J., Link, T. E., Marks, D., and Unsworth, M. H. 2005. The importance of canopy structure in controlling the interception loss of rainfall: Examples from a young and an old-growth Douglas-fir forest. *Agric. For. Meteorol.*, 130(1-2):113–129. → pages 88

Raymond, C. L. and Peterson, D. L. 2005. Fuel treatments alter the effects of wildfire in a mixed-evergreen forest, Oregon, USA. *Can. J. For. Res.*, 35(12):2981–2995. → pages 128

Renaud, V., Innes, J. L., Dobbertin, M., and Rebetez, M. 2011. Comparison between open-site and below-canopy climatic conditions in Switzerland for different types of forests over 10 years (1998-2007). *Theor. Appl. Climatol.*, 105(1):119–127. → pages 3, 9, 25

Resco de Dios, V., Fellows, A. W., Nolan, R. H., Boer, M. M., Bradstock, R. A., Domingo, F., and Goulden, M. L. 2015. A semi-mechanistic model for predicting the moisture content of fine litter. *Agric. For. Meteorol.*, 203:64–73. → pages 72, 73

Rosin, K. 2010. *Development, evaluation, and application of dominant runoff generation processes in hydrological modeling*. PhD thesis, University of British Columbia. → pages xiii, 18, 124

Rothermel, R. 1972. A mathematical model for predicting fire spread in wildland fuels. Research Paper INT-117. Technical report, US Department of Agriculture, Forest Service, Intermountain Forest & Range Experiment Station. → pages 4, 47, 80, 101

Rothermel, R., Wilson, R. A., Morris, G. A., and Sackett, S. S. 1986. Modeling moisture content of fine dead wildland fuels. Research Paper INT 359. Technical report, US Department of Agriculture, Forest Service, Intermountain Research Station. → pages 78, 79, 148, 152

Rutter, A. J., Morton, A. J., and Robins, P. C. 1975. A predictive model of rainfall interception in forests. II. Generalization of the model and comparison with observations in some coniferous and hardwood stands. *J. Appl. Ecol.*, 12(1):367–380. → pages 87, 88

Samran, S., Woodard, P., and Rothwell, R. 1995. The effect of soil water on ground fuel availability burning conditions by fuel moisture. *For. Sci.*, 41(2):255–267. → pages 4, 10, 102, 150

Sato, Y., Kumagai, T., Kume, A., Otsuki, K., and Ogawa, S. 2004. Experimental analysis of moisture dynamics of litter layersthe effects of rainfall conditions and leaf shapes. *Hydrol. Process.*, 18(16):3007–3018. → pages 9

Schunk, C., Wastl, C., Leuchner, M., Schuster, C., and Menzel, A. 2013. Forest fire danger rating in complex topography-Results from a case study in the Bavarian Alps in autumn 2011. *Nat. Hazards Earth Syst. Sci.*, 13(9):2157–2167. → pages 10

Sharples, J. J. 2009. An overview of mountain meteorological effects relevant to fire behaviour and bushfire risk. *Int. J. Wildland Fire*, 18(7):737–754. → pages 2

Simard, A. J. 1968. *The moisture content of forest fuels 1: A review of the basic concepts. Information Report FF-X-14*. Department of Forestry and Rural Development. Forest Fire Research Institute. → pages 4

Skaar, C. 1988. *Wood-Water Relations*. Springer-Verlag, Berlin. → pages 5, 58

Smith, J. A. and Goltz, S. M. 1994. Updated thermal model using simplified short-wave radiosity calculations. *Remote Sens. Environ.*, 47(2):167–175. → pages 53

Smith, J. K., Lyon, L. J., Huff, M. H., Hooper, R. G., Telfer, E. S., Schreiner, D. S., and Others 2000. Wildland fire in ecosystems. Effects of fire on fauna. General Technical Report 42. → pages 1

Smith, J. W. 2002. *Mapping the thermal climate of the HJ Andrews Experimental Forest, Oregon*. PhD thesis, Oregon State University. → pages 24, 25

Soetaert, K. E. R., Petzoldt, T., and Setzer, R. W. 2010. Solving differential equations in R. *R J.*, 2:1–25. → pages 53

Spittlehouse, D. L. 1998. Rainfall interception in young and mature conifer forests in British Columbia. In *Proc. 23rd Conf. Agric. For. Meteorol.*, pages 2–6. → pages 88

Stambaugh, M. C., Guyette, R. P., and Dey, D. C. 2007. Forest fuels and landscape-level fire risk assessment of the Ozark Highlands, Missouri. *Proc. 15th Cent. Hardwood For. Conf.*, pages 1–9. → pages 77

Stathers, R. J. 1989. Summer frost in young forest plantations. *FRDA Rep.* → pages 25

Stephens, S. L. and Ruth, L. W. 2005. Federal forest-fire policy in the United States. *Ecol. Appl.*, 15(2):532–542. → pages 1

Stull, R. B. 1988. *An Introduction to Boundary Layer Meteorology*. Kluwer Academic Publishers, Norwell, MA. → pages 58

Suggitt, A. J., Gillingham, P. K., Hill, J. K., Huntley, B., Kunin, W. E., Roy, D. B., and Thomas, C. D. 2011. Habitat microclimates drive fine-scale variation in extreme temperatures. *Oikos*, 120:1–8. → pages 24, 25, 26, 27

Sullivan, A. L. and Matthews, S. 2012. Determining landscape fine fuel moisture content of the Kilmore East Black Saturday'wildfire using spatially-extended point-based models. *Environ. Model. Softw.* → pages 8, 78

Tanskanen, H., Granström, A., Venäläinen, A., and Puttonen, P. 2006. Moisture dynamics of moss-dominated surface fuel in relation to the structure of Picea abies and Pinus sylvestris stands. *For. Ecol. Manage.*, 226(1):189–198. → pages 78

Thornton, P. E., Running, S. W., and White, M. A. 1997. Generating surfaces of daily meteorological variables over large regions of complex terrain. *J. Hydrol.*, 190(3–4):214–251. → pages 21, 25

Turner, M. G., Romme, W. H., Gardner, R. H., and Hargrove, W. W. 1997. Effects of fire size and pattern on early succession in Yellowstone National Park. *Ecol. Monogr.*, 67(4):411–433. → pages 1

Valente, F., David, J. S., and Gash, J. H. C. 1997. Modelling interception loss for two sparse eucalypt and pine forests in central Portugal using reformulated Rutter and Gash analytical models. *J. Hydrol.*, 190(1):141–162. → pages xvi, 85, 86

Valigura, R. A. and Messina, M. G. 1994. Modification of Texas clear-cut environments with loblolly pine shelterwoods. *J. Environ. Manage.*, 40(3):283–295. → pages 26

Van Wagner, C. 1972. Equilibrium moisture contents of some fine forest fuels in eastern Canada. Information Report PS-X-36. Technical report, Canadian Forest Service, Petawawa Forest Experiment Station. → pages 5

Van Wagner, C. 1987. Development and structure of the Canadian forest fire weather index system. Forestry Technical Report 35. Technical report, Canadian Forestry Service. → pages 6, 10, 23, 47

Van Wagner, C. E. 1969. Drying rates of some fine forest fuels. *Fire Contr Notes Washingt.* → pages 4

Van Wagner, C. E. 1979. A laboratory study of weather effects on the drying rate of jack pine litter. *Can. J. For. Res.*, 9(2):267–275. → pages 5, 6, 7

Vanwalleghem, T. and Meentemeyer, R. K. 2009. Predicting forest microclimate in heterogeneous landscapes. *Ecosystems*, 12(7):1158–1172. → pages 25, 26

Vejmelka, M., Kochanski, A. K., and Mandel, J. 2016. Assimilation of perimeter data and coupling with fuel moisture in a wildland fire–atmosphere DDDAS. *Int. J. Wildland Fire*, 25(5):558–568. → pages 6

Vercauteren, N., Destouni, G., Dahlberg, C. J., and Hylander, K. 2013. Fine-resolved, near-coastal spatiotemporal variation of temperature in response to insolation. *J. Appl. Meteorol. Climatol.*, 52(5):1208–1220. → pages 24

Viney, N. 1991. A review of fine fuel moisture modelling. *Int. J. Wildland Fire*, 1(4):215–234. → pages 3, 4, 5, 56

Vo, S. T. K. 2001. *Duff water balance in the Canadian boreal forest*. PhD thesis, University of Calgary. → pages 102

Wadsö, L. 1993. Measurements of water vapour sorption in wood. *Wood Sci. Technol.*, 28(1):59–65. → pages 61

Whitehead, D. and Kelliher, F. M. 1991. A canopy water balance model for a Pinus radiata stand before and after thinning. *Agric. For. Meteorol.*, 55(1-2):109–126. → pages 88

Whitehead, R. J., Russo, G. L., Hawkes, B. C., Taylor, S. W., Brown, B. N., Barclay, H. J., and Benton, R. A. 2006. Effect of a spaced thinning in mature lodgepole pine on within-stand microclimate and fine fuel moisture content. In *Fuels Manag. How to Meas. success. Conf. Proceedings.–Andrews PL, Butl. BW, eds*. → pages 3, 9, 25, 78, 102, 131, 148

Wilkes, K. E. 1979. Thermophysical properties data base activities at Owens-Corning Fiberglas. In *Proc. ASHRAE/DOE-ORNL Conf. Therm. Perform. Exter. Envel. Build.*, pages 662–677. → pages 175

Winkler, R. D., Moore, R. D., Redding, T. E., Spittlehouse, D. L., Carlyle-moses, D. E., and Smerdon, B. D. 2010. Hydrologic Processes and Watershed Response. In *Compend. For. Hydrol. Geomorphol. Br. Columbia. BC*, pages 133–178. British Columbia Ministry of Forests and Range, Forest Science Program, Victoria, BC. → pages 9, 10

Zou, C. B., Barron-Gafford, G. A., and Breshears, D. D. 2007. Effects of topography and woody plant canopy cover on near-ground solar radiation: Relevant energy inputs for ecohydrology and hydropedology. *Geophys. Res. Lett.*, 34(24):1–6. → pages 3, 27, 148

Zuur, A., Leno, E. N., and Smith, G. M. 2007. *Analysing Ecological Data*. Springer Science & Business Media, New York. → pages 38

Appendix A

Temperature, humidity, and fuel moisture bias correction

A.1 Methods

The LogTags were set to measure ambient temperature and humidity in the lab for three days before and after the field season. For both periods and both variables, an average value across all LogTags was calculated and biases from this inter-LogTag mean were calculated for each LogTag. After checking that these biases remained stable over the field season, that is, the biases were the same for both calibration periods, these individual biases of each LogTag were removed.

From a brief pre-field test it was apparent that the three fuel moisture sensors exhibit biases relative to one another when co-located. These biases were removed before comparisons were made between fuel moisture measurements at different sites. This was accomplished with an approach similar to the LogTag bias correction. The three moisture sensors were co-located at the Base Station for the first 20 days of the field season. After the field season the moisture sensors were again set up to take co-located measurements at the UBC climate station for an additional 15 days. The first comparison period was used to calculate the biases of the sticks relative to one another. Once these biases were removed, the second comparison period was used to test the stability of these biases. Here I will focus on reducing the bias during the dry, low-moisture periods with no rain, because these

periods represent the majority of the season and are the most important from a fire behaviour stand point.

Pre-field tests also indicated that the LogTags had biases relative to higher-quality sensors. These biases were quantified by comparing the LogTag data to the data from the co-located high-quality sensors located at Fuel Moisture 1 and 2 and the Base Station. Initial analysis indicated that the LogTag biases were not constant; they changed with the changing humidity and temperature. Moreover, these relationships between the absolute value of the variable and the bias were non-linear. Therefore, a generalized additive model (GAM) from the R package mgcv was used to quantify these non-linear relationships. To account for the non-linear relationships, these variables were first passed through a thin plate regression spline smoothing function. The amount of smoothing was chosen automatically through cross validation. These models were then used to estimate the bias at each time step which was then removed from the LogTag data.

A.2 Results

A.2.1 Logtag bias corrections

Based on the two comparison periods, the individual systematic biases of the Log-Tags were stationary throughout the field season, and were within the $\pm 1°C$ and ± 5 % humidity instrument error reported by the manufacturer. Individual humidity and temperature biases averaged across both periods were therefore removed from each LogTag before further analysis.

Figure A.1 provides a comparison between all Rotronic and uncorrected Log-Tag observations taken at these three sites. The smoothed function fitted by the GAM model is also shown. The humidity bias is most prominent at the higher values where the LogTag sensors underpredict by a few percentage points. Conversely, the LogTag sensors overpredict temperature especially at the higher values. This is reflected in the comparison statistics shown in Table A.1.

Once the GAM-modelled errors were removed the comparison statistics improved, with most of the improvement seen in the biases. Example relative humidity time-series are shown in Figure A.2 for both pre and post adjustment while

169

error statistics are provided in Table A.1. The root mean square errors saw marginal improvements while the correlations did not change. This is expected as it is evident from Figure A.1 that much of the error is due to the spread rather than any systematic bias. It is likely that the slower response time of the LogTag sensors is responsible for much of this error. However, as we are primarily interested in daily ranges and seasonal trends, this error will not impact the final results of this analysis.
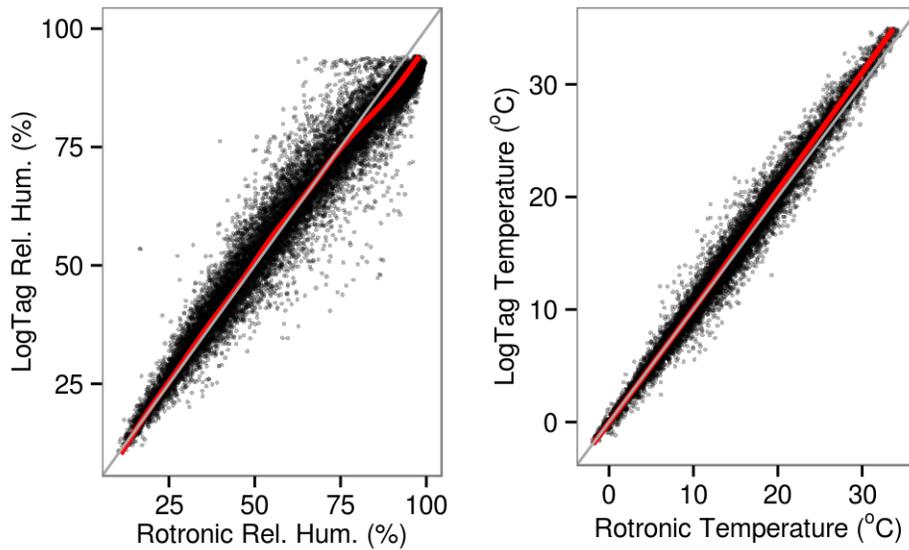

Figure A.1: Comparison of all co-located LogTag and Rotronic temperature and relative humidity observations. The *red line* is the smoothed GAM function. A 1:1 line is provided for reference.

Table A.1: LogTag vs. Rotronic comparison statistics for both relative humidity and temperature. Values provided for before and after the bias adjustment.

|	Relative Humidity			Temperature		
	Bias	Cor.	RMSE	Bias	Cor.	RMSE
	(%)		(%)	(^oC)		(^oC)
Pre-Adj.	-0.68	0.98	5.16	0.28	0.99	1.09
Post-Adj.	0.00	0.98	4.79	-0.00ww	1.00	
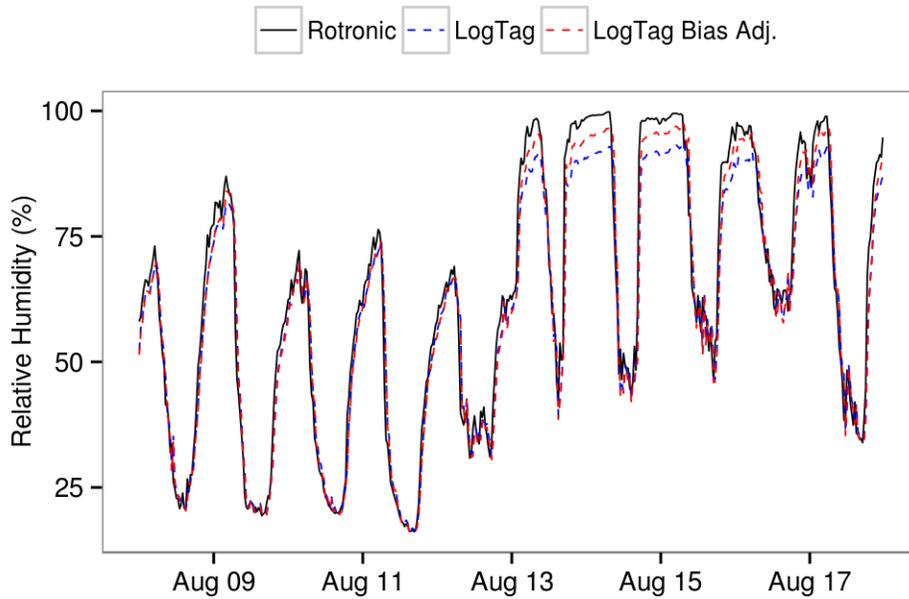
Figure A.2: Example relative humidity measurements by the Rotronic and LogTag sensor at the Base Station along with bias-adjusted LogTag data.

A.2.2 Fuel moisture sensor bias corrections

A comparison of un-adjusted co-located fuel moisture data from all three sensors is presented in Figure A.3. Below the fibre saturation point of 30% moisture content, where liquid water begins to form on the surface of the sticks, the sensors track each other very closely with correlations between 0.94 and 0.98. Sensors 1 and 3 show little bias between each other (.11 %) while sensor 2 has a consistent negative bias relative to the other two sensors (-3.2 % and -3.1 %). Above the fibre saturation point the sensors are much less consistent: the correlations between sticks are lower (r ranges from 0.86 to 0.94) and no one stick shows a consistent bias compared to the others. However, the late-season comparison period shows much more agreement above the fibre saturation point compared to the early-season period. This may be due to the relatively modest rainfall amount during the late-season period, i.e., as the sensors approach the saturation point of around 60%, agreement

diminishes substantially.
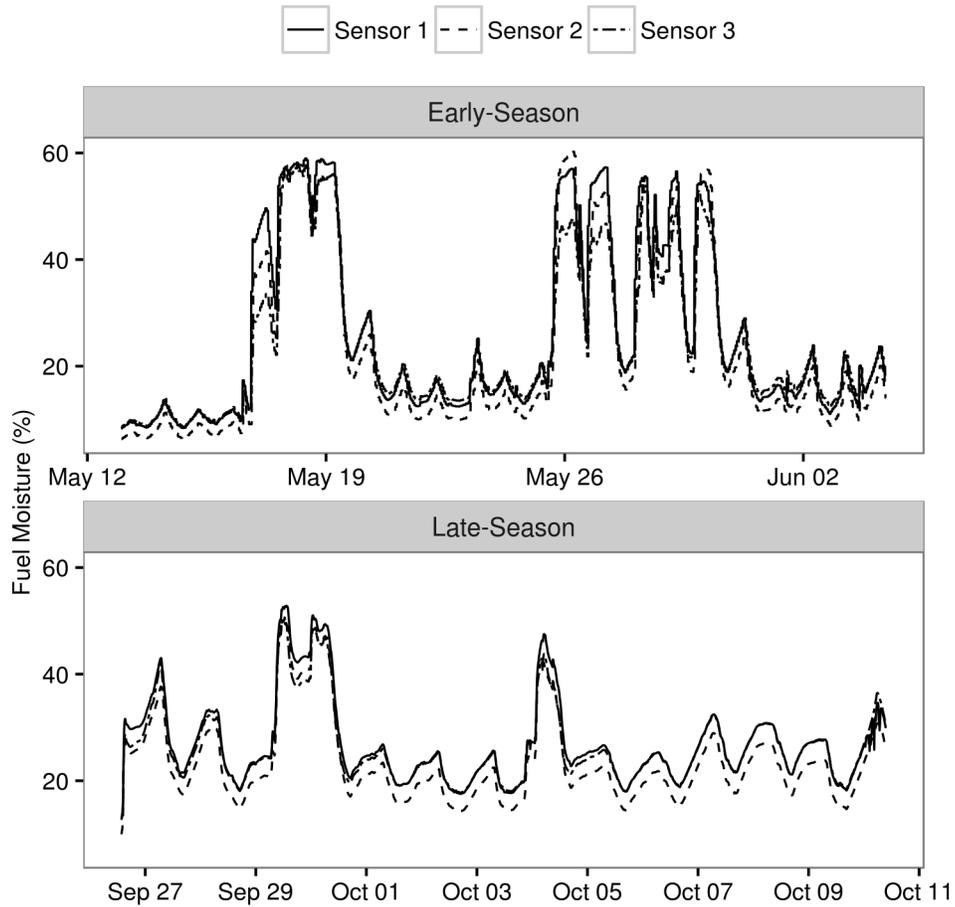
Figure A.3: Early and late-season comparison of co-located moisture sensors before bias adjustment.

Biases from an inter-sensor mean were calculated for each sensor using the early-season data. These biases were then removed from the late-season data and comparison statistics were calculated. In general, when below the fibre saturation point, biases between sensors seemed to be consistent over the season, although over the course of the season the spread between sensors increased slightly. When the early-season biases were removed the remaining late-season biases between

172

sensors ranged from 0.18 to 0.65%.

Because the biases seemed to be consistent over the season, I calculated season-wide sensor biases from the inter-sensor mean using both comparison periods and removed these biases from data. Because the periods below the fibre saturation point represent the majority of the season and are the most significant to this research, I calculated these biases using just the data below the fibre saturation point. Comparison statistics after removing these biases are presented in Table A.2. The root mean square error between sensors ranges from 1.52 to 2.25%. The adjusted fuel moisture time-series are shown in Figure A.4.

Table A.2: Intercomparison of moisture sensors after the bias adjustment using both comparison periods. Statistics are calculated for data below and above the Fibre Saturation Point as well as for all the data. Comparisons are made between sensors 1 and 2 ('1v2'), 1 and 3 ('1v3') and 2 and 3 ('2v3').

|	Correlation			Bias (%)			RMSE (%)		
	1v2	1v3	2v3	1v2	1v3	2v3	1v2	1v3	2v3
Above FSP	0.94	0.86	0.89	-0.48	4.52	5.00	3.52	6.47	6.79
Below FSP	0.98	0.94	0.96	0.00	0.00	0.00	1.52	2.25	1.52
All Data	0.99	0.97	0.98	-0.12	1.14	1.26	2.20	3.78	3.65
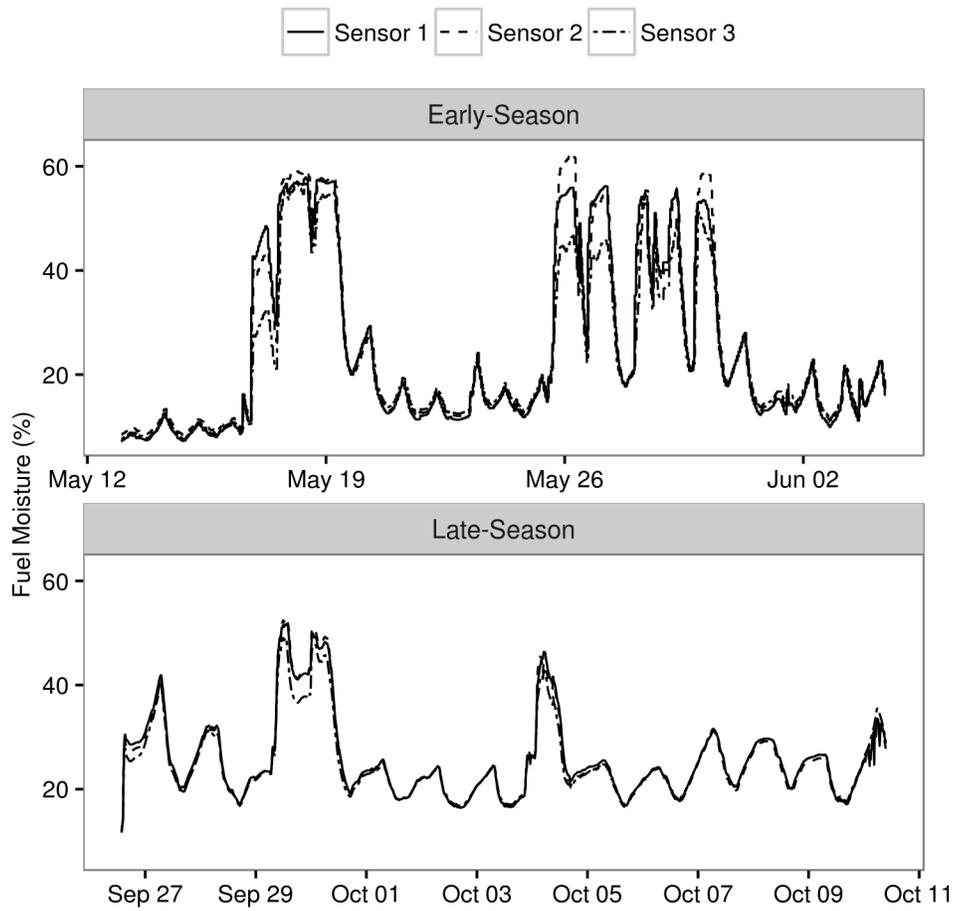
Figure A.4: Early and late-season comparison of co-located moisture sensors after bias adjustment.

Appendix B

Fuel moisture model details

B.1   Stick specific heat calculation

Following Wilkes (1979) the change in c_s with moisture and temperature is calculated as:

$$c_s = \frac{c_{wood} + m\,c_{water}}{1 + m_s} + c_{bound} \tag{B.1}$$

where m is the average stick moisture, $c_{water}\,(4200 \text{ J K}^{-1}\text{ kg}^{-1})$ is the specific heat of water, and c_{wood}, the specific heat of dry wood, is estimated as :

$$c_{wood} = 103.1 + 3.867\,T_s \tag{B.2}$$

c_{bound} accounts for the energy absorbed by the bound water below the fibre saturation point and is given as an empirical function of temperature and moisture:

$$c_{bound} = \begin{cases} \left(23.55\,T_s - 1320\,m_s - 6191\right)m_s & : m_s < m_{fsp} \\ 0 & : m_s \geq m_{fsp} \end{cases}$$

B.2   Division of shortwave radiation into diffuse and direct components

The ratio of diffuse to total radiation is:

$$\frac{K_{d,diff}}{K_d} = \begin{cases} 1.0 - 0.09n & n \geq 0.22 \\ 0.951 - 0.1604n + 4.388n^2 & \\ -16.638n^3 + 12.336n^4 & 0.22 > n \geq 0.80 \\ 0.165 & n > 0.80 \end{cases}$$

where n, the clearness index, is calculated as the ratio $K_d/K_{d,max}$, where $K_{d,max}$ is the theoretical maximum solar radiation achievable under a cloud free sky and is calculated as:

$$K_{d,max} = K_{solar}\tau^{p/p_{sea-level}}\sin\phi \tag{B.3}$$

where K_{solar} is the solar constant (1367 W m^{-2}), τ is the atmospheric transmissivity which is set to 0.75, p and $p_{sea-level}$ are the pressure at the site and at sea-level, respectively, and ϕ is the solar elevation angle.

The downwelling longwave radiation, L_d (W m^{-2}), is calculated by estimating an atmospheric emissivity, ε. Following Prata (1996) we can first calculate a clear sky emissivity, ε_0 as:

$$\varepsilon_{clear-sky} = 1 - (1+w)\exp\left(-(1.2 + 3.0w)^{0.5}\right) \tag{B.4}$$

where w is the precipitable water content (cm) which is estimated as:

$$w = 465\left(\frac{M q_a}{R}\right) \tag{B.5}$$

We need to account for cloudiness to estimate a final atmospheric emissivity, ε_a, from the clear-sky case, $\varepsilon_{clear-sky}$. Following Arnold et al. (1996), this can be done by using the clearness index, n, calculated above. Specifically, ε_a is calculated as:

$$\varepsilon_a = (1 + \beta m)\varepsilon_{clear-sky} \tag{B.6}$$

where m is the cloudiness factor and β is a constant based on cloud type. β is taken to be a constant value of 0.26 which is an average value for a variety of cloud types (Braithwaite and Olesen, 1990). m is calculated from n:

176

$$m = \begin{cases} 1 - n & : n > 0.2 \\ 1 & : n \leq 0.2 \end{cases}$$

B.3 Absorbed radiation

To calculate the diffuse radiation absorbed by the cylindrical fuel sticks, L_{abs} and $K_{abs,diff}$ (W), we will first assume that all incoming diffuse radiation is isotropic. We can then integrate the equation for the intensity of diffuse radiation on a inclined plane over the surface of the cylinder.

Iqbal (1983) provided the diffuse radiation intensity, I (W m^{-2}), for an inclined plane exposed to both upwelling and downwelling isotropic diffuse radiation:

$$I_d = I\frac{1}{2}(1 + cos\theta), \quad I_u = I\frac{1}{2}(1 - cos\theta) \tag{B.7}$$

where θ is the angle relative to the horizontal. We apply these two equations to the infinitesimal segment in Figure B.1. For the upper half of the cylinder the radiation absorbed, $I_{abs,top}$ (W), will be:

$$I_{abs,top} = I \int_0^{\pi/2} 1 + \cos(\pi/2 - \theta)lrd\theta \tag{B.8}$$

The symmetry of the problem allows us to double the integral from 0 to $\pi/2$ (which cancels out the 1/2 factor in equation B.7). For the lower half we use the same geometry as in Figure B.1 but we take the radiation to be upwelling towards the infinitesimal segment (i.e., we flip the geometry around the horizontal axis). Therefore, the limits of integration remain the same but we use the equation for I_u instead:

$$I_{abs,bott} = I \int_0^{\pi/2} 1 - \cos(\pi/2 - \theta)lrd\theta \tag{B.9}$$

The total absorbed diffuse radiation, I_{abs}, (in J s^{-1}) is then:

$$I_{abs} = I_{abs,bott} + I_{abs,top} + I_{abs,edge} =$$

$$lrI \int_0^{\pi/2} 2\,d\theta + I2\pi r^2 = I(\pi lr + 2\pi r^2) \quad \text{(B.10)}$$

$I_{abs,edge}$ is the power absorbed by both stick edges and is derived by applying equation B.7 to those vertical faces. We can apply this result to our problem, and calculate the shortwave and longwave diffuse radiation absorbed by the stick using the terms defined in section **??**:

$$L_{abs} = (\pi lr + 2\pi r^2)\,e_s(L_d + L_u) \quad \text{(B.11)}$$

$$K_{abs,diff} = (\pi lr + 2\pi r^2)(1 - \alpha_s)(K_{d,diff} + K_u) \quad \text{(B.12)}$$
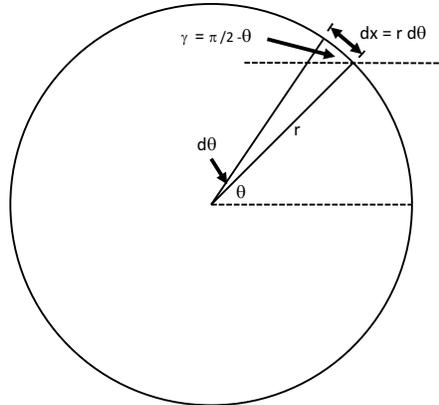
Figure B.1: Integral geometry for the absorption of diffuse radiation by the fuel moisture stick.

Appendix C

Supplementary information for Chapter 6
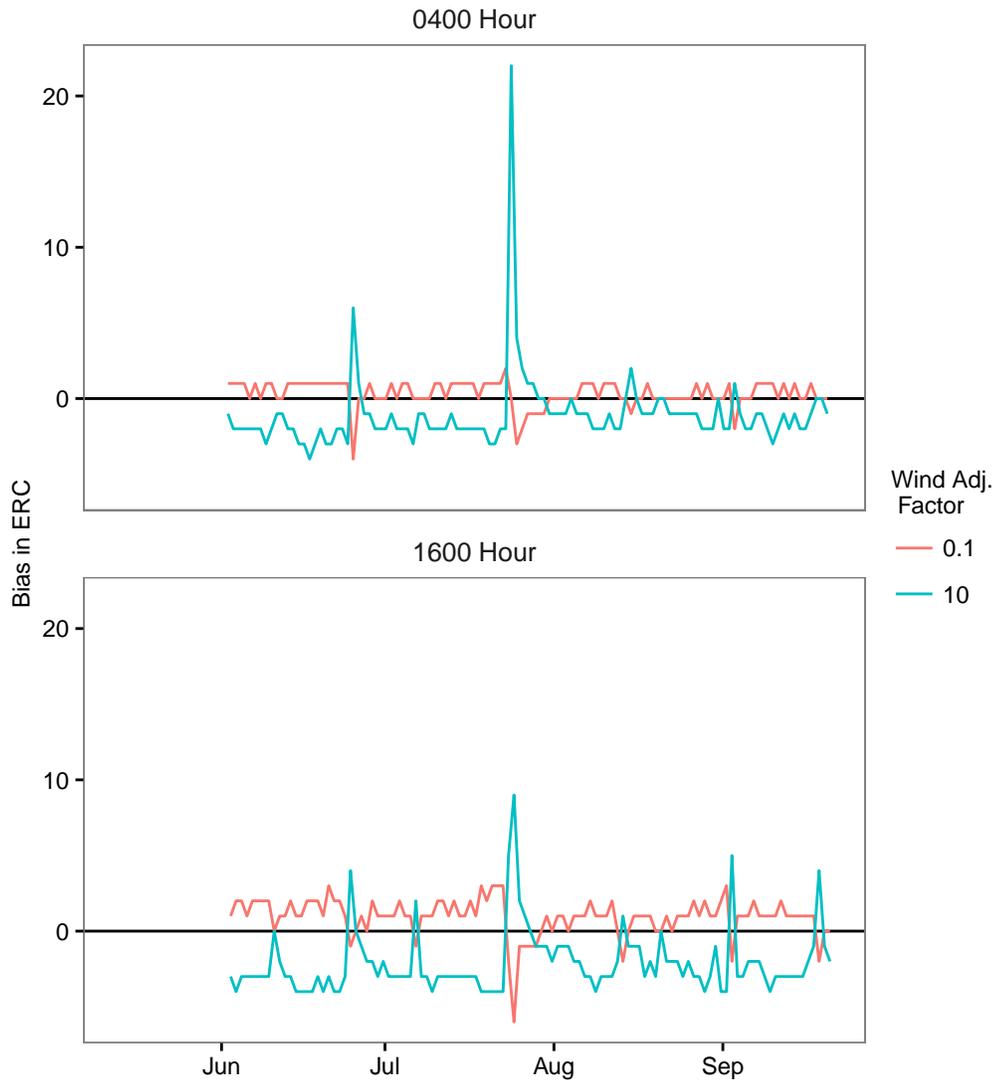
Figure C.1: Change in ERC at the Base Station resulting from the adjustment of wind speed by constant factors of 0.1 and 10.
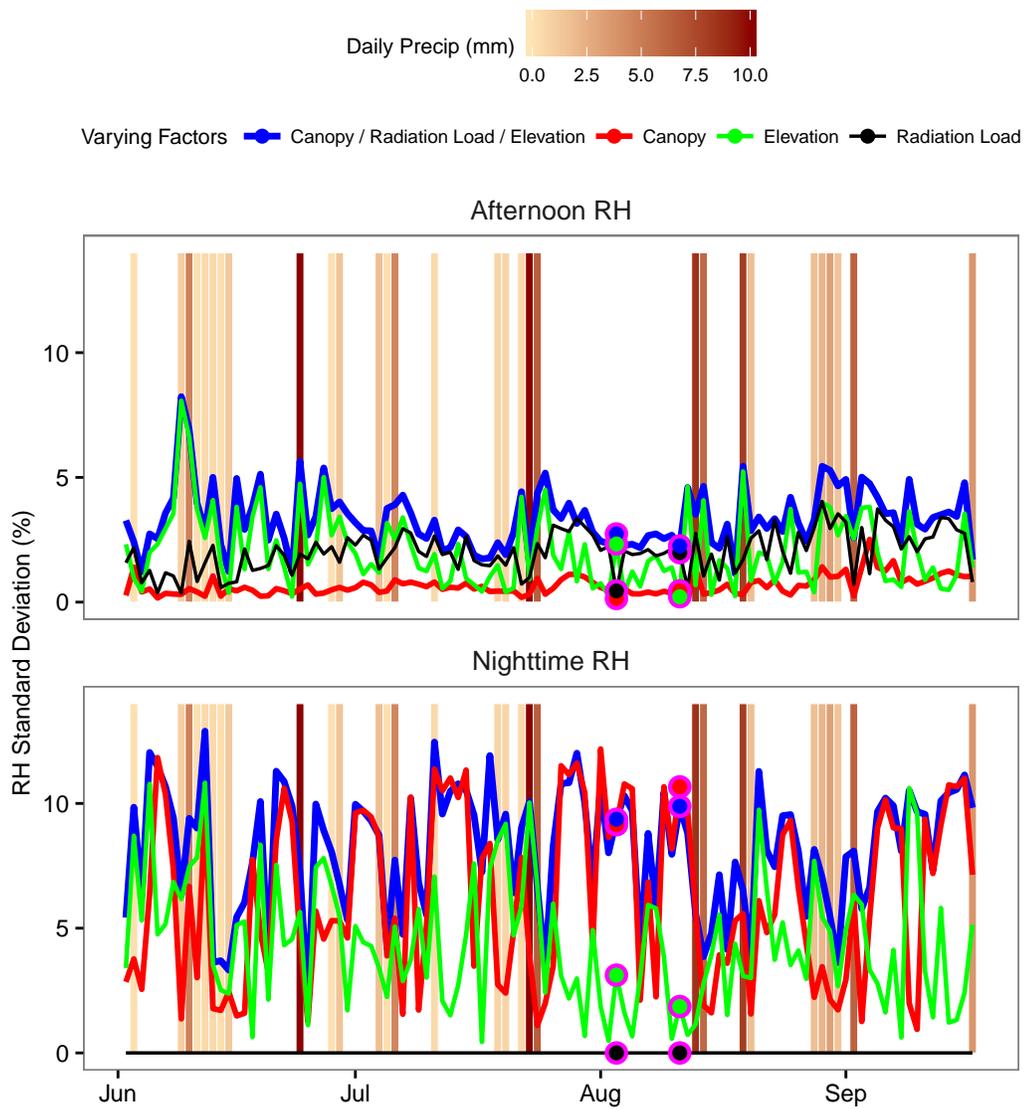
Figure C.2: Standard deviations of afternoon and nighttime relative humidity across the entire study region. The results from four different simulations are shown here: three runs in which all but one of the three spatial factors were kept constant, and one when all three factors varied across the landscape. The points indicate the two days which are shown as rasters in Figures 6.8 and 6.9
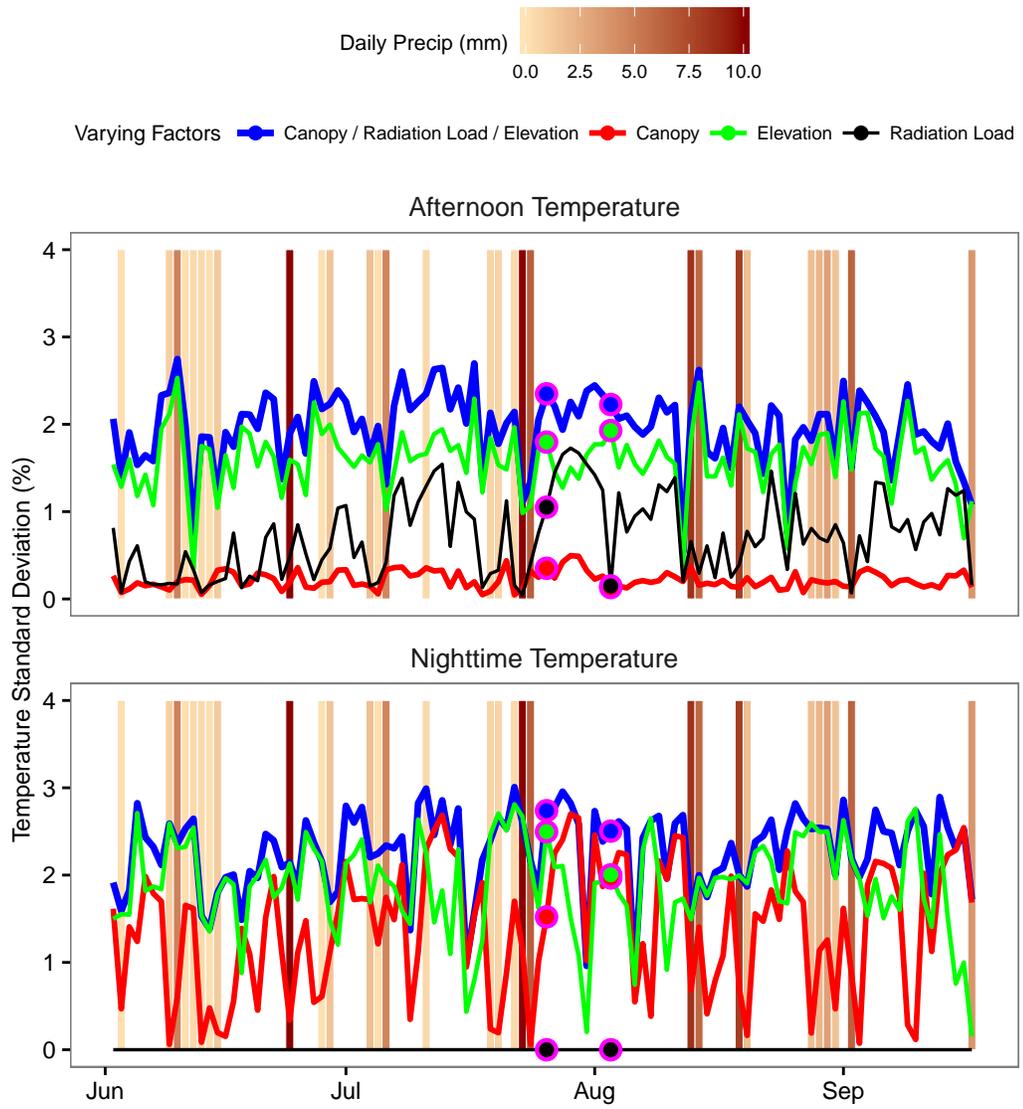
Figure C.3: As in Figure 6.7, but for temperature
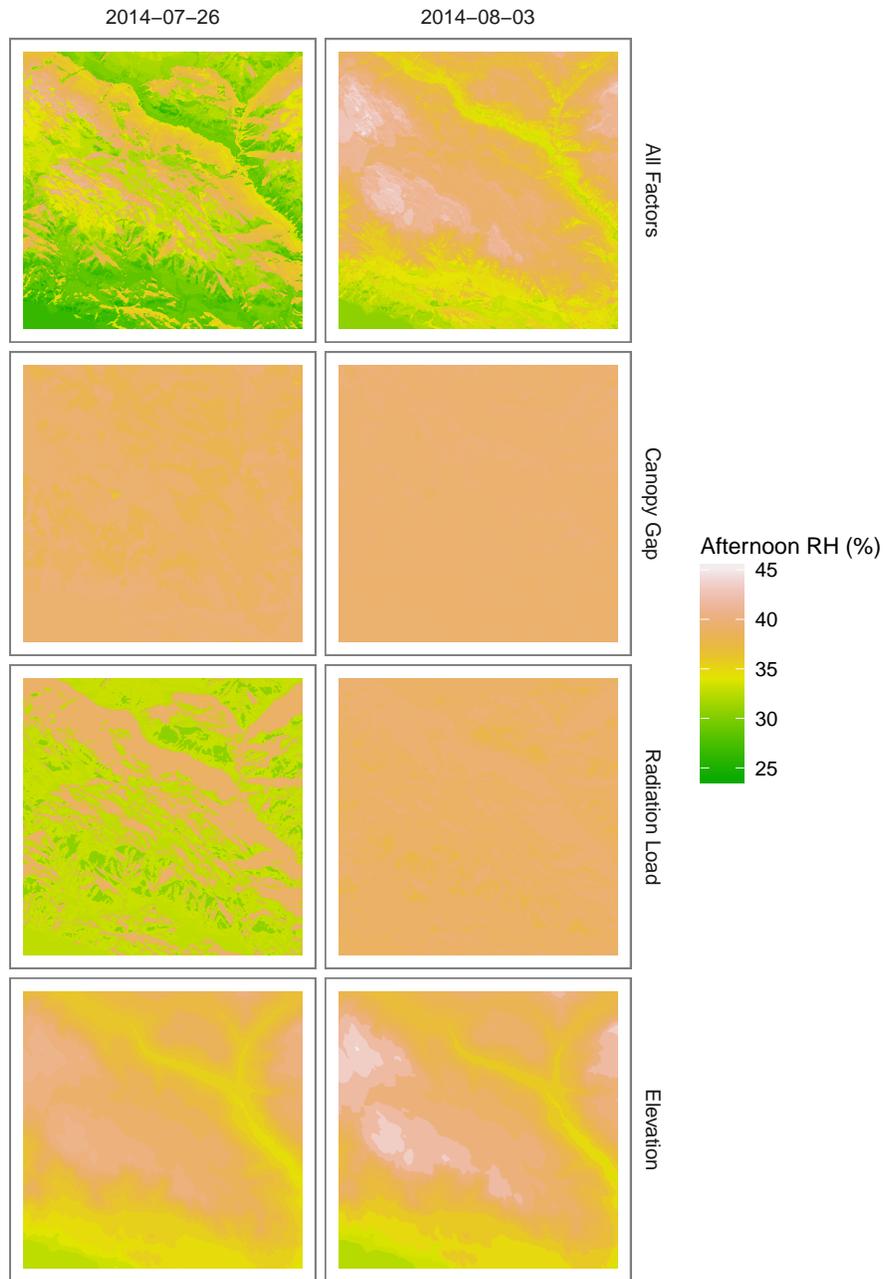
Figure C.4: Rasters of afternoon relative humidity for two different days (*columns*, indicated in Figure 6.7). Rasters driven by all factors, and the three factors individually (*rows*) are provided.
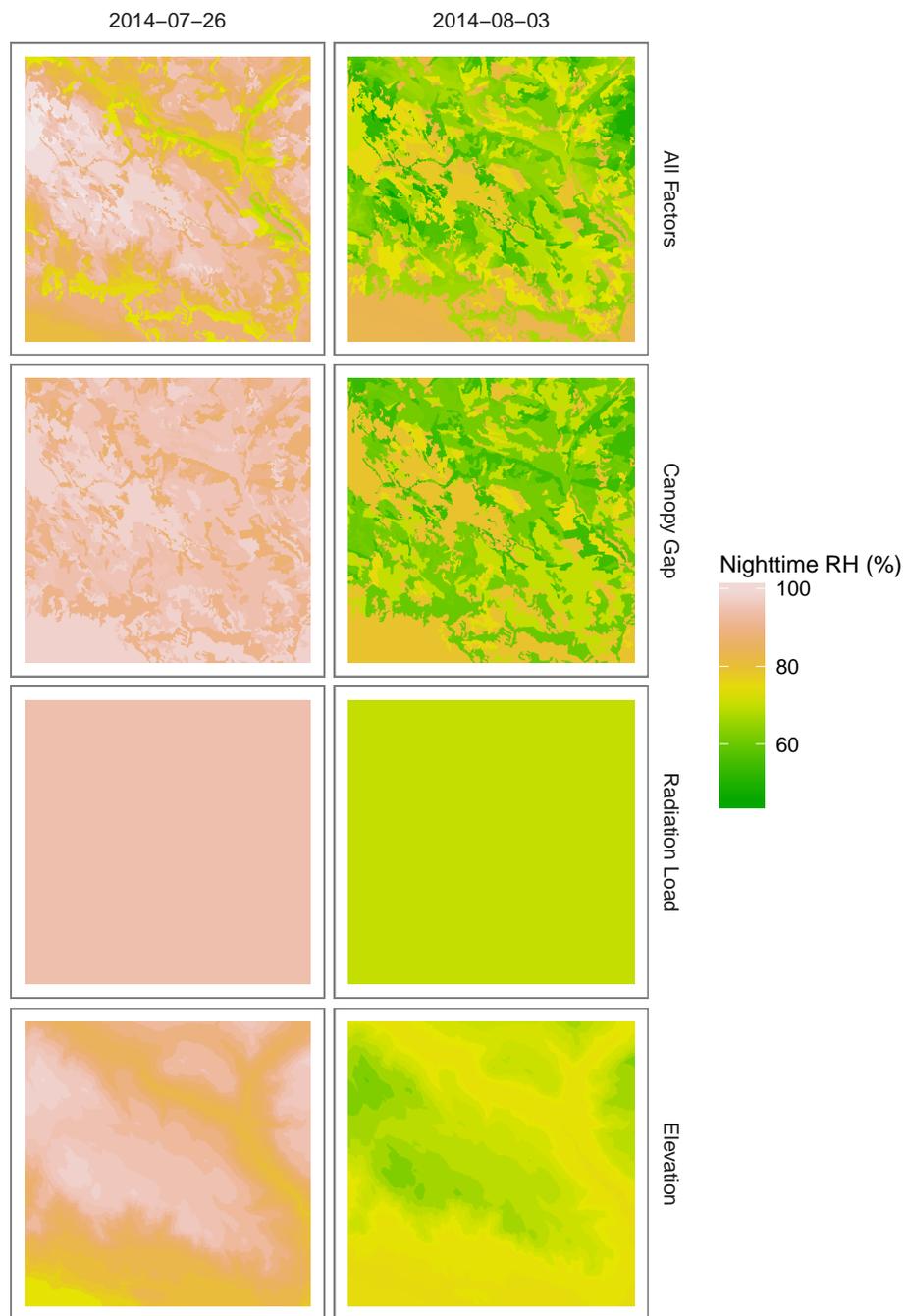
**Figure C.5:** As in Figure 6.8, but for nighttime relative humidity.
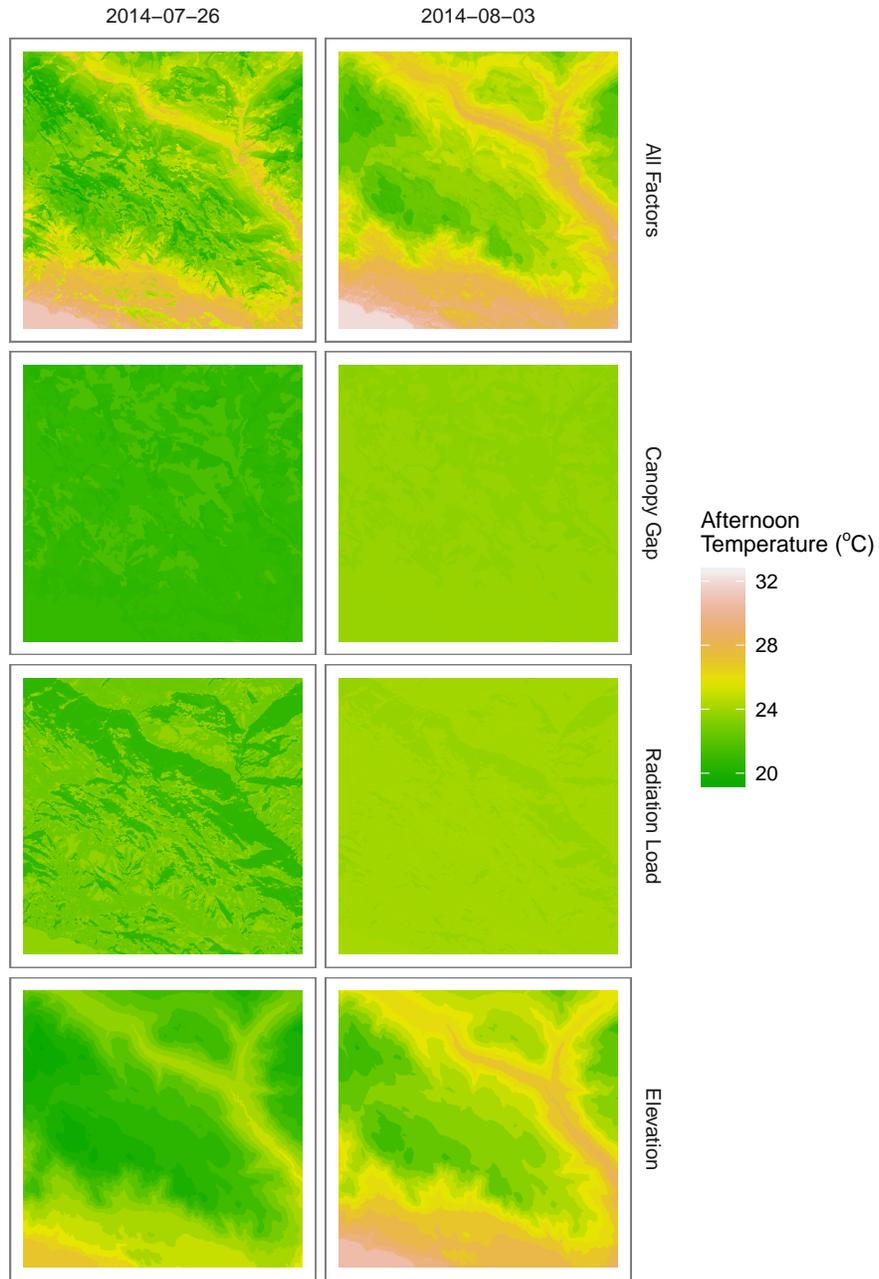
**Figure C.6:** As in Figure 6.8, but for afternoon temperature
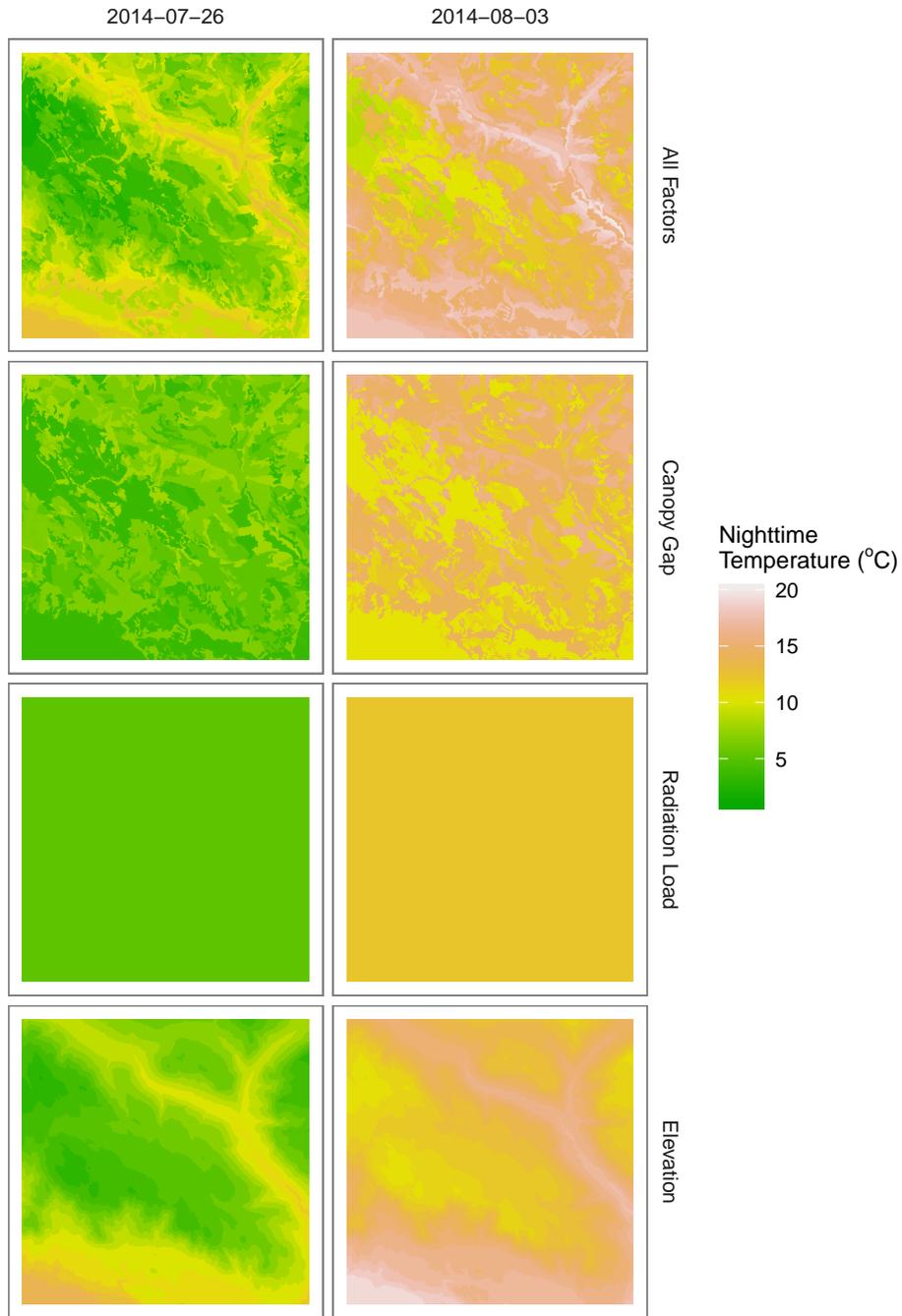
Figure C.7: As in Figure 6.8, but for nighttime temperature.